FEASIBILITY ANALYSIS ON THE UTILIZATION OF THE IRIDIUM SATLLITE COMMUNICATIONS NETWORK FOR RESIDENT SPACE OBJECTS IN LOW EARTH ORBIT

THESIS

John Robert Claybrook, Civ, USAF

AFIT-ENY-13-M-04

DEPARTMENT OF THE AIR FORCE
AIR UNIVERSITY

AIR FORCE INSTITUTE OF TECHNOLOGY

Wright-Patterson Air Force Base, Ohio

AFIT-ENY-13-M-04

FEASIBILITY ANALYSIS ON THE UTILIZATION OF THE IRIDIUM SATELLITE COMMUNICATIONS NETWORK FOR RESIDENT SPACE OBJECTS IN LOW EARTH ORBIT

THESIS

Presented to the Faculty

Department of Aeronautics and Astronautics

Graduate School of Engineering and Management

Air Force Institute of Technology

Air University

Air Education and Training Command

In Partial Fulfillment of the Requirements for the

Degree of Master of Science in Astronautical Engineering

John Robert Claybrook, BS

Civ, USAF

March 2013

AFIT-ENY-13-M-04

FEASIBILITY ANALYSIS ON THE UTILIZATION OF THE IRIDIUM SATELLITE COMMUNICATIONS NETWORK FOR RESIDENT SPACE OBJECTS IN LOW EARTH ORBIT

John Robert Claybrook, BS

Civ, USAF

Approved:

_____	_____
William E. Wiesel, PhD (Chairman)	Date
_____	_____
Eric D. Swenson, PhD (Member)	Date
_____	_____
Jonathan T. Black, PhD (Member)	Date

Abstract

In recent years, space has become more congested and contested, particularly in low Earth orbit (LEO), generating the need for a low-latency capability to provide precise orbital knowledge and accurate space situational awareness information. This thesis investigates the feasibility of resident space objects (RSOs) in LEO communicating continuously with ground operators or users through the Iridium Satellite Communications Network. Due to the problem's complexity and required time for computation, a test-industry technique called Design of Experiments is implemented in order to efficiently study the feasibility of the communication link. Specifically, an optimal response surface method is chosen to design the computation test matrix of orbital parameters in Design Expert for simulations using Systems Tool Kit. The results provide a statistical polynomial model for predicting the total Iridium-network access times and windows under specified orbital parameters. Initial assessments and physical constraints provide the model-space envelope, including a discussion on representing specific orbital parameters within the model prediction space.

To my father for his guidance, my mother for her unconditional support, and my brother for his everlasting friendship

Acknowledgments

I would like to express my gratitude to my research advisor, Dr. William Wiesel, for his willingness and desire to share his expertise, not only in the lectures that I had the fortune to learn, but throughout this entire thesis effort. I truly appreciate his excitement in the classroom of astrodynamics and his patient support with my evolving thesis.

I would like to express my appreciation to my academic advisor and thesis committee member, Dr. Eric Swenson, for his personal guidance and support throughout my time at AFIT, particularly during the Space Vehicle Design sequence and my thesis.

I would like to thank my thesis committee member, Dr. Jonathan Black, for his support and feedback during the Space Vehicle Design sequence and with my thesis.

John Robert Claybrook

Table of Contents

Page

List of Figures

Page

List of Tables

Page

FEASIBILITY ANALYSIS ON THE UTILIZATION OF THE IRIDIUM SATELLITE COMMUNICATIONS NETWORK FOR RESIDENT SPACE OBJECTS IN LOW EARTH ORBIT

I. Introduction

1.1 Background Information

The United States Strategic Command (USSTRATCOM) currently collects observations for more than 22,000 man-made objects, 10 centimeters or larger, orbiting the Earth (31). With such a large number of objects and this number only growing, the United States Air Force (USAF) has focused on the problems of conjunction analysis and space situational awareness (SSA) (4). Furthermore, the latency to collect information for conjunction analysis and SSA and send to the appropriate end user is critical in monitoring, addressing, or resolving the aforementioned problems.

A few decades ago, the only way to provide global wireless communications was via geosynchronous (GEO) satellites. A minimum of three satellites separated by 120 degrees could potentially offer coverage anywhere on the surface of the Earth, except above 70 degrees. Some major disadvantages of using GEO satellites included the amount of power required as a consequence of long-distance propagation losses, perceivable time-delay in voice-communications, and high relative costs for both the satellite acquisition process and a terminal user. During the 1990s and 2000s, three LEO satellite constellations were built and launched into operation, namely Iridium, Globalstar and Orbcomm. In LEO, either a Polar constellation or a Walker constellation provides an efficient global coverage method with different tradeoffs. A Polar constellation covers

the entire globe, while a Walker constellation only covers below certain latitudes. However, if the two constellations have the same number of satellites, then the Walker constellation has more diversity, and thus typically a slight edge on availability and reliability (6). This thesis assesses utilizing the Iridium network, a Polar constellation, and therefore the Globalstar and Orbcomm networks are not discussed in further detail.

Today, a market of terrestrially-based modems that can communicate with a particular LEO network of communications satellites has been fully exploited for purposes of tracking, monitoring, and locating. More specifically, the Iridium 9602 Transceiver is a next-generation Short Burst Data (SBD) modem that can transmit approximately 300 bytes of information, which has been industry proven in applications such as asset identification and tracking, sending telemetry, and environmental monitoring and alarming (9, 10). In order to perform conjunction analysis and acquire SSA information, there must be a system capability to identify and track the resident space object (RSO), send the RSO's orbital and health status information to the ground, and report or transmit potential impacting events. The status quo is utilizing either GEO satellites or traditional ground stations when the RSO passes overhead to collect and transmit data and information. However, as previously stated, GEO communications require large amounts of power. And traditional ground stations require that the RSO be in view, which for a typical LEO satellite will only be about two or three consecutive passes per day. The next technological step is then to leverage the industry success of terrestrially-based modems onto a space system capability that can communicate with an existing LEO communications network, thereby reducing power requirements, end-to-end latency, and the need for a dedicated ground station.

1.2 Motivation

The USAF has a need to develop a self-sufficient, low-cost, low-SWAP RSO identification and precision tracking capability for future SSA Architecture.

Recent trends that the space environment is becoming more congested and contested are described in the 2011 National Security Space Strategy Unclassified Summary (4). As space becomes more congested, the number of reported conjunctions increases, and subsequently more attention and resources are required in tracking active national assets. By collecting Global Positioning System (GPS) data and performing on-orbit determination, the satellite's position and covariance, or positional error ellipsoid, can be accurately estimated. In general, performing continuous on-orbit determination will result in a smaller covariance, in comparison to ground-based tracking, and subsequently fewer conjunction reports. As space becomes more contested, the requirement for SSA becomes more demanding. By providing a platform for a suite of space environmental sensors, the satellite can detect, measure and potentially analyze changes in the space environment, albeit natural changes or man-made threats. Furthermore, by leveraging existing LEO communications networks, such as Iridium, there will be no costs incurred in the development and construction of a dedicated ground station. Finally, by designing the capability to a cubesat-class design, the size, weight and power can be minimized.

Therefore, an initial space systems capability to collect GPS data, perform on-orbit determination, and transmit the desired information down to the ground user has been studied by professors, staff, students, and interns at the Air Force Institute of Technology (AFIT). Explicitly within the 2013 graduating class, Capt Landon Bastow

studied space collision avoidance, and Lt Rex Newman studied the solar power and battery module configuration.

1.3 Problem Statement

The Doppler effect is the primary inherent difficulty with satellite-to-satellite communications. The relative orbital motion of the two satellites results in a frequency shift when sending or receiving electromagnetic energy between a source and an observer. In the case of Iridium, there is a specific electromagnetic frequency range that it uses to communicate with voice and data transceivers, generically within the radio frequency (RF) range. The type of data transceiver to be flown on orbit also has minimum link duration requirements, or network processing times, in order to successfully route the flow of information. Additionally, there are physical limitations on equipment and particular configurations that restrict the domain of capable geometries for satellite-to-satellite communication. In short, the frequency shift, network processing time and physical constraints dictate the occurrence of communications opportunities and the duration of occurrences. By modeling and analyzing various orbits against an Iridium-like constellation model, a statistical relationship between orbital parameters and the number of occurrences, frequency of occurrences, and durations can be obtained. This relationship can then be tested against nominal orbits for purposes of validation.

1.4 Research Focus

The focus of this thesis is to statistically quantify the satellite-to-satellite communications link, including the effects of orbital parameters, constraints on range and range rate, and payload antenna beam width.

1.5 Methodology

This thesis utilizes the Systems Tool Kit (STK) 10.0 software package to perform numerical computations of individual orbital simulations. Due to the large number of required simulations for complete analysis, a technique called Design of Experiments is implemented to reduce experimental test points while maintaining the quality of the results and analysis and the validity of the conclusions. The Design Expert 8.0 software package is used to perform the experimental design analysis as well as the statistical analysis of the data obtained from STK.

1.6 Assumptions/Limitations

Due to the proprietary nature of the Iridium network, various critical details are excluded from this thesis and replaced with engineering judgment or generalized based on open source literature. One example of using engineering judgment is the modeling of the constellation. Specific details and information regarding the satellite control boxes, or regions in which the satellite is permitted to drift without maneuvering, is proprietary. Instead, the constellation is modeled as if the satellites are kept at the center of the control boxes and propagated forward in time according to the J_2 perturbation. One example of generalization is the modeling of the individual spot beams, or representations of the field-of-view (FOV), for each satellite. All satellites have the same beam patterns and are generically derived from provided proprietary link margin footprints and available open source information on Iridium in order to keep this study within full distribution. Complete details of assumptions and limitations will be discussed further while developing the methodology of study in Chapter Three.

1.7 Overview

This thesis is divided into five chapters, including this first chapter on the background and problem to be researched. Chapter Two is a literature review that provides supporting information on the Iridium network, relevant astrodynamic theory, and previous efforts. Chapter Three discusses the methodology of the study by describing the setup and appropriate tools to research the problem. Chapter Four presents the results from the study with detailed discussions. And Chapter Five presents the conclusions, summarizes the effort, and discusses potentially meaningful future efforts.

II. Literature Review

2.1 Chapter Overview

The purpose of the Literature Review is to provide the relevant and pertinent research to the problem. In the case of our study, understanding the Doppler effect and the complete Iridium network is critical to defining the scope of the problem and bounding the experimental design space.

2.2 The Doppler Effect and Satellite Communications

For satellite communications in general, the Doppler effect must be accounted for in order to achieve and sustain a communications link between a satellite in orbit and a ground station. The Doppler effect is the apparent change in frequency of a wave received by an observer moving relative to a source of waves. In general, the motion of the wave medium, such as air for sound waves, must also be accounted for in accurately determining the frequency shift. As a consequence of Einstein's Theory of Relativity, only the relative motion between observer and source impact the frequency shift for electromagnetic energy. If neither the source nor the observer is moving, then the frequency observed is the frequency emitted. In situations where the observer or the source is moving, or both, the frequency observed can be different from the frequency emitted. For satellite-to-satellite communications, the scenarios for the Doppler effect are more complex than for satellite-to-ground communications. At orbital velocities, the range rates between satellites can result in extremely large frequency shifts. Conversely the range rates between satellites can result in lower frequency shifts as the relative velocities approach zero. Communication links are often governed by the amount of

frequency shift the physical equipment can accommodate. In other words, a communications device, such as a transceiver, will vary the transmitted frequency according to the Doppler shift (11). In the case of the Iridium network, the permitted frequency shift is +/-37.5 kHz (17). Without getting into specific details that involve proprietary information, part of establishing the communications link involves the transceiver and satellite components determining what the frequency shift actually is under a particular configuration. This determination is part of the data processing time. Equation 1 shows the frequency shift according to the Doppler Effect. The frequency shift is related to the relative velocity along the line of sight $\dot{\rho}$, or also the rate of change of the scalar distance, or range rate, and calculated from

$$\Delta f = f\frac{v\cos(\theta)}{c} = f\frac{\dot{\rho}}{c} \tag{1}$$

where v is the relative velocity between the two satellites, θ is the angle between the relative velocity vector and the direct line of sight, c is the speed of electromagnetic energy in a vacuum.

More details on Iridium communications will be discussed in later sections, but for now if we take the center frequency f for the Iridium user-service to be 1621.25 MHz, then the maximum range rate $\dot{\rho}$ is approximately ±6.94 km/s.

2.3 The Iridium Network

The Iridium Network was conceived in the late 1980s by Motorola and became operational in the late 1990s (8). The objective was to provide telecommunications service to any user anywhere on the planet using a constellation of satellites in LEO. Being a communications satellite in LEO, an Iridium vehicle has a sophisticated antenna

array configuration that maximizes the field-of-view (FOV), or ground coverage. Figure 1 is a sketch of an Iridium communications satellite. The satellite has three mission antennas that receive and transmit user signals. The mission antennas are configured to maximize the FOV. Further the satellite has a combination of four inter-satellite link (ISL) antennas and four Gateway antennas that are used for relaying signals as necessary. More details on FOV and ISLs are discussed later in this section.

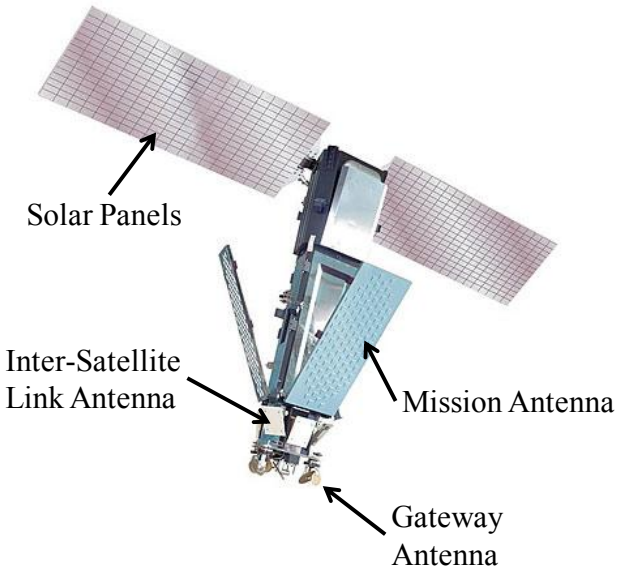

Figure 1. Iridium Communications Satellite

The original concept envisioned 77 satellites orbiting the Earth, and subsequently the name was inspired after the 77th chemical element, Iridium, which has 77 orbiting electrons. However, in an effort to reduce costs the constellation concept was reduced to 66 satellites (7). The original concept also envisioned the usage of 12 ground station "Gateways" that linked the individual Iridium Satellites with terrestrial terminals, such as landline networks for phones and facsimiles (8). Figure 2 illustrates the evolved concept of the Iridium network.

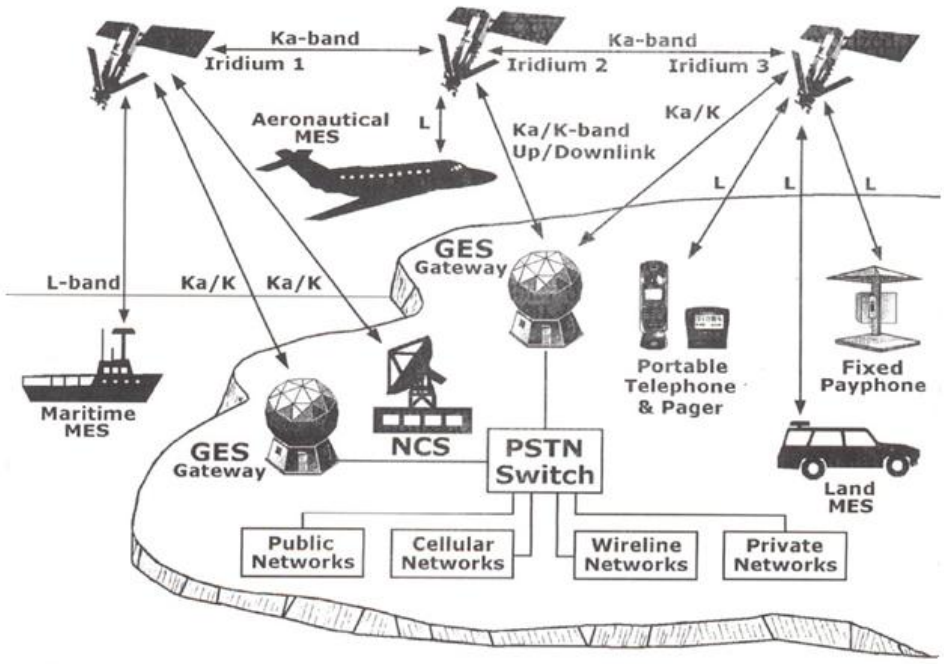

Figure 2. Utility Concept of the Iridium Network (8)

However, the currently unique capability of the Iridium inter-satellite links (ISLs) enables the ground infrastructure to fully operate with only a single primary Gateway located in Tempe, AZ (26). The Gateway comprises three communication towers. An individual tower is pictured in Figure 3.

Figure 3. Iridium Network Gateway Tower

2.3.1 Iridium Constellation

The Iridium constellation consists of 66 satellites, not including spares, spread over six planes in near-circular orbits at approximately 780 kilometers in altitude and 86.4 degrees inclination. The co-rotating planes are spaced apart by 31.6 degrees (22). Within each of the six planes, the 11 satellites are spaced out in approximate equal intervals. Figure 4 shows a snapshot of the Iridium constellation at a moment in time.

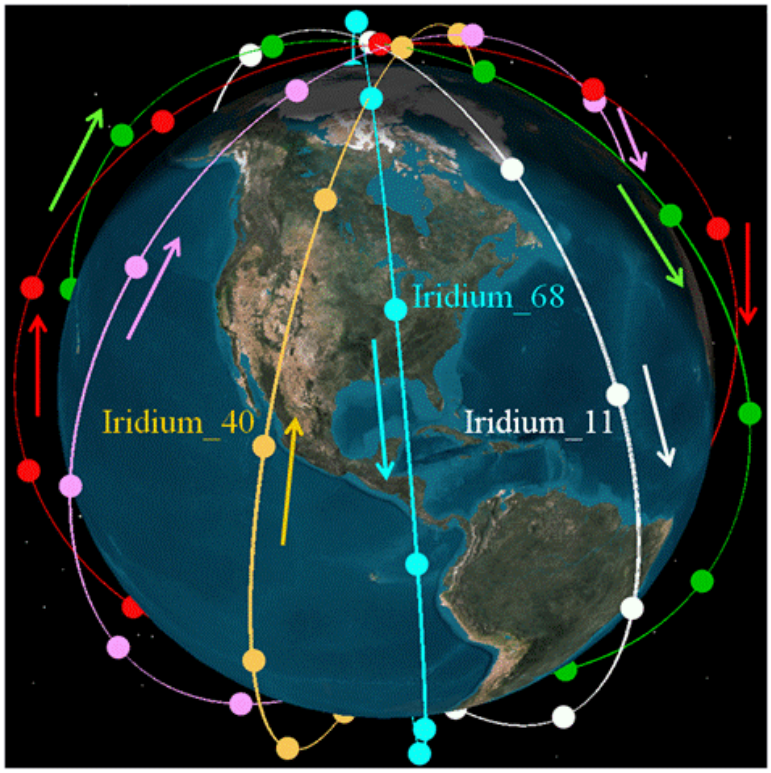

Figure 4. Iridium Communications Satellite Constellation

Note the spacing between the turquoise-colored plane (containing Iridium_68) and orange-colored plane (containing Iridium_40) compared to the spacing between the turquoise-colored plane and the white-colored plane (containing Iridium_11). The turquoise-colored and orange-colored planes can be thought of as planes one and six, respectively. Consequently, planes one and six are the counter-rotating planes. To be

more specific, at the moment shown in Figure 4 over the United States, the turquoise-colored plane is descending, or transiting north to south, and the orange-colored plane is ascending, or transiting south to north.

Due to drift from perturbing forces the satellites are not always spaced exactly 32.727 degrees apart. Instead, the individual satellites are permitted to drift within a control box. The control box is better thought of as a control ellipsoid, or region of space where the satellite is permitted to drift without a correction maneuver, that has dimensions on the order of kilometers. When the satellites approach the edge of the box, correction maneuvers are executed to return the satellite to the center (or near the center) of the box (7).

A current unique feature of the Iridium network compared to other LEO communications networks is the capability of ISLs. Also known as cross-links, the ISLs operate in the Ka-band and allow adjacent satellites to relay communications. Each satellite has four ISLs as shown in Figure 5.

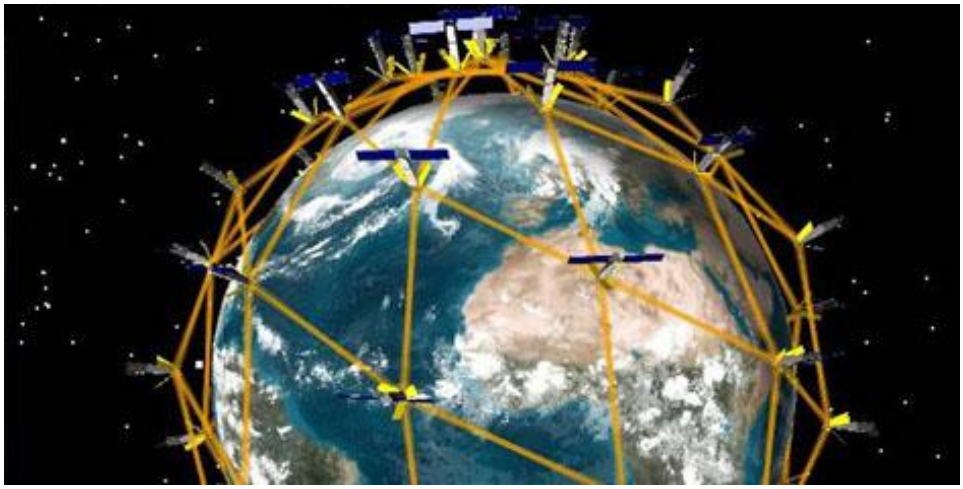

Figure 5. Iridium Constellation Inter-Satellite Links

Each satellite is permanently linked with the intra-plane forward and aft adjacent satellites. The satellite is dynamically linked with the inter-plane adjacent satellites. Dynamic links refer to those that are established and terminated regularly while the satellite orbits the Earth. ISLs do not exist between the counter-rotating planes since large angular rates exist between adjacent satellites (22). The ISLs provide flexibility with network paths to deliver communications. As a result, the flexibility improves communications delivery efficiency and system reliability (8). As a consequence, the Iridium ISLs increase autonomy in contrast to GEO networks, and there are fewer necessary Gateways since the satellites can route the communications. In fact, Iridium utilizes only one primary Gateway to connect the constellation to ground networks (22).

2.3.2 Iridium and the Doppler Effect

Another contrast between a LEO communications network and a GEO communications network is the difference in orbital velocities, and more specifically the velocity relative to the ground. By definition, a GEO satellite rotates with the Earth at the equatorial speed. Ideally, the GEO satellite remains directly overhead in the absence of perturbing forces. Of course, perturbing forces exist and cause a figure-eight type of drifting motion, but the relative velocity to the ground is fairly small, and the satellite remains over the desired field-of-view essentially until the satellite is disposed from its GEO orbit. With a LEO satellite, the satellite will have a faster orbital speed and will move from horizon to horizon in a relatively short amount of time. A rough estimate of the orbital speed v can be calculated from the two-body *vis-viva equation* (32)

$$v^2 = \mu\left(\frac{2}{r} - \frac{1}{a}\right) \tag{2}$$

where μ is the standard gravitational parameter of the Earth, r is the orbital radius of the satellite, and a is the semi-major axis of the satellite.

An estimate of the orbital period *P* can be calculated from Kepler's Third Law (32) as

$$P = 2\pi\sqrt{\frac{a^3}{\mu}} \tag{3}$$

Assuming a circular orbit and mean Earth radius of 6371 km, then for the case of Iridium, with a semi-major axis equal to 7151 km, equations 2 and 3 estimate an orbital speed of 7.47 km/s and an orbital period of 100.3 minutes, respectively.

As we discussed in section 2.1, the Doppler Effect impacts the ability to establish and maintain communications. Since the Doppler shift depends on the relative velocity, we can calculate the range ρ and range rate $\dot{\rho}$ can be calculated from

$$\rho = \sqrt{(x_2 - x_1)^2 + (y_2 - y_1)^2 + (z_2 - z_1)^2} \tag{4}$$

where x, y, and z are the position coordinates, and the subscripts *1* and *2* specify the two objects under consideration, and

$$\dot{\rho} = \frac{d\rho}{dt} = \frac{(x_2 - x_1)(\dot{x}_2 - \dot{x}_1) + (y_2 - y_1)(\dot{y}_2 - \dot{y}_1) + (z_2 - z_1)(\dot{z}_2 - \dot{z}_1)}{\rho} \tag{5}$$

where $\dot{x}$, $\dot{y}$, and $\dot{z}$ are the velocity coordinates.

In this problem to gauge the significance of the Doppler Effect we use the Earth-Centered Inertial coordinate frame depicted in Figure 6 to perform our calculations.

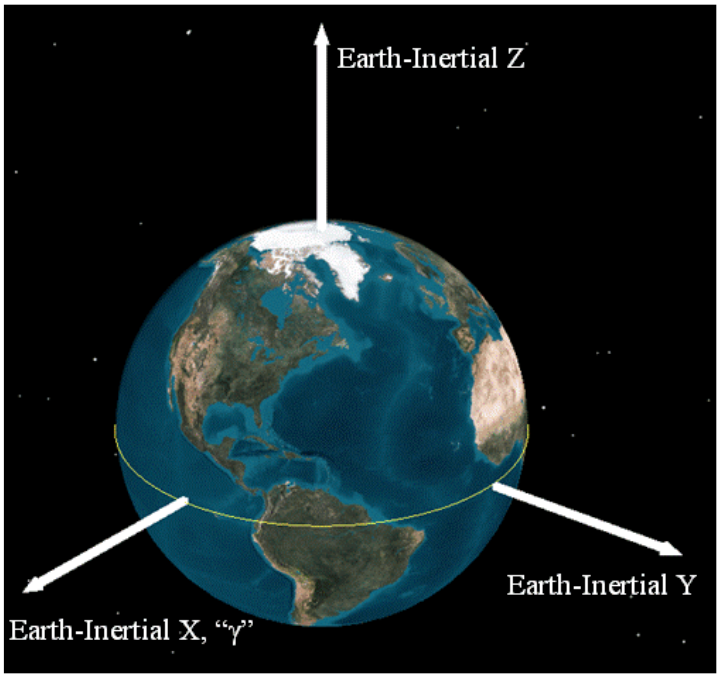

Figure 6. Earth-Centered Inertial Coordinate System (from STK)

Without explicit computation we can observe that if the Iridium satellite under consideration is directly overhead of a mobile user, then the range rate will equal zero. For example, if at this moment of occurrence, both the satellite and mobile user are along the x-axis, then the x-velocities are zero, the y-positions are zero, and the z-positions are zero. By definition, this is the point of closest approach. Instead, we can gauge the general maximum values for the range rate between the satellite and mobile user by assessing the situation at the time when the Iridium satellite first comes over the horizon and enters into the user's view. The minimum elevation angle El for a user to view an Iridium satellite from the ground is 8.2 degrees (22), but unless noted otherwise, this study will use a minimum elevation angle of 10 degrees. Figure 7 shows the geometry between a ground user and an Iridium satellite at the ascension point over the horizon.

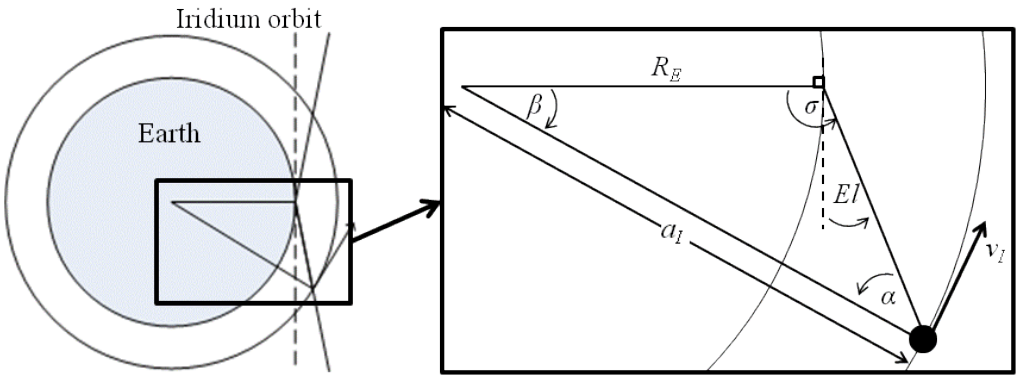

Figure 7. Iridium Satellite Viewing Geometry from Ground User

From Figure 7, the parameters important for assessing the significance of the Doppler effect are:

α is the satellite slant angle to the ground;

β is the Earth-central angle between the ground user and satellite;

σ is the angle between the Earth's radial vector to the ground user and elevation line to the satellite;

a_I is the semi-major axis for the satellite;

El is the elevation angle of the ground user to the satellite;

R_E is the radius of the Earth;

v_I is the orbital speed of the satellite.

From Equation 5, we need to calculate the position and velocity coordinates of both the user and the Iridium satellite at the moment when the satellite ascends over the horizon. Like before we will assume circular Keplerian motion for the satellite. Also, we will impose that the mobile user is at the equator in the *xz*-plane and that the satellite is within

the *xz*-plane at the instant of ascending over the horizon. Thus, the inertial position and velocity coordinates for the Iridium satellite are calculated from

$$\begin{aligned} x_I &= a_I \cos(\beta) \\ y_I &= 0 \\ z_I &= -a_I \sin(\beta) \\ \dot{x}_I &= v_I \sin(i)\sin(\beta) \\ \dot{y}_I &= v_I \cos(i) \\ \dot{z}_I &= v_I \sin(i)\cos(\beta) \end{aligned} \tag{6}$$

where i is the inclination angle of the Iridium satellite. In order to calculate the Iridium satellite coordinates, we must calculate the Earth-central angle β. However, to calculate the Earth-central angle we must first calculate the satellite slant angle α using the Law of Sines as

$$\frac{\sin(\sigma)}{a_I} = \frac{\sin(\alpha)}{R_E} \tag{7}$$

where we can use the trigonometric identity between sine and cosine as

$$\sin(\sigma) = \sin(90° + El) = \cos(El) \tag{8}$$

Therefore, the satellite slant angle α is 61.3 degrees. Then from the triangle

$$\beta = 180° - \sigma - \alpha \tag{9}$$

and the Earth-central angle β is 18.7 degrees. Then, using an inclination angle of 86.4 degrees the Iridium coordinates can be calculated and are located in Table 1.

Next the user coordinates need to be calculated. We cannot ignore that the mobile user on the ground has a velocity due to the rotation of the Earth. The rotation of the Earth is calculated from

$$\omega = \frac{2\pi \text{ rad}}{1 \text{ sidereal day}} \tag{10}$$

where one sidereal day is 23 hours, 56 minutes, 4.09 seconds, and therefore the rotation rate of the Earth is 7.292E-5 rad/s. Then, the inertial position and velocity coordinates for the mobile user on the ground are calculated from

$$\begin{aligned} x_u &= R_E \\ y_u &= 0 \\ z_u &= 0 \\ \dot{x}_u &= 0 \\ \dot{y}_u &= R_E \omega \cos(\lambda_E) \\ \dot{z}_u &= 0 \end{aligned} \tag{11}$$

where λ_E is the latitude of the user. In this problem, the user is located at the equator and has zero latitude. Also, since the user is located at the equator we will use the equatorial Earth radius of 6378 km. The calculated coordinates for the user are located in Table 1.

Table 1. Iridium Satellite and User Coordinates at Moment of Horizon Ascension

Coordinate	Iridium Satellite	Mobile User
x	6774 km	6378 km
y	0 km	0 km
z	-2293 km	0 km
$\dot{x}$	2.387 km/s	0 km/s
$\dot{y}$	0.468 km/s	0.465 km/s
$\dot{z}$	7.052 km/s	0 km/s

As it turns out, the inclination angle of the Iridium satellite results in an eastwardly motion nearly equal to the Earth equatorial speed.

Now we can assess the significance of the Doppler effect to our communications. Table 2 shows the results from the calculations for range, range rate, and frequency shift from Equation 4, Equation 5, and Equation 1, respectively.

Table 2. Range, Range Rate, and Frequency Shift at Horizon Ascension

Range	Range Rate	Frequency Shift
2327 km	-6.58 km/s	-35.4 kHz

If the z-position and x-velocity of the satellite change signs, namely negative to positive and positive to negative, respectively, then the ranges are equal, the range rates are equal in magnitude but opposite in sense, and the frequency shifts are equal in magnitude but opposite in sense.

In addition to considering the impact of the frequency shift for our communications, we should also calculate the time duration for when the satellite is in view. In contrast to a GEO satellite, a LEO satellite will have very short durations for viewing time. We can view the satellite as long as the elevation angle El is greater than our minimum requirement. The previous statement holds true for a total Earth-central angle of 2β. Then the in-view time $T_{in-view}$ is calculated from

$$T_{in-view} = \left(\frac{2\beta}{360°}\right) P_{Iridium} \tag{12}$$

where $P_{Iridium}$ is the orbital period of an Iridium satellite as calculated previously from Equation 3. Equation 12 yields a viewing time of 10.4 minutes.

Now, we shall gauge the range rate between an Iridium satellite and a mobile user satellite in LEO. From this point, we shall refer to a mobile user satellite as the spacecraft. In general terms the process is the same as previously preformed, and so this time only the highlights are emphasized. Figure 8 is essentially identical to Figure 7 except now we have replaced the radius of the Earth for the semi-major axis of the LEO spacecraft. We have also included the representation of the spacecraft velocity since, generally speaking, the LEO spacecraft will have a nonzero inclination angle which results in a nonzero *z*-component of the velocity.

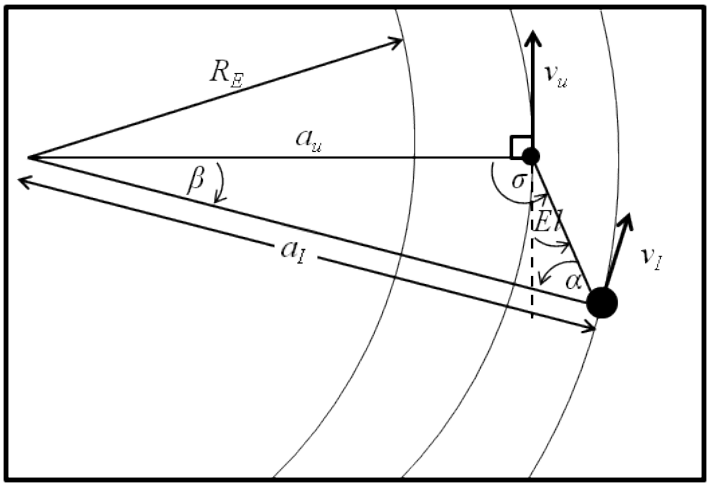

Figure 8. Iridium Satellite Viewing Geometry from LEO Satellite User

Qualitatively, we can observe that by increasing the spacecraft semi-major axis, the arc that the Iridium satellite subtends when in view has decreased in size. In other words we can say that the Earth-central angle β has decreased.

We will assume the spacecraft follows circular Keplerian motion where the semi-major axis a_s is 6771 km, the inclination i_s is 40°, and the spacecraft is ascending in its transit. Figure 9 illustrates that with a nonzero inclination, the spacecraft will have an inertial *z*-component of velocity in addition to the *x*- and *y*-components of velocity as it

orbits the Earth. The spacecraft orbital velocities are significantly greater than what we calculated for the equatorial velocity of the Earth.

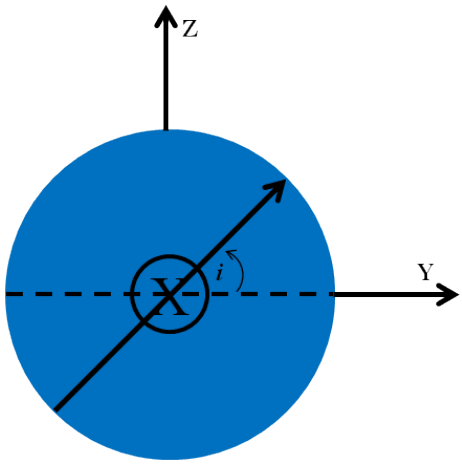

Figure 9. Inclination of Spacecraft

Additionally we will impose that the spacecraft is located directly over the equator in the *xz*-plane and that the Iridium satellite is within the *xz*-plane at the moment of ascension over the horizon. We start by calculating the inertial position and velocity coordinates for the LEO spacecraft from

$$\begin{aligned} x_s &= a_s \\ y_s &= 0 \\ z_s &= 0 \\ \dot{x}_s &= 0 \\ \dot{y}_s &= v_s \cos(i_s) \\ \dot{z}_s &= v_s \sin(i_s) \end{aligned} \tag{13}$$

where the subscript *s* refers to the LEO spacecraft. As stated above, since the LEO spacecraft has a larger radius than the Earth, the values for the angles in Figure 8 are not

necessarily identical to the values for the angles in Figure 7. We can see this by suggesting for a moment that the elevation angle El remains at 10 degrees. Then we can calculate the satellite slant angle α from the Law of Sines

$$\frac{sin(\sigma)}{a_I} = \frac{sin(\alpha)}{a_s} \tag{14}$$

and in this example, we compute a satellite slant angle of 68.8 degrees. Without describing the exact details at this moment in the thesis, we shall simply state that the real maximum satellite slant angle for an Iridium Satellite is 62 degrees. Therefore, we will use the value of 62 degrees for the satellite slant angle. Next, using Equation 14 we compute an elevation angle of 21.2 degrees. Finally, using Equation 9 we compute an Earth-central angle of 6.8 degrees. Now returning to Equation 6 and Equation 13 we compute the inertial position and velocity coordinates, which are shown in Table 3.

Table 3. Iridium satellite and LEO spacecraft coordinates at first viewing moment

Coordinate	Iridium Satellite	LEO Spacecraft
x	7101 km	6771 km
y	0 km	0 km
z	-847 km	0 km
$\dot{x}$	0.882 km/s	0 km/s
$\dot{y}$	0.468 km/s	5.876 km/s
$\dot{z}$	7.393 km/s	4.930 km/s

Then, Table 4 shows the calculated range, range rate and frequency shift between the Iridium satellite and the LEO spacecraft

Table 4. Doppler shift between Iridium satellite and LEO spacecraft

Range	Range Rate	Frequency Shift
909 km	-1.97 km/s	-10.4 kHz

Therefore, the magnitude of the Doppler shift has actually decreased as a consequence of the particular configuration of the two orbits. We should emphasize that based on the problem setup, the Iridium satellite and LEO spacecraft both had positive *z*-components of velocity. We shall define this configuration such that the LEO spacecraft is co-rotating with the Iridium satellite constellation. However, if everything else stays the same except that we now impose the LEO spacecraft is descending in its transit (*z*-component of velocity is negative), then we get a significantly different result in the frequency shift as shown in Table 5. We shall define this configuration such that the LEO spacecraft is counter-rotating against the Iridium satellite constellation.

Table 5. Small Doppler shift between Iridium satellite and LEO user

Range	Range Rate	Frequency Shift
909 km	-11.2 km/s	-60.3 kHz

The magnitude of 60.3 kHz as a Doppler shift exceeds the capability of the Iridium transceiver to establish a link with the Iridium satellites.

We can now infer one general trend for the Doppler shift at orbital altitudes and velocities. For co-rotating orbits the Doppler shift will actually decrease relative to the ground-based shift and should not inhibit the communications link. For counter-rotating

orbits, the Doppler shift will significantly increase relative to the ground-based shift and exceed current allowable frequency shifts within the transceiver equipment.

2.3.3 Iridium Satellite Footprint and Spot Beams

Each Iridium satellite has three antennas with 16 spot beams for a total of 48 spot beams. The full 48-beam footprint has an approximate diameter of 2800 miles, or about 4500 km, on the ground. Individual spot beams have an approximate diameter of 250 miles, or about 400 km, on the ground, which means there is significant overlap with adjacent spot beams. The overlap ensures reliability in handing off voice calls between spot beams (27). Due to the proprietary nature of the diagrams that detail the spot beam layout and link margins no representative figure is included in this section; but the spot beams are organized roughly into four groups: three inner beams, nine outer-inner beams, 15 middle beams, and 21 outer beams (29). Many of the beam patterns are irregularly shaped and the beams in each group are not quite evenly distributed azimuthally, but the deviations are small. All adjacent spot beams do overlap, but there is not any overlap with spot beams in the same group that are not adjacent. A generalized model of the satellite spot beams is discussed in section 3.2.3 and shown in Figure 13.

2.3.4 Iridium Short Burst Data

The Iridium network has a user uplink and downlink frequency range of 1616 MHz to 1626.5 MHz (22). The Iridium network has the capability to send short messages with relatively low latency between terminal originator and terminal end, otherwise known as Short Burst Data (SBD). SBD is a service that sends and receives information via email or direct IP. Iridium has released three generations of the SBD

transceiver: Iridium 9601, Iridium 9602, and Iridium 9603. This study considers the Iridium 9602 transceiver shown in Figure 10.

Figure 10. Iridium 9602 Transceiver

Typically the message size is on the order of 300 bytes. The transfer of information typically only takes about a few seconds. However, there is more to the process than just sending the message because the transceiver and satellite must pass setup messages, but the details of the process are proprietary. Overall, the consequence is that the full message transfer process is on the order of several seconds (30). The transceiver-to-satellite processing time has been tested and measured by the United States Naval Academy. The results are discussed section 2.6.3.

There are two types of SBD transmissions. The first is a Mobile Originated (MO) transmission which is a message that originates with a mobile user that uses the Iridium network to transmit the message through the Gateway and out to the intended email or IP address. The second is a Mobile Terminated (MT) transmission which is a message that originates within the internet that sends the message to the Gateway which then uses the Iridium satellites to relay the message to the intended mobile user. There are subtle differences between the two types of transmissions in order to ensure that the Gateway

properly routes the information (9). For the purposes of modeling and simulation, this study does not consider whether the communications link is a MO or MT transmission.

2.4 Satellite Propagation Methods

The nature and accuracy of predicting satellite positions at times in the future is critically dependent on the selected satellite propagation method. Only brief descriptions of typically-selected methods are discussed. For detailed derivations and explanations, consult any quality astrodynamics textbook, such as those by Wiesel or Vallado.

2.4.1 Keplerian Motion

The simplest orbital problem is that under pure Keplerian motion, otherwise known as two-body motion. The combination of Newton's Second Law of Motion, Newton's Universal Law of Gravitation, and Kepler's three laws are the foundation for the study of orbital motion (32). Any orbital mechanics text starts a derivation of the basic two-body equation from these laws, but the final form of the two-body equation, as shown in Vallado is

$$\ddot{r} = -\frac{\mu}{r^2}\frac{\vec{r}}{r} \tag{15}$$

where $\vec{r}$ is the radius vector from the central-body to the satellite and μ is the standard gravitational parameter of the Earth. Two-body motion, which relies only on one central gravitational force, can be utilized as a first approximation for certain situations and for consideration of short time intervals. However, the accuracy of prediction using two-body motion equations diverges immediately since there are real perturbing forces influencing a satellite's orbital motion (35).

2.4.3 J_2 Perturbation

Aside from the historical considerations of third-body interactions, say that of the Sun-Earth-Moon system, the next often considered orbital perturbation is due to a non-spherical Earth. Since the Earth rotates and is not a rigid mass, the planet bulges at the equator and slightly compresses at the poles. The J_2 perturbation accounts for this type of mass distribution. Starting with Poisson's Equation for a satellite orbiting in space

$$\nabla^2 V = 0 \tag{16}$$

Wiesel derives the geopotential expansion and corresponding Hamiltonian function in spherical harmonics in (34). A critical result with the geopotential expansion comes out of the first non-vanishing zonal harmonic or otherwise known as the J_2 perturbation. This term is on the order of one-thousandth that of the Newtonian point mass term and is the most dominant geopotential term after the point mass term. Further, Wiesel derives the J_2 disturbing function, R_2, and breaks it into periodic and secular terms. Ultimately, the J_2 secular effects result in the node of the orbital plane regressing and the precession of the orbit. No large effects are observed for the semi-major axis, the orbital eccentricity, or the orbital inclination.

2.4.4 Other Methods

General and special perturbations are two other classes of orbit propagation methods. General perturbations is an analytical method, and special perturbations is a numerical method. The most familiar type of general perturbations is that of SGP4, or simplified general perturbations, and is used with two-line element sets (TLEs) for predicting a satellite's orbital position at some time in the future. Special perturbations is a class that relies on specific initial conditions for each situation. However, the unique

nature of this method typically results in better orbit determination than general perturbations, but requires computation of each individual set of initial conditions.

2.5 Relative Satellite Motion

Relative satellite motion has been studied and analyzed since the beginning of the manned space program (12b). However, the studies and analysis have primarily focused on the applications of rendezvous, which includes spacecraft docking and conjunctions, and formation flying. In particular, the study of two spacecraft orbiting the Earth in close proximity to one another has been analytically understood for some time. Without showing the derivation, which is available in (23), the general three-dimensional form for relative satellite motion assuming only Keplerian motion is

$$\begin{aligned} \ddot{x} - 2\dot{f}\left(\dot{y} - y\frac{\dot{r}_c}{r_c}\right) - x\dot{f}^2 - \frac{\mu}{r_c^2} &= -\frac{\mu}{r_d^3}(r_c + x) \\ \ddot{y} + 2\dot{f}\left(\dot{x} - x\frac{\dot{r}_c}{r_c}\right) - y\dot{f}^2 &= -\frac{\mu}{r_d^3}y \\ \ddot{z} &= -\frac{\mu}{r_d^3}z \end{aligned} \tag{18}$$

where x, y, and z are the deputy satellite position components in the rotating chief Hill frame, r_c is the orbit radius of the chief satellite, and r_d is the orbit radius of the deputy satellite. Since these are second-order, coupled, nonlinear equations, the problem is difficult to solve analytically. The equations of motion can be simplified through the assumption that the relative orbit coordinates x, y, and z are small compared to the chief orbit radius, and that the orbit of the chief satellite is circular. If

$$r_d = \sqrt{(r_c + x)^2 + y^2 + z^2} \tag{19}$$

then

$$r_d \approx r_c \sqrt{1 + 2\frac{x}{r_c}} \tag{20}$$

The resulting equations are known as Hill's equations or the Clohessy-Wiltshire equations (33). Additionally, Wiesel derives the Clohessy-Wiltshire solution in two matrix/vector equations (35). The restriction of small relative orbital elements in Hill's or the Clohessy-Wiltshire equations provides a limited set of orbits for our study. Since the LEO RSO and Iridium satellite under consideration for analysis will, in general terms, be at vastly different altitudes and have large deviations in inclination and true anomaly, this type of analytical method is not sufficient for our study.

Another study of relative satellite motion examines the scenario where two satellites have nearly identical altitudes but lie in different orbital planes. Here, the relative motion depends only on the difference in the two inclinations and the two spacecraft longitudes (33). Spacecraft longitude is used in place of both the argument of perigee and mean anomaly for the case of circular orbits. In the case of circular orbits, the argument of perigee and mean anomaly do not behave well, but the sum of the argument of perigee and mean anomaly, or spacecraft longitude, does behave well. If the payload satellite has to be at the same altitude as the Iridium satellite, then this creates two problems. The first problem is that there are an infinite number of orbits that can be utilized that are not at the same altitude as the Iridium constellation. And the second problem is that since Iridium was originally designed to be used from terrestrial or near-terrestrial locations, the mission antenna arrays on the Iridium satellites do not point

sideways which means that communication only occurs at altitudes below the Iridium constellation. Therefore, this type of analytical method is not sufficient for our study.

More recently, some focus has turned to the large-scale relative satellite motion. Applications in this field of study include satellite-to-satellite communications and space-based observation of other space objects. The Newman-Omran model has been developed which includes the nonlinear terms that the Clohessy-Wiltshire equations exclude. The Newman-Omran model currently assumes Keplerian motion with the chief satellite in a circular orbit (25). Work is being done to acquire an analytical solution under J_2, but is not currently complete (15). Lovell provides a concise representation of the three-dimensional Newman-Omran model equation. Stringer provides the solution for the time dependent deputy positions and describes that the positions are nonlinear functions of the initial position and velocity. Since the equations take up a lot of space and are available in the references, they are not explicitly written out in this thesis. In the future, it may be possible to study the problem focused in this thesis with a Newman-Omran model that considers more than just Keplerian dynamics. However, since the Newman-Omran model is not currently complete for orbital perturbations, this analytical method is not sufficient for our study.

As a result of insufficient analytical methods to study the problem focused on LEO spacecraft communicating with the Iridium constellation, we turn our attention to numerical methods and more specifically a platform that performs satellite propagation using numerical integration and computation.

2.6 Relevant Efforts

2.6.1 Iridium Flight Modem

NASA's Kennedy Space Center and Wallops Flight Facility conducted a joint proof-of-concept project in 2003 with the objective to attach an Iridium modem to launch vehicles to provide real-time tracking, communications and control during launch events. The project investigated "the feasibility of using the Iridium satellite system for low-rate full duplex two-way communications" (24). In summary, the project conducted four aviation flight tests and zero orbital tests. The tests demonstrated reasonable success of passing GPS data through the Iridium network with latencies on the order of one second and horizontal position errors on the order of 150 meters for slow-moving aircraft (20).

In 2004, the joint project focused on the applicability of the Iridium Flight Modem for balloons and sounding rockets. The balloon flights indicated that the modems will function at -70 degrees Celsius with adequate insulation for about 100 minutes. The modem was integrated in two test flights on sounding rockets. The first test flight resulted in only 14 seconds of modem data transmitted out of an approximate flight time of 430 seconds. The second flight test resulted in modem data transmitted from liftoff to an apogee of 120 km at 161 seconds. After a brief disconnect, the modem reacquired signal and transmitted through ground impact plus an additional 25 minutes. The project concluded that "the Iridium Flight Modem is most appropriate for relatively slow-moving vehicles" (21).

2.6.2 US Naval Academy (18)

With the use of satellite communications becoming critical to overseas operations, the US Naval Academy partnered with a contractor to perform testing on two data

services, namely SBD and Short Message Service (SMS). The testing occurred since there is a lack of available open information regarding the performance details of the two message services. Experiments were designed to capture and quantify the performance of the message services; and of particular interest was the performance of the Iridium SBD service.

The experiments utilized an Iridium phone with the Iridium 9522 L-Band transceiver. The experiments transmitted messages between the mobile unit and an email address through the Iridium Gateway. At the time of testing, it was suggested that the SBD service was relatively new and not quite ready for production usage as several problems were encountered, including anomaly-emails being incorrectly generated to the device queue. The results indicate that the MO processing was more reliable and controllable than the MT processing. For the second set of testing, the researchers were permitted access to the SBD service for the military with enhanced performance. The modem processing times were longer for MT transmissions versus MO transmissions. And for MT transmissions, the modem processing times were a function of message size. In summary, the average processing time for completion ranged between 7.1 seconds and 22.2 seconds and was typically a function of both the MT and MO sizes. The researcher's discussion of the results states that the average time it takes to send one MO message is between 6 and 22 seconds. This time period is the modem processing time, which includes signaling channel negotiations from the modem to the satellite. The modem processing time is a function of message size. To measure full system latency requires the addition of another two to four seconds to account for the message travel time between the Gateway and email server.

Under good conditions, the average error rate for MO transmissions was about 3%. The MT process is not set up the same way as the MO process. The receiver must check for messages. If messages are not retrieved, and a source sends additional messages, then the messages build up in a large queue and actually increase end-to-end latency. While the size of the MT message did not impact the send process, the variation in size resulted in a range between 6 and 20 seconds for the receiver to retrieve the message. A recommendation by the tester was to wait for queue acknowledgement before sending the next message to avoid queue back-ups. Overall, the average time between sending a message and receiving an acknowledgement of receipt back was about 30 seconds. With the correct setup, there appeared to be no message errors. The Gateway can handle when the queue grows extremely well. The tester notes a significant observation that was also verified by Iridium. The tester stated that the message sequence number (MSN) attached to the MT transmission is different than the MSN received on the receiving side.

2.6.3 Using Satellite Communications with Ground-based Beacons (16)

In 2006, Maher examined the design of a beacon that could transmit GPS data through a LEO satellite communications network. The objective of the thesis was to design low power ground-based beacons for tracking applications that transmitted data through the satellite network. The effort included a brief comparative study of a variety of satellite networks, and ultimately the thesis focused on using Globalstar due to the ease of obtaining a compatible device.

2.6.4 Nanosatellite Communications in LEO

In 2008, Khan studied data communication with a nanosatellite using the Globalstar Network for his thesis at the University of Central Florida. Khan first compared the International Maritime Satellite Network, Thuraya Satellite Network, Iridium Satellite Network, and Globalstar Satellite Network. Then it was concluded that the Globalstar system would provide more coverage than the Iridium system, and ultimately the Globalstar system was chosen for simulation and analysis (13).

NASA's Florida Space Grant Consortium funded researchers at Florida International University in 2009 to investigate using the Iridium network for nanosatellite communications. The investigation considered Iridium 9522A and 9601 transceivers. Simulations indicate that for a nanosatellite at an altitude of 700 km, the Doppler shift between the nanosatellite and an Iridium satellite is 270 Hz if the two satellites are moving in the same direction and -81.087 kHz if the two satellites are moving in opposite directions (2).

2.6.5 AFIT Efforts (1)

In 2011, as part of the Astronautical Engineering Space Design Vehicle specialty sequence, a team of AFIT students studied the concept and designed a CubeSat for reducing the dependence on a dedicated ground station by passing information through the Iridium network. By using the Iridium network, any computing device with internet access could become a ground station for communicating with the CubeSat, thereby reducing the time between ground station passes from hours to essentially zero. The mission objectives were to communicate basic telemetry, tracking and control (TT&C) information, as well as unique on-orbit events. An electromagnetic energy detector was included in the design as a secondary payload to experiment with the notification of and response to an energy detection event.

The team's modeling studies yielded that a satellite at an altitude of 300 kilometers with 65 degrees inclination had an Iridium-access time about 34.5% of the analysis period. At an altitude of 700 kilometers and 65 degrees inclination, the satellite had an Iridium-access time about 0.9% of the analysis period. The model results also yielded that the best case average duration of access to Iridium for the case of an orbit at an altitude of 300 kilometers with 0 degrees inclination was 155 seconds.

The team performed a link margin analysis between the payload and an Iridium satellite. To summarize, a crosslink distance range of 81-6321 kilometers was considered. The payload patch antenna had a gain of 2 dBi with the Iridium antenna gain estimated to be 2 dBi. The transceiver data rates ranged 9-1000 bps. This resulted in a nominal transmit power requirement of 10 milli-Watts.

The effort also considered the Doppler Shift effects on communications. The team found that with the case of using the center Iridium frequency of 1620 MHz and a maximum range rate between the designed CubeSat and an Iridium satellite of 13 km/s, the resulting Doppler Shift is 70.2 kHz. Since this implied that only 1.56% of the available bandwidth was not usable, the team determined that the frequency shift due to the high range rates was not a limiting factor of the system.

2.6.6 Re-entry Break-up Recorder

The Aerospace Corporation performed an experiment attempting to pass information from a re-entering object through the Iridium network using the Iridium 9601 transceiver. There have been multiple attempts at using a Re-entry Break-Up Recorder (REBR) to collect and transmit re-entry data. "REBR is a small autonomous device that is designed to record temperature, acceleration, rotation rate, and other data as a spacecraft reenters the Earth's atmosphere" (3). While communication was not intended for orbit, the effort focused on collecting re-entry data and GPS data and transmitting the information through commercial communications satellites to the appropriate ground station. To date, both successes and failures have been encountered. Overall, the communication objective has been to transmit data between the transceiver and Iridium satellites during re-entry (12, 14, and 28).

III. Methodology

3.1 Chapter Overview

This chapter discusses the methodology used in analyzing the prospective orbits that can regularly link to the Iridium network.

3.2 Modeling the Iridium Constellation in Systems Tool Kit

The platform chosen for modeling and simulation of the Iridium constellation is Systems Tool Kit (STK), version 10.0. In reality, each Iridium satellite is referenced against a control box in which it drifts around a center over time. As the satellite drifts from the center of the control box and approaches the "edge," maneuvers are performed to reduce the satellite's offset from the center. The specific size of the control box (technically an ellipsoid) is proprietary, but it can be said that the individual radial, in-track, and cross-track dimensions are on the order kilometers. For near-real simulations, either special or general perturbations methods are necessary to propagate the satellites, but it is assumed that the box centers are propagated using the J_2 perturbation. Additionally, the correction maneuvers require an update to the initial states for perturbations, and thus complicate long-term position predictions for the individual satellites. Therefore, the control box centers are modeled as the individual Iridium satellites, and subsequently the satellites are propagated using the J_2 perturbation for a period of three days to minimize large deviations between propagation methods.

3.2.1 Setting Up the Satellites

The parameters and values for the Iridium Network satellite constellation previously discussed throughout Chapter Two are modeled in STK. For convenience,

Table 6 lists the parameters for the model of the Iridium Network satellite constellation. The individual orbital element sets are located in Appendix 1.

Table 6. Iridium Constellation Model Setup

Iridium Network Satellite Constellation	Model Parameter Value
Number of satellites	66
Semi-major Axis	7151 km
Orbital Eccentricity	0
Orbital Inclination	86.4 degrees
Planar Separation	31.6 degrees
Satellite Separation	32.727 degrees
Inter-plane Satellite Offset	15.8 degrees

.

3.2.2 Iridium Satellite Orbit Propagator

After constructing the model, we must select an appropriate propagation method to accurately estimate the number and duration of communication-access windows. The 66 Iridium satellites are propagated in STK using the J_2 perturbation. The J_2 perturbation is sufficient for the general purposes of modeling and statistically quantifying the communications-access opportunities and durations.

3.2.3 Modeling the Iridium Satellite Footprint and Individual Spot Beams

As stated earlier, the Iridium satellite footprint comprises 48 individual spot beams. The primary assumptions for modeling the Iridium spot beams are to assume a simple conic distribution for each spot beam and that each spot beam has the same simple

conic half-angle. These assumptions are not bad when considering the overall footprint of the spot beams in the proprietary diagrams. Due to the nature and complexity of the CubeSat-to-Iridium communications link problem, it was determined that precise effects are difficult to quantify because of the environment and lack of legacy projects (30). Therefore, sensor objects defined in STK are used to represent the individual mission antenna array cells. Sensor objects do not require specific communications details like that of the transmitter, antenna, and receiver objects in STK. Manual constraints can be imposed on the model configuration as appropriate to adequately represent limitations due to physics or other practical engineering capabilities. Therefore by just using sensor objects in STK to model the individual antenna cells, simpler access computations can be performed that yield access opportunities and durations. To calculate the whole Iridium footprint and individual spot beam footprints, we start with Figure 11.

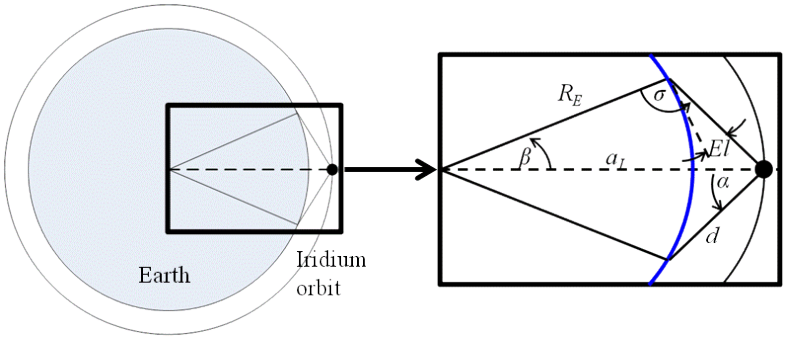

Figure 11. Iridium Satellite Ground Coverage Geometry

From Figure 11, the parameters to consider are:

a_I is the semi-major axis for the satellite;

d is the distance from the satellite to the edge of the FOV;

El is the elevation angle of the ground user to the satellite;

R_E is the radius of the Earth;

α is the satellite slant angle to the ground;

β is the Earth-central angle between the satellite semi-major axis and the edge of the FOV

σ is the angle between the Earth's radial vector to the ground user and elevation line to the satellite;

The physical difference between the whole Iridium footprint and an individual spot beam footprint is the size of the slant angle, which will subsequently impact the value of the Earth-central angle, the value of the ground elevation angle, or possibly both values.

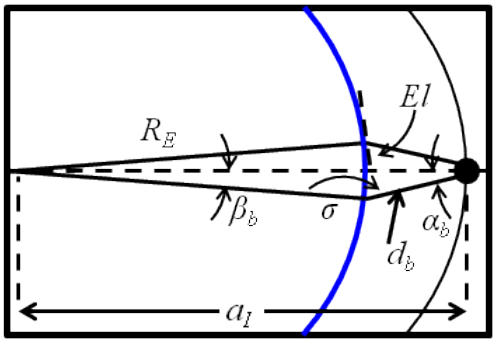

Figure 12. Iridium Satellite Spot Beam Coverage Geometry

From Figure 12, the spot beam parameters different from Figure 11 are:

d_b is the distance from the satellite to the edge of the spot beam FOV;

α_b is the satellite slant angle to the ground;

β_b is the Earth-central angle between the satellite semi-major axis and the edge of the FOV

The larger slant angle is used to consider the entire Iridium footprint on the ground, while the smaller slant angle is used to consider one individual spot beam. Thus, the same process will be used to find both slant angles, noting that the more useful slant angle to know is for the spot beam. From the Iridium datasheets mentioned in the section 2.3.3, the Iridium ground footprint diameters for full view and individual spot beam are 2800 miles and 250 miles, respectively. Or, the diameters can be approximated to 4500 km and 400 km, respectively. Assuming a mean Earth radius R_E of 6371 km, the Earth-central angles β and β_b can be found from trigonometry using the footprint diameters as the arc lengths s and s_b.

$$\begin{aligned} s &= R_E(2\beta) \\ s_b &= R_E(2\beta_b) \end{aligned} \tag{21}$$

Using Equation 21 we compute Earth-central angles for the full Iridium footprint and individual spot beam footprint of 20.23 degrees and 1.80 degrees, respectively. Using the Law of Cosines, the distance to the edge of the footprints can be calculated from

$$\begin{aligned} d &= \sqrt{{R_E}^2 + {a_I}^2 - 2R_E a_I cos(\beta)} \\ d_b &= \sqrt{{R_E}^2 + {a_I}^2 - 2R_E a_I cos(\beta_b)} \end{aligned} \tag{22}$$

With Equation 22 we compute distances to the edge of the full coverage footprint and individual spot beam footprint of 2493 km and 808 km, respectively. Rearranging the Law of Cosines, the satellite and individual spot beam slant angles can be calculated from

$$\alpha = arccos\left(\frac{{R_E}^2 - {a_I}^2 - d^2}{-2a_I d}\right)$$
$$\alpha_b = arccos\left(\frac{{R_E}^2 - {a_I}^2 - {d_b}^2}{-2a_I d_b}\right) \quad (23)$$

Using Equation 23 we compute a satellite slant angle of 62 degrees and an individual spot beam slant angle of 14 degrees. Therefore, the Iridium satellite mission antenna array spot beams are modeled in STK as sensor objects with simple conic distributions with a half-angle of 14 degrees.

The more difficult challenge is to sufficiently model the distribution configuration for the 48 spot beams. A published spot beam layout can be found in (17), but more attention was paid to other schematics that are not openly available. In this sense, more emphasis was placed on attempting to represent the spot beam footprints on the ground. Figure 13 shows the final layout implemented into STK for each Iridium satellite. As described in section 2.3.3, the 48 spot beams are distributed amongst four generic groups based on the elevation angle. The details regarding the specific elevation and azimuth angles for the spot beam distribution are located in Appendix 2. For reference, an elevation angle of 90° is directed nadir from the satellite, and an azimuth angle of 0° is considered in-track with the satellite's orbital motion.

A link margin analysis was also performed, but not all necessary information was available. Therefore, some information was approximated according to (33) and reverse engineered based on (30). Ultimately, a range constraint of 2500 km was applied to the sensors, but this constraint only impacted group four.

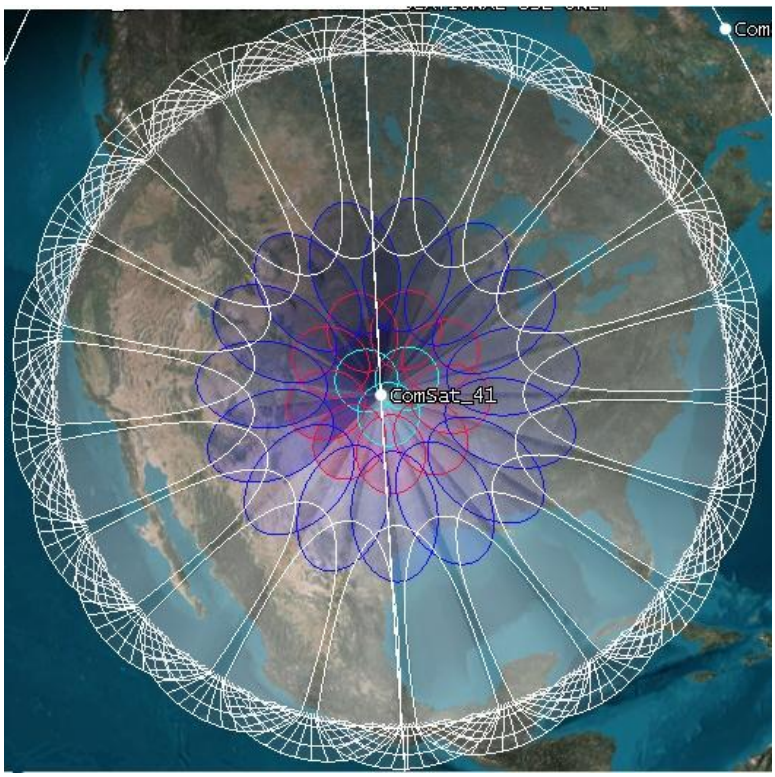

Figure 13. Model of Iridium Satellite Spot Beams

3.3 The TestSat

The TestSat represents an arbitrary resident space object. Attached to the TestSat is a sensor object that represents an Iridium transceiver modem with antenna. The TestSat will be confined to the LEO regime, but various orbital configurations within the LEO regime can be analyzed for access to the Iridium network. Additional details on the selected orbital configurations are discussed in the section below titled Implementation of Design of Experiments using Design Expert.

3.3.1 TestSat Sensor Object

The physical construct of a specific Iridium transceiver does not impact the analysis. However, the performance of the transceiver and the beam pattern and direction

of the antenna are critical parameters to be implemented into the model. Similar to the Iridium satellite spot beams, the transceiver can be represented by a simple sensor object in STK with the necessary constraints and characteristics. An AntCom Dual Iridium/GPS antenna as shown in Figure 14 has been considered for our satellite to be flown in space.

Figure 14. AntCom Dual Iridium/GPS Antenna

The Iridium antenna has a half-power beam width (HPBW) of about 100°. In STK, a HPBW angle of 100° translates into a simple conic angle of 50° for the sensor object. The sensor FOV is fixed and directed zenith from the center of the TestSat. The Iridium 9602 Transceiver modem has been considered for the satellite to be flown in space. Currently, the modem has a Doppler shift limit of ±37.5 kHz for a communications link between itself and an Iridium satellite. In STK, a Doppler shift limit of ±37.5 kHz translates into a range rate of about ±7.0 km/s. Additionally, there is a plan in place to make a modification to the modem to allow for double the current Doppler shift due to the potential for much larger Doppler shifts on orbit. Thus, both a range rate constraint of ±7.0 km/s and ±14.0 km/s are considered. Based on the latency measurements from (17) and discussions with (30), minimum communications duration to count as an access

within the STK simulations shall be 10 seconds. Finally, the sensor object will be constrained for access to only latitudes between -80° and 80°. In reality, Iridium turns off various satellites as they near the poles. The satellites are turned off in such a way so that one satellite remains on in order to maintain full global coverage. Without knowing the exact Iridium process, this cannot be accounted for in STK. Therefore, rather than have an overstated number of accesses, the modem has the zonal constraint of -80° to 80° in latitude.

3.4 Implementation of Design of Experiments using Design Expert

The complete STK model consists of 66 satellites, each with 48 sensors, plus the TestSat with modem sensor for a total of 3,236 objects within the STK scenario. Recall that results from numeric propagation methods are only accurate for the specific set of initial conditions selected for the computation. Therefore, we must individually simulate each scenario for a given set of initial conditions. Despite the scenario analysis time of only three days, each update of the TestSat orbital elements, and subsequent access computations, requires approximately five minutes, not including the time required to create and save the access and event reports. This is the major drawback to using a platform such as STK in contrast to performing the numerical computations with custom software code. Generally speaking, however, the required time of five minutes is not a significant issue until considering the number of factors and potential levels of factors involved. If, as one example, a completely full factorial analysis was performed on a test matrix that factored in the six orbital elements all with six levels of consideration, the maximum range rate constraint with two levels of consideration, and the half-power

beam width HPBW of the TestSat modem-antenna with two levels of consideration, then this would require 186,624 simulations. Even if, as another example, the eccentricity is kept at zero and subsequently is removed along with the argument of perigee from consideration, this still requires 5,184 simulations. Further, we could only consider the intended communications antenna to be used and thus remove the HPBW factor from consideration which still leaves us with 2,592 simulations. Equivalently, we can say the data collection time period is approximately 216 hours. Therefore, the goal is to reduce the data collection time without compromising the integrity of the data, results, and conclusions by implementing the technique of Design of Experiments.

3.4.1 Design of Experiments concept

In the test and evaluation (T&E) community, Design of Experiments (DOE) can be implemented when testing resources are limited. Often, the number of test points is restricted due to cost. The reduction of test points can introduce uncertainty into conclusions and reduce confidence in inferred relationships or interactions between factors that may or may not exist in the results. Montgomery states that results and conclusions are dependent upon the process of data collection (19). The full field and study of Design of Experiments is beyond the scope of this thesis, but Montgomery is a quality reference for the concepts of experimental design, particularly statistical experiments and the analysis of experimental data. Selected concepts implemented in this thesis are discussed below because they are critically important to the assessment of the quality and validity of the results and conclusions.

3.4.2 Analysis of Variance

The underlying null hypothesis of our experiment is that the means, or averages, of our responses are equal. Therefore, by varying a factor or factors we can assess the effect of the factor or factors. Analysis of Variance (ANOVA) is a data analysis process for evaluating the equality of the response means. The single-factor ANOVA model is governed by

$$y_{ij} = \mu + \tau_i + \epsilon_{ij} \begin{cases} i = 1, 2, \dots, a \\ j = 1, 2, \dots, a \end{cases} \tag{24}$$

where y_{ij} is the response, μ is the overall mean, τ_i is the ith factor effect, and ϵ_{ij} is random error.

Next, there are two subset models within the ANOVA model based on what specifically is being tested: fixed effects and random effects. The fixed effects model focuses on the factor means and our conclusions will apply only to those factor levels under consideration. The fixed effects model is best-suited for categoric factors that, by definition, have specific set levels. Categoric factors do not have an inference space between levels. The random effects model focuses on the variability of the factors, and it aims to make conclusions about the entire factor population, regardless of their consideration in or exclusion from the experiment. The random effects model is best-suited for numeric factors, particularly continuous numeric factors. Numeric factors have an inference space between levels, and consequently predictions can be statistically meaningful, dependent on the data fit of the random effects model. Before moving forward into understanding the critical details of ANOVA, it is pertinent to emphasize an important and defining difference between categoric and numeric factors. As we

consider higher order model fits, categoric factors cannot interact with themselves while numeric factors can have self-interaction terms. To say this in a more familiar way, a model fit with only categoric factors does not consider power terms such as A^2, B^3, C^4D^5, etc. The only appropriate higher order terms for models with only categoric factors are interaction terms such as AB, AC, BD, etc. Models with numeric factors can have any combination of interaction terms up to the appropriate order of the polynomial fit.

Montgomery derives the fundamental ANOVA identity, shown in Equation 25. The identity relates the total variability in the data to differences between factor averages and the overall mean plus differences of individual points within factors from the factor average.

$$SS_T = \sum_{i=1}^{a}\sum_{j=1}^{n}\left(y_{ij} - \bar{y}_{..}\right)^2 = n\sum_{i=1}^{a}((\bar{y}_{i.} - \bar{y}_{..})^2) + \sum_{i=1}^{a}\sum_{j=1}^{n}\left(y_{ij} - \bar{y}_{i.}\right)^2 \tag{25}$$

A different way to consider Equation 25 is

$$SS_T = SS_{Factors} + SS_E \tag{26}$$

where SS refers to the quantity of sum of squares and the subscripts *T*, *Factors*, and *E* refer to the total, factors, and random error, respectively. After computing the sum of squares, the mean squares for factors and random error are calculated from

$$\begin{aligned} MS_{Factors} &= \frac{SS_{Factors}}{a-1} \\ MS_E &= \frac{SS_E}{a(n-1)} \end{aligned} \tag{27}$$

where MS is mean squares and $a-1$ and $a(n-1)$ are the degrees of freedom for a factor and the random error, respectively. Then upon applying Cochran's Theorem we

calculate the F-value, or the test statistic for the hypothesis of zero differences between factor means, from (19)

$$F_0 = \frac{MS_{Factors}}{MS_E} \tag{28}$$

Finally, the F-value for the factor can be used to assess the significance of the factor to the model fit. It is also common, and usually more direct, to use the associated p-value based on the F-table found in most statistics textbooks.

Fortunately, Design Expert 8.0 performs the ANOVA and allows for manual removal of the insignificant factors. With the case of multiple factors, we must also consider the interactions among factors. However, within the process to include or remove model terms, the interaction terms are still treated with the process of mean squares testing described above.

3.4.3 Understanding the Quality of the Data

Montgomery provides detailed sections on assessing the quality of the data from the experiment. Only a brief overview is included below in order to understand the nature of some of the material presented in Chapter Four. Design Expert 8.0 incorporates the tools described below.

First, a good assessment uses a normal probability plot. With Design Expert, the residuals are plotted. The premise here is that if the underlying error within the data has a normal distribution, then the plot will resemble a straight line. Generally speaking, deviations from this straight line have little meaning for fixed effects models, but have great importance for random effects models. However, scatter is typically expected, and

judgment must be used in determining the amplitude and impact of any deviations. One example is that with even good model fits, there will be noticeable scatter at the tails.

Second, a good assessment utilizes a plot of the residuals versus the predicted fit values. Under the premise that the ANOVA model is correct, then the plot of residuals should be structure-less or have no identifiable pattern. Specifically, we want the plot to show that the experiment has approximately constant variance. Of particular concern is variance growth, which can be characterized by a megaphone structure. If there are equal sample sizes in all factors, then variance non-homogeneity only slightly affects the F-test for the fixed effects model, but can drastically impact the F-test for the random effects model. For situations with variance non-homogeneity, a common practice is to perform a transformation. This alters the ANOVA model into a model that applies to the transformed populations based on the transformed data points.

3.4.4 Experimental Designs

In general terms, factorial designs are the most efficient for experiments with two or more factors. In this type of experimental design, we test all possible combinations of factor levels. The efficiency is derived from comparing the number of required runs between two designs. The standard for comparison is the one-factor-at-a-time design. In the case of a two-factor two-level experiment (A^+,A^-,B^+,B^-), a one-factor-at-a-time design would require a minimum of six observations (two observations at each factor level changing only one factor at a time will equate to: A^+B^-, A^-B^-, A^-B^+, A^+B^-, A^-B^-, A^-B^+). With a factorial design, a data point is collected at the A^+B^+ test point. This now technically qualifies as making two observations at each level. In this case, only four total observations are necessary (A^+B^-, A^-B^-, A^-B^+, A^+B^+), thus reducing the number of

required observations. Further, if an interaction exists between the two factors, then the conclusion about the response at the A^+B^+ test point is in serious question under the one-factor-at-a-time design. With the factorial design, data is actually collected at the A^+B^+ test point, and this allows a more confident conclusion. Or in other words, we obtain meaningful mean squares results on A, B and AB (here, the factors are considered to be categorical). For consideration of four orbital elements at six levels and the maximum range rate constraint at two levels, this will equate to 6^4 test points two times, or a total of 2,592 points. However, with some engineering judgment and the proper experimental design, we can significantly reduce the total number of test points without compromising the integrity of the data.

As implied earlier, this study has more complexity given the number of factors and levels within each factor. First, the orbital elements are not categorical factors. They are continuous numeric factors, and if we attempt to represent them as categorical in nature, thereby attempting to apply a fixed effects model, then we lose prediction integrity between the factor levels across all the factors. This is the statistical consequence that the values between our factor levels are not part of the inference space. Thus, we must use the random effects model so that we can randomly assign factor levels for our numeric factors in such a way that allows us to draw conclusions that can be expanded to a larger population of values for the factor. Fundamentally, the ANOVA identity and process remains identical to that of the fixed effects model, but now we are testing hypotheses about the variance components. Also, treating the factors as numeric dictates that we are no longer utilizing a factorial design, but instead we want to use a response surface method design which requires more data points for meaningful results.

The previous sentence is a powerful general statement where the justification is beyond the scope of this thesis. However, we can return to the two-factor-two-level experiment discussed in the previous paragraph to say that if A and B are now continuous numeric factors, then the factorial experimental design of only four test points is not sufficient for model fits greater than first order. Without collecting data along the edges or at the center of the design space, we have little to no statistical confidence in the model for the inference space. Nothing fundamentally changes within the experimental design process, but now the entire population within the design space bounds is under consideration. We can then, in the case of a two-factor study, formulate a response surface that traditionally is used for optimization but can also be formulated for prediction accuracy.

Finally, ignoring for a moment, again, that the orbital elements and range rate constraints are real numbers, there would be 31 total model terms for a full fifth order model {A,B,C,D,E,AB,AC,…,ABCDE}. However, a higher order model, and subsequently more model terms, is not necessarily better. Having more model terms requires more management effort and diligence to maintain prediction integrity, but most importantly higher order models require more data points for statistically meaningful results. But when we return to consider the orbital elements and range rate constraint to be real numeric values, this opens the door to the power terms and the power terms with interactions $\{A^2,\ldots, A^2B,\ldots, A^2BC,\ldots, A^2B^2,\ldots, A^3B,\ldots, E^5\}$. Fortunately, with ANOVA we can remove terms with insignificant mean squares. Thus, the true utility of ANOVA is to be able to ultimately determine the best polynomial model order and terms to fit the data. However, ANOVA only determines the order of the model as precisely as the available data permits. If higher order model fits are expected or desired, then more

data points must be tested within the design space, including the replication of select data points. If the test matrix is optimally designed for obtaining a quadratic model, then, for example, a fifth-order model would be extremely suspect even though the ANOVA process can produce it. Ideally, the simpler the model, the easier it is to comprehend the effects among factors and factor levels within the results.

3.4.5 Selection of Experimental Design and Process

After everything considered in the previous section, the selection and selection method of the experimental design space are critical to the quality of results and validity of conclusions if we are not to collect the complete factorial matrix. Practical constraints and limited resources restrict our ability to collect the infinite number of observations required for a complete and perfect model fit when experimenting with continuous numeric factors.

Therefore, this study will use a response surface method for designing the test matrix. It is not required but intuitive to limit the number of numeric factors to two since we are considering a response surface. However, for each combination set of categoric factors we will have a response surface for the two numeric factors. As stated, the complexity of this study does not allow any kind of simplistic reduction in the number of factors, but there are engineering judgments and initial assessments that can provide opportunity for some factor reduction and perhaps reduce the consideration of our experiment to no more than two numeric factors and some number of categoric factors. Recall, that responses to categoric factors only have meaningful statistics at the prescribed categoric factor levels. Therefore, to transform a numeric factor into a

categoric factor, we need to be able to justify the generalization of the factor as well as the loss of the inference space.

First, we shall use our engineering judgment to construct some initial assessments that will provide us the insight into constructing our primary experimental test matrix. We can start by suggesting that over an analysis period of three days the orbital elements semi-major axis, eccentricity, inclination, and right ascension of the ascending node (RAAN) will be important factors in the study of a LEO spacecraft having access to the Iridium Network satellite constellation. Further, we can suggest that the orbital elements argument of perigee and true anomaly will have little or no importance in the problem. From a statistical perspective, we will have problems with direct mathematical relationships between the orbital elements.

3.4.6 Problem of Using Semi-major Axis and Eccentricity Elements

The eccentricity of an ellipse can have any numeric value between zero and one for any given semi-major axis. However, this statement is only true for general mathematics. In the problem of orbital mechanics, the radius of the Earth provides a constraint for the smallest distance between the ellipse focus and edge. Given a particular value for the semi-major axis of a satellite in orbit, the eccentricity has a real maximum value before perigee intersects the surface of the Earth. Mathematically, there is nothing that prevents performing the ANOVA process with a variety or semi-major axis values and eccentricity values. However, no eccentricity values above the maximum value can be simulated in STK. Equation 29 provides the realistic maximum eccentricity for a given semi-major axis value.

$$e = \frac{a - R_E}{a} \tag{29}$$

Table 7 shows an example of the experimental constraint involving only the eccentricity and semi-major axis values.

Table 7. Maximum eccentricity values within experimental space

Semi-major Axis (km)	Maximum Eccentricity
6528	0.0230
6678	0.0449
6828	0.0659
6978	0.0860
7128	0.1052

As the experiment considers larger semi-major axis values the possible range of eccentricity values also increase, but the larger eccentricities cannot be considered for the smaller semi-major axis values. The consequence is multicollinearity between the semi-major axis and eccentricity factors. During the experimental design matrix evaluation, the problem of multicollinearity is indicated by large variance inflation factors (VIFs). Another way to describe the problem is to say that there is a large standard error of design for the experimental matrix since "the standard error of a model coefficient increases in proportion to the square root of the VIF" (5). Ideally, we want VIFs of 1.0. VIFs above 10 indicate strong multicollinearity. It should be noted in full disclosure that VIF values are not only dependent on the selection of the test points but also on the number of test points and the predicted polynomial model fit. For a meaningful

comparison, an arbitrary response variable is predicted to have a quadratic polynomial model fit given two factors. Term A represents the semi-major axis factor, and term B represents the eccentricity factor. Both terms A and B are considered to be continuous numeric factors.

Table 8. Quadratic Design Matrix Evaluation for Semi-major Axis and Eccentricity

	Inclusion of All Eccentricity Values		**Only Permitted Eccentricity Values**	
Term	*Std Error*	*VIF*	*Std Error*	*VIF*
A	0.37	1.00	1.34	10.42
B	0.37	1.00	1.34	10.42
AB	0.49	1.00	1.51	9.33
A^2	0.60	1.10	0.93	2.25
B^2	0.60	1.10	0.93	2.25

The left portion of Table 8 is meaningless in reality since there are data points that cannot be simulated due to unrealistic eccentricity values. The right portion of Table 8 indicates a poor experimental design. Before data is entered into the test matrix there is an assumed standard deviation of 1.0 for the experimental design, and therefore standard errors of design near or greater than 1.0 are a first indication of poor experimental design. Second, with VIFs near and larger than 10.0 there is a strong possibility of multicollinearity being present in the experimental design. When multicollinearity is present, the design evaluation and model fit statistics are rendered useless.

Since we want to at least acquire an understanding of the effects due to the altitude of our TestSat, we shall impose that the eccentricity is zero, thereby removing it from consideration as a factor in the study. This subsequently eliminates the argument of perigee as a factor since it is undefined for an eccentricity of zero.

3.4.7 Angular Orbital Elements

Next, we shall consider the angular orbital elements and verify or reject our suggestion that the inclination and right ascension of the ascending node are important and the initial true anomaly value is unimportant over a period of three days. As an initial assessment, we can set up a general factorial experiment with the angular elements considered categoric factors. Again, we lose confidence in predicting the response at factor levels not considered, but here the purpose is not of prediction but assessing factor significance in the response. We consider the inclination at levels of 0 degrees, 45 degrees, and 90 degrees. We consider the RAAN at 0 degrees, 90 degrees, 180 degrees, and 270 degrees. And we consider the initial true anomaly at 0 degrees, 120 degrees, and 240 degrees. We can perform a full factorial assessment which equates to 36 simulations. Since we want to perform a full factorial assessment and we are not interested in accurate response data, we can save time by using a modified Iridium Network satellite constellation model in STK. The modified model has only a single spot beam under each Iridium satellite that represents the full field-of-view (FOV) based on our calculations in section 3.2.3. This reduces the computation time for each simulation to a few seconds, while providing sufficient insight to assess the significance of the angular factors in modeling the response variable. Figure 15 shows the modified STK model that only utilizes the full satellite FOV versus individual spot beams.

The semi-major axis is held constant at 6771 km, and eccentricity is zero. At orbital altitudes, the Iridium satellite FOV is drastically reduced. Figure 16 depicts the coverage of an altitude of approximately 400 km. The response variable chosen for this initial assessment is the total access time to the constellation.

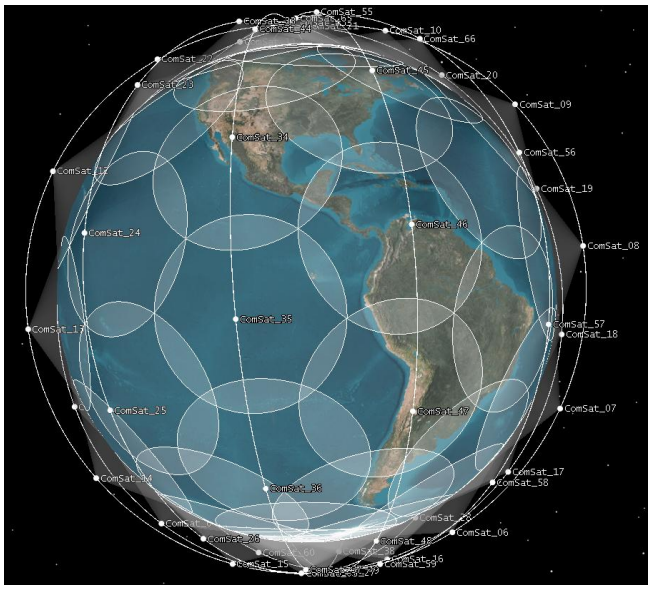

Figure 15. Iridium Constellation Model in STK with Single FOV Spot Beams

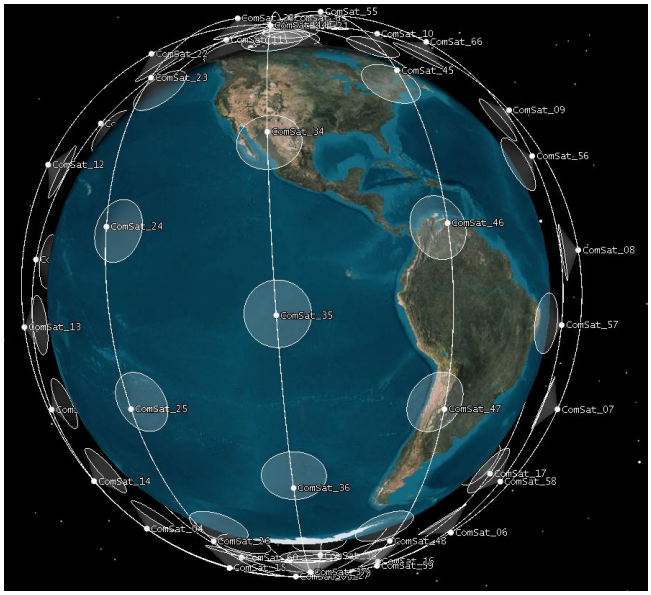

Figure 16. Iridium Constellation Coverage for 400-km-Spacecraft Altitude Orbit

The complete results of the 36 simulations are available in Appendix 4. Note that factor A represents the inclination, factor B represents the RAAN, and factor C represents the initial true anomaly. Table 9 shows the complete ANOVA results.

Table 9. Complete ANOVA Results for Inclination, RAAN, and True Anomaly

Source	Sum of Squares (SS)	Degrees of Freedom (df)	Mean Square
Model	1.955E9	35	5.586E7
A	*1.187E9*	*2*	*5.936E8*
B	*2.824E8*	*3*	*9.412E7*
C	*1.815E4*	*2*	*9.073E3*
AB	*4.842E8*	*6*	*8.070E7*
AC	*3.416E5*	*4*	*8.541E4*
BC	*3.029E5*	*6*	*5.048E4*
ABC	*6.707E5*	*12*	*5.589E4*
Pure Error	0.000	0	

It is seen that the mean squares values for factor C and the interaction terms AC, BC and ABC are of considerably smaller order than the factors A and B and the interaction term AB. Therefore the results confirm that the initial true anomaly value is not an important factor. As a main effect, the initial true anomaly has the smallest mean squares value by four orders of magnitude compared to the other two main effects. The interaction terms with the initial true anomaly have the smallest mean squares values by three orders of

magnitude compared to the other interaction term. Table 10 shows the ANOVA results of the reduced model fit where the initial true anomaly factor has been removed from consideration.

Table 10. Reduced ANOVA Results for Inclination and RAAN

Source	Sum of Squares (SS)	Degrees of Freedom (df)	Mean Squares	F-value	P-value
Model	1.955E9	11	1.776E8	3197.04	< 0.0001
A	*1.187E9*	*2*	*5.936E8*	*10685.59*	*< 0.0001*
B	*2.824E8*	*3*	*9.412E7*	*1694.16*	*< 0.0001*
AB	*4.842E8*	*6*	*8.070E7*	*1452.63*	*< 0.0001*
Residual	1.333E6	24	5.556E5		
				R^2	0.9993
				Adj R^2	0.9990
				Pred R^2	0.9985
				Ad. Prec.	183.416

Once the model has been reduced by any number of terms, the ANOVA process yields F-values, corresponding p-values and the correlation fit coefficients R^2, adjusted-R^2, and predicted-R^2. As described above, the F-value is the ratio of the term mean squares value to the residual mean squares value. The p-value, or probability value, is the

proportion of the area under the F-distribution curve beyond the calculated F-value. The ANOVA results indicate that terms A, B, and AB all have a probability of 0.01% that they are attributed to only noise in the experiment. In other words, terms A, B, and AB are all significant to the model. The model is a perfect fit if R^2 has a value of one. When R^2 is less than one, the adjusted-R^2 and predicted-R^2 values provide additional insight into the quality of the model fit. From a conceptual level, if the adjusted-R^2 and predicted-R^2 values are not within 0.20 of one another, then there is likely a problem with either the data or the model. Therefore with everything considered, a model fit using the terms A, B, and AB best represents the data from the full factorial experiment involving the inclination, RAAN, and the initial value of the true anomaly. Figure 17 provides a graphical representation of the ANOVA results by plotting the normal effects of each term, which show that only terms A, B, and AB are important in the model fit. The line in Figure 17 should fit the most number of terms possible. Each term that fits the line has an insignificant effect on the model. The terms that do not fit the line are significant to the model, and more specifically that effect is quantified. The terms that fit the line, which are not labeled, include C, AC, BC, and ABC.

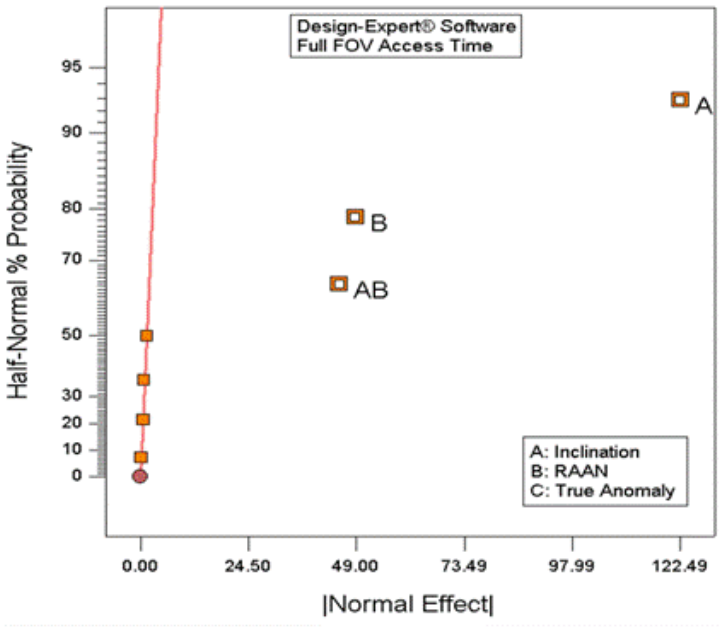

Figure 17. Normal Effects Plot of Inclination, RAAN, and True Anomaly

There is further intrigue with the selected model F-values despite the fact that all the F-values and corresponding p-values indicate model significance. The F-value of term A is about a full order of magnitude larger than terms B and AB. This is also seen in the normal effects plot that shows terms B and AB have less than half the effect of term A. Figure 18 shows the interaction between terms A and B in the experiment.

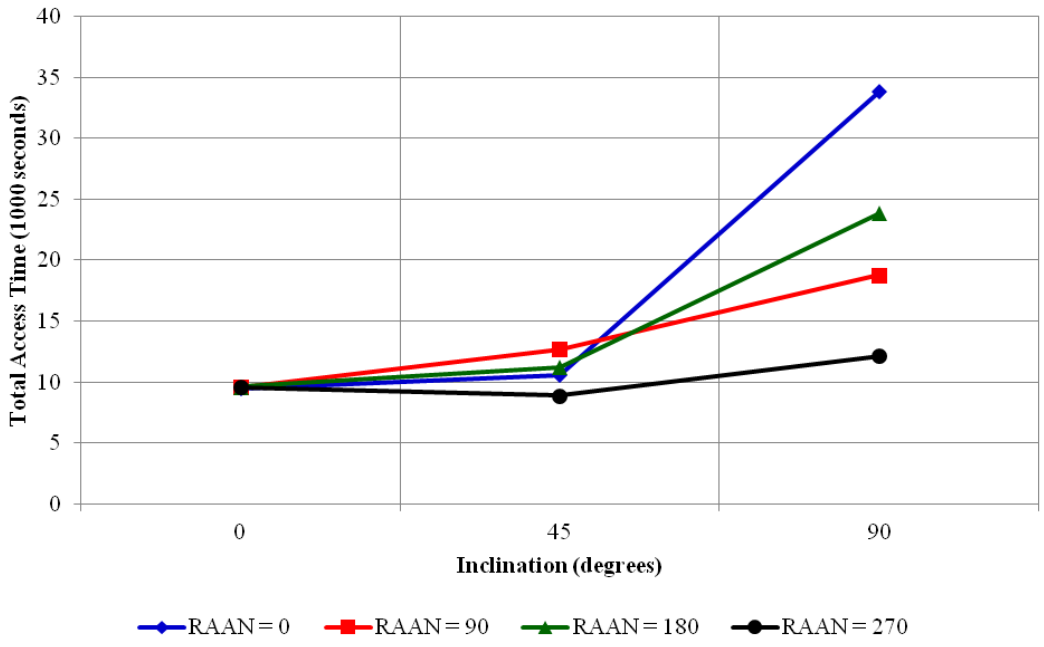

Figure 18. Spacecraft Factor Interaction Plot for Access to Iridium Satellite

Firm conclusions cannot be formulated from Figure 18, but it does provide hints to the necessity of a follow-up experiment involving only spacecraft inclination and RAAN. Recall that in our preliminary assessment both inclination and RAAN are treated as categoric factors. Therefore we have discrete levels indicated for inclination of 0, 45, and 90 degrees, and we have separate RAAN profiles of 0, 90, 180, and 270 degrees. We cannot make any inferences about the space between the discrete levels and therefore normally it would be improper to connect discrete data. However, here we connect the data not to infer trends within the inference space, but to assess interactions between our two categoric factors. When the profiles intersect, as they do above, there is some form of combination(s) of the two factors that interact to yield different trends in the response parameter. There is essentially no spread in the total access time at an inclination of 0 degrees and little spread at an inclination of 45 degrees, but there is a large spread at an

inclination of 90 degrees. Further the slopes of the RAAN profiles between inclinations of 45 degrees and 90 degrees are not parallel, which is another indication of strong interaction at an inclination of 90 degrees. We can also observe that at an inclination of 90 degrees, the total access time response is ordered from highest to lowest by RAAN values of 0, 180, 90, and 270 degrees. Comparing this to the model of the Iridium satellite constellation configuration, we observe a loose pattern to this order. At RAAN values of 0 and 180 degrees, the TestSat spends the majority of its orbit directly underneath an Iridium satellite orbit. At RAAN values of 90 and 270 degrees, the TestSat spends the majority of its orbit offset from being directly underneath an Iridium satellite orbit. Additionally, RAAN values of 0 and 90 degrees result in the TestSat co-rotating with the Iridium satellite constellation, while RAAN values of 180 and 270 degrees result in the TestSat counter-rotating with the Iridium satellite constellation. Thus, the two highest response values occur when the TestSat spends the majority of its orbit directly underneath an Iridium satellite orbit, and the two lowest response values occur when the TestSat spends the majority of its orbit offset from being directly underneath an Iridium satellite orbit. Also, within each pair, the higher of the two responses occurs when the TestSat is co-rotating with the Iridium satellite constellation. This result provides a potential opportunity to represent the RAAN, which in reality is a continuous numeric factor, as a combination of two categoric factors.

In order to justify representing the RAAN as two categoric factors, we can design a follow-up experiment to further assess this interaction. Figure 19 and Figure 20 show the total access time to the Iridium satellite constellation for orbital inclinations of 45 and 90 degrees, respectively, across the range of possible RAAN values for three days.

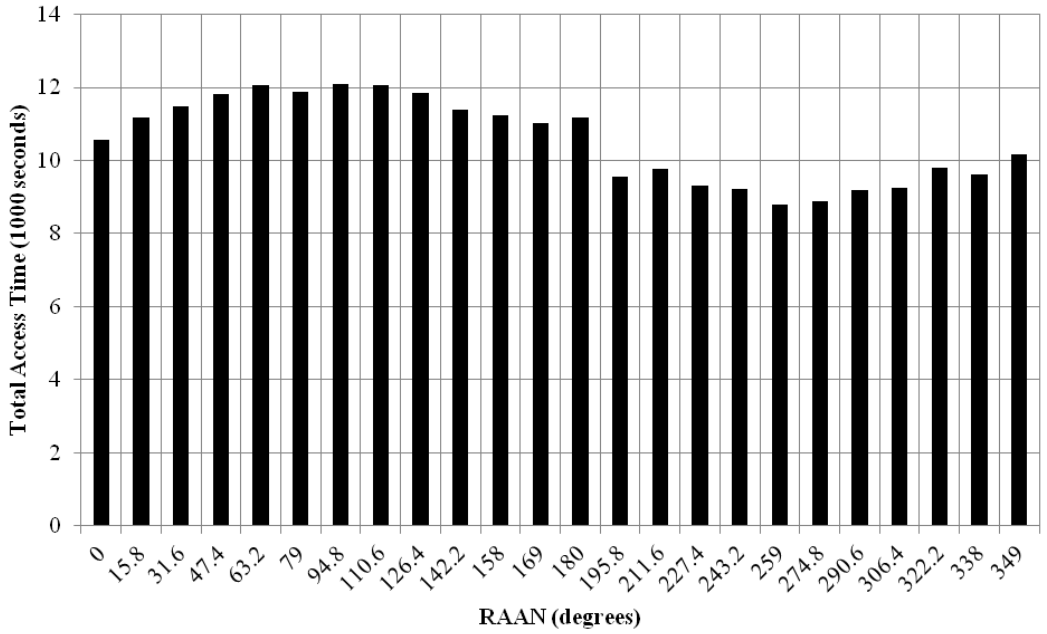

Figure 19. Spacecraft Total Access Time at Inclination of 45 degrees for Three Days

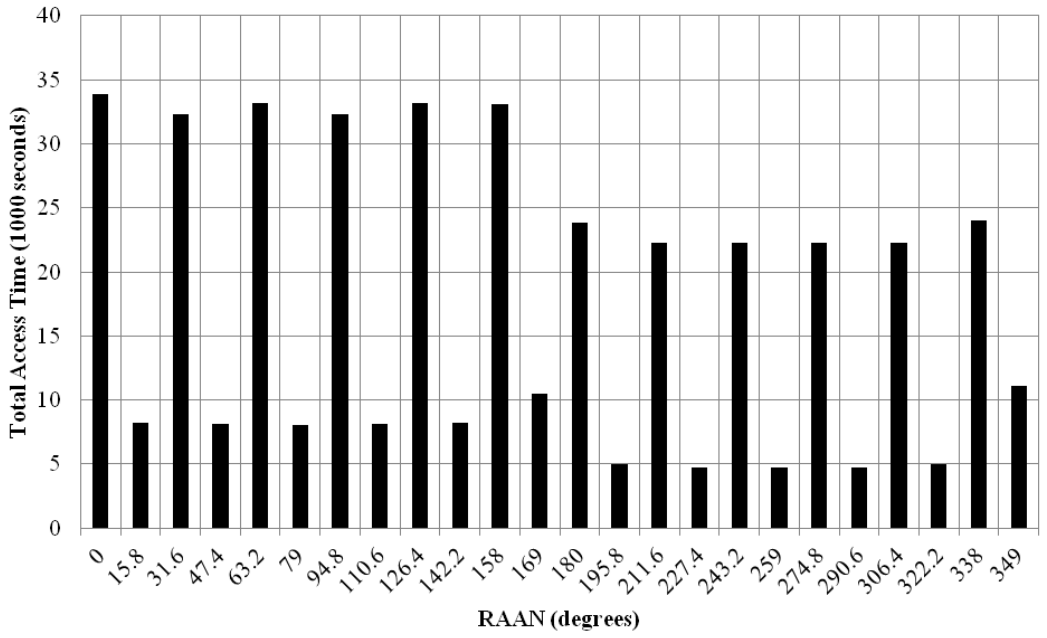

Figure 20. Spacecraft Total Access Time at Inclination of 90 degrees for Three Days

In Figure 19 we can see a periodic but relatively constant access time across the range of RAAN values in contrast to the significant differences in access time across the range of RAAN values in Figure 20. The RAAN values are the planar-mid-offset values and planar-equal values. However, we observe four approximately constant values that turn out to be grouped based on the RAAN values. The planar-equal, co-rotating RAAN values have the highest total access times which are approximately constant. Next, the planar-equal, counter-rotating RAAN values have the second-highest total access times which are approximately constant. Then the planar-mid-offset, co-rotating RAAN values have the third-highest total access times which are approximately constant. Finally, the planar-mid-offset, counter-rotating RAAN values have the lowest total access times which are approximately constant. The two outlier points occur at RAAN values of 169 and 349 degrees. Both of the outlier points occur between the first and sixth Iridium planes, which have a plane separation of only 22 degrees thereby meaning the mid-offset points are 11 degrees from the plane instead of 15.8 degrees. We can see the profile of how the total access time typically changes between the Iridium planes in Figure 21. Here, the specific profile is for the case of co-rotating in the area between the third and fourth Iridium planes. However, for the case of counter-rotating, the profile is similar except with lower values at each point. Similarly, in the case of the areas between the first and sixth Iridium planes the profile minimum will be larger in contrast to the other profiles.

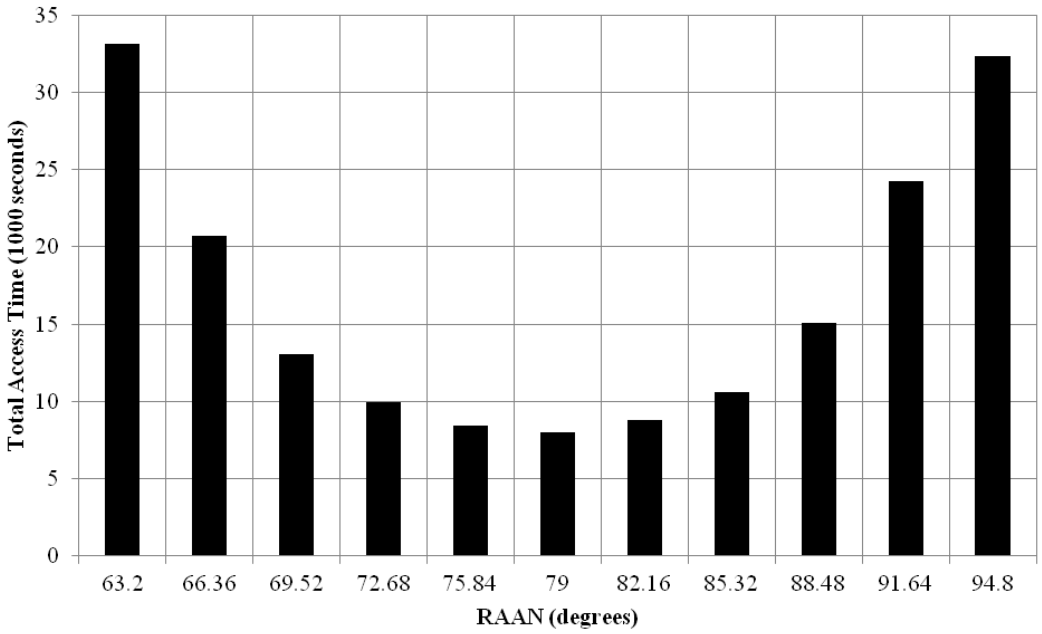

Figure 21. Total Access Time Profile Trend between Adjacent Planes 3 and 4

Therefore, we will represent the RAAN as a combination of two categoric factors. Table 11 demonstrates how we represent the range of RAAN values as two categoric factors each with two levels.

Table 11. Numeric RAAN Values Represented as Two Categoric Factors

Range of RAAN Values	Categoric Factor and Level
$\Omega_{Iridium} \pm 3°$	RAAN / Equal
$\Omega_{Iridium} + 3° < \Omega < \Omega_{Iridium} + 28.6°$	RAAN / Mid-Offset
$0° \leq \Omega \leq 180°$	Orbit / Co-rotating
$180° < \Omega < 360°$	Orbit / Counter-rotating

Then for the purposes of simulation in STK, the RAAN values that will be input for the TestSat are shown in Table 12.

Table 12. Spacecraft RAAN Values in STK for RAAN Categoric Factors

RAAN Group	TestSat RAAN Value in STK
Equal RAAN / Co-rotating Orbit	94.8°
Equal RAAN / Counter-rotating Orbit	274.8°
Mid-offset RAAN / Co-rotating Orbit	79°
Mid-offset RAAN / Counter-rotating Orbit	259°

The values in Table 12 are chosen based on utilizing the near-symmetry of the Iridium satellite constellation and the average access time values indicated in previous figures. A validation experiment is conducted to assess the quality of the categoric representation of the RAAN parameter.

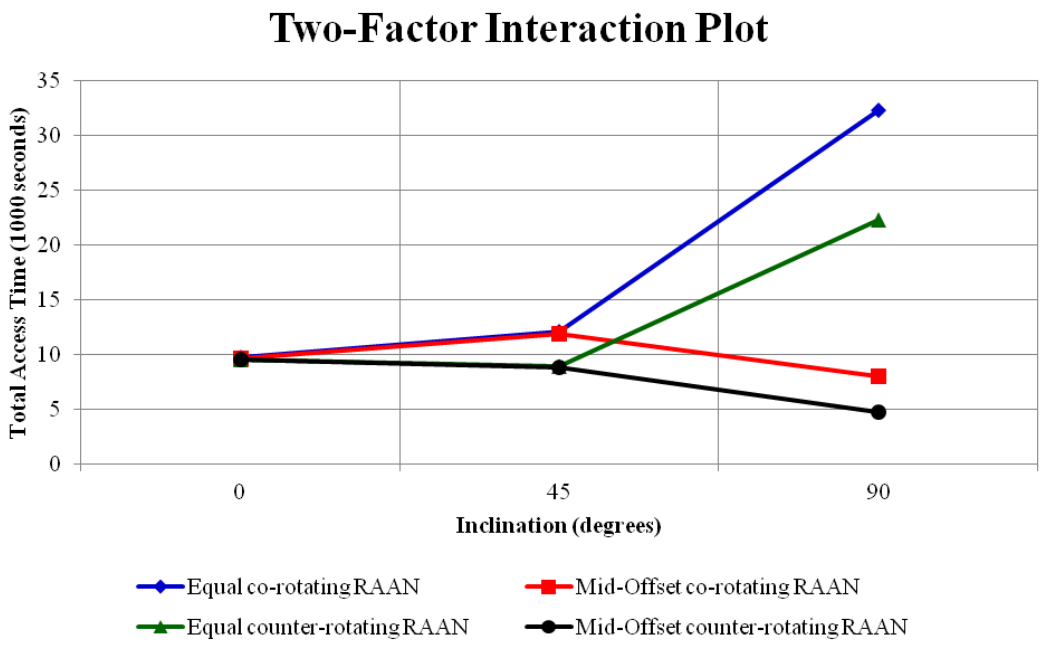

Figure 22. Spacecraft Factor Interaction Plot for Inclination and RAAN

Figure 22 turns out to be similar to Figure 18. Further, the interaction trends are intact. Therefore, it is suggested that for the purposes of this study the RAAN will be represented as a combination of two categoric factors.

3.4.8 Range Rate Constraint Factor

Lastly, we consider the range rate constraint of the communication link. Since both the current Doppler shift constraint of the Iridium 9602 transceiver and the planned Doppler shift constraint of the Iridium 9602 transceiver after the modification are specific discrete values, we can treat the range rate constraint as a categoric factor. This is justified since we do not have an interest in varying the constraint below the current capability since these data points would be meaningless. Further, we have little interest in varying the range rate constraint value between the current and planned capability levels. There could potentially be a general academic benefit understanding this knowledge in case the modification is unable to be implemented into the system, but this only adds complexity into the experiment. Further, since the risk of not implementing the modification at this time is relatively low, it is appropriate and justified to treat the range rate constraint as a categoric factor.

3.4.9 Experimental Design

Therefore, the problem study is broken into five factors. The semi-major axis and inclination parameters are considered to be continuous numeric factors with lower and upper bounds. The semi-major axis is bound between 6528 km and 7028 km with a set eccentricity value of zero. The RAAN is considered to be a combination of two categoric factors. The first factor has levels that describe whether the node is equal in value to any of the RAANs for the six planes of the Iridium satellite constellation, including the value

plus 180°, or is offset into the middle between two adjacent planes. The second factor has levels that describe whether the TestSat is approximately co-rotating with the Iridium constellation or approximately counter-rotating with the Iridium constellation. To say further, co-rotating implies a RAAN value between 0 and 180 degrees, and counter-rotating implies a value between at 180 and 360 degrees. The range rate constraint is a two-level categoric factor with levels of 7 and 14 km/s.

As a result of having two numeric factors mixed with three categoric factors, and the desire to minimize the number of simulations, or test points, an Optimal Response Surface Method design is implemented for the study. Optimal designs not only minimize the number of test points in general, but optimal designs are also an efficient choice for experiments with a mixture of numeric and categoric factors. However, with five factors it is not a trivial process to determine the minimum number of test points. Fortunately, the Design Expert 8.0 software package is equipped to provide this information. Using Design Expert, the specific test matrix design is a IV-optimal design. IV-optimal designs are best applied for studies where prediction is important. The selection of test points is processed through an algorithm that minimizes the integral of the prediction variance across the design space. It would be an unfortunate result but with five factors we can predict a worst case of requiring a sixth order model to fit the data. The algorithm states a minimum of 146 test points are necessary. However, this does not account for estimating lack of fit which is critical for quality purposes when dealing with higher-order models. The 146 test points also do not account for any replicates. Since the study is collecting results from STK, which will provide the same results given a particular set of initial conditions, it is not absolutely critical to incorporate replicates. However, for

the sake of evaluating the test matrix before the experiment, we want to have an adequate number of degrees of freedom for the pure error in the model. Finally, since we do have available time resources, we are also increasing the number of experimental data points. Therefore, 300 total test points are chosen for the study. For the interested reader, the test matrix evaluations dependent on the predicted model order are included in Appendix 4.

3.4.9 Experimental Response Parameters

The response parameters of interest in this study are chosen to be the total access time and the number of unique 10-second windows.

IV. Analysis and Results

This chapter presents the results of the study, and discusses the impacts of those results on the prospective project.

4.1 Total Access Time Results

The total access time is calculated from the summation of access durations of a minimum of 10 seconds and greater over the analysis period of three solar days in STK. For reference, if the TestSat has complete, continuous access to the Iridium constellation for the entire analysis period, then the total access time would equal 259,200 seconds.

Table 13, Table 14, and Table 15 show the fit summary information for the data according to Design Expert. In short, the tables compare the variety of fit-orders against the quality of the fit.

Table 13. Data Fit Summary Results

Source	Sum of Squares	df	Mean Squares	F-Value	p-value
Mean vs Total	3.28E+11	1	3.28E+11		
Linear vs Mean	2.46E+11	5	4.92E+10	169.47	< 0.0001
2FI vs Linear	3.70E+10	10	3.70E+09	21.69	< 0.0001
Quadratic vs 2FI	8.51E+09	2	4.26E+09	30.06	< 0.0001
Cubic vs Quadratic	2.20E+10	20	1.10E+09	16.08	< 0.0001
Quartic vs Cubic	1.01E+10	28	3.62E+08	10.89	< 0.0001
Fifth vs Quartic	3.46E+09	36	9.62E+07	4.41	< 0.0001
Sixth vs Fifth	1.82E+09	44	4.12E+07	2.54	< 0.0001
Residual	2.50E+09	154	1.62E+07		
Total	6.59E+11	300	2.20E+09		

Table 14. Model Lack of Fit Results

Source	Sum of Squares	df	Mean Squares
Linear	8.54E+10	275	3.11E+08
2FI	4.84E+10	265	1.83E+08
Quadratic	3.99E+10	263	1.52E+08
Cubic	1.79E+10	243	73746261
Quartic	7.78E+09	215	36181889
Fifth	4.32E+09	179	24107757
Sixth	2.5E+09	135	18522690
Pure Error	0	19	0

Table 15. Model Summary Statistics

Source	Std. Dev.	R-Squared	Adjusted R-Squared	Predicted R-Squared	PRESS
Linear	17045.41	0.742	0.738	0.730	8.96E+10
2FI	13059.04	0.854	0.846	0.831	5.59E+10
Quadratic	11898.23	0.880	0.872	0.858	4.72E+10
Cubic	8270.323	0.946	0.938	0.921	2.63E+10
Quartic	5765.765	0.977	0.970	0.954	1.53E+10
Fifth	4668.446	0.987	0.980	0.964	1.19E+10
Sixth	4029.569	0.992	0.985	0.961	1.31E+10

The results in Table 13 indicate that every order through the sixth order is significant to the model based on the p-values. No F-values, nor subsequent p-values are in Table 14 as a consequence that the results of for two STK simulations with identical initial conditions are equal, thereby yielding zero pure error. However, we can note that

the mean square values are of order 10^8 and high 10^7 through the cubic model, and low 10^7 for quartic and higher models. For lack of fit, we want the lowest F-value. In this situation with zero pure error, the smaller the mean square value, the better the model fits the data. Table 15 provides the model summary statistics which reiterate essentially the same results from Table 14. All of the correlation coefficients increase as the model increases in polynomial order. Recall from Chapter Three that we stated having higher order models is not necessarily a good solution. The attempt to model every possible response deviation or change based on an optimal response surface method actually increases the risk of the quality of the model. Generally speaking, the higher-order models have reduced normality even after response transformations intended to improve normality. Further, while the VIFs of the specific model terms improve from the pre-experiment values, the change is not typically significant. In other words, if a term had a high VIF value before the experiment and it turned out to be a term included in the model, then its updated VIF value will still be high, and similarly for acceptable VIF values. We can also note that while Design Expert suggests using a sixth-order model, the corresponding mean square values added into the model by the fifth- and sixth-order terms are drastically smaller than the contribution from the lower order terms. In fact, we can see the fifth- and sixth-order terms are two orders of magnitude smaller than the total mean squares value. Further, numerous terms within the fifth- and sixth-order models have VIF values larger than the recommended maximum. Therefore, we shall exclude the fifth- and sixth-order model terms from consideration in our data fit.

Next, deciding on whether to include or exclude the quartic model terms requires more of an engineering judgment decision. Using the arguments from the previous

paragraph, it is a sound decision to remove the quartic model terms from consideration in the data fit and select the cubic polynomial model fit. However, one contradicting result is the fact that the mean squares value from the lack of fit for a quartic model implies still a drastic data fit improvement from a cubic model to a quartic model. This can also be noted by the correlation constants in Table 16.

Table 16. Comparison of Quartic and Cubic Correlation Constants

	Quartic	**Cubic**
R-Squared	0.974	0.945
Adj R-Squared	0.970	0.940
Pred R-Squared	0.961	0.928
Adeq Precision	81.897	72.565

While not explicitly shown here, it also turns out that the quartic model has the largest signal-to-noise ratio of all models from first order to sixth order indicated by the adequate precision value.

The cubic model is well above a generally accepted value of 0.8, and in fact it is above 0.9. The quartic model does improve the predicted-R^2 constant about 3.5%, however the quartic model includes several terms with high p-values that have to be kept in the model for purposes of hiearchy. Another way to say this is that the quartic model is carrying terms that are unnecessary and noisy but yet required to maintain structure for higher order terms that are important in the model. Since we have a mixture of numeric and categoric factors we do not want to place too much emphasis on the VIF values, but the quartic model still has a couple of terms with VIF values over 10, even after model reduction. The study shall accept the risk of a slightly reduced polynomial fit in

exchange for a fewer number of terms. Another benefit of carrying fewer terms is that the standard error of terms that contribute to both the quartic and cubic models decreases as a percentage of the overall response standard deviation. This is a typical behavior, but the cubic model happens to be the point in the curve where the change flattens out. With everything considered, the cubic response model is selected for the total access time.

4.1.1 Cubic Model Results

Appendix 3 shows the reduced (noise-attributed terms removed except for terms facilitating hierarchy) cubic model results.

We can also measure the quality of the model by examining the normal probability plot as shown in Figure 23 and the plot of the residuals against the predicted values in Figure 24. If these two plots lead us to the conclusion of a sufficient model fit and that no response transformation is necessary, then we can visually assess the quality of the fit by comparing the model predicted values against the actual values as shown in Figure 25.

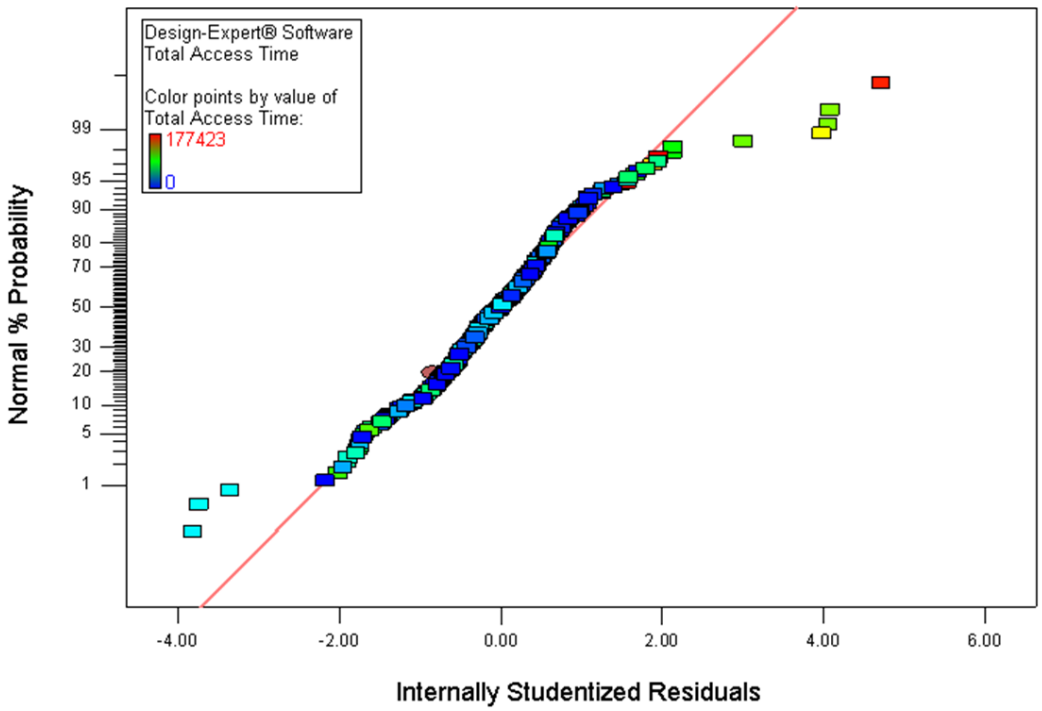

Figure 23. Normal Probability Plot of Cubic Polynomial Model Fit

There is some scatter with a few data points. Since the data points that are scattered from the normal distribution line are at the tails, the scatter is not considered an issue. There does appear to be a hint of curvature which can be an indication of a problem in either the data or the model, especially for random effects models. Fortunately, the curvature is not significant and only slightly deviates from the normal line over a small range. Figure 23 is one measure of validating the selection of the cubic model to fit the data.

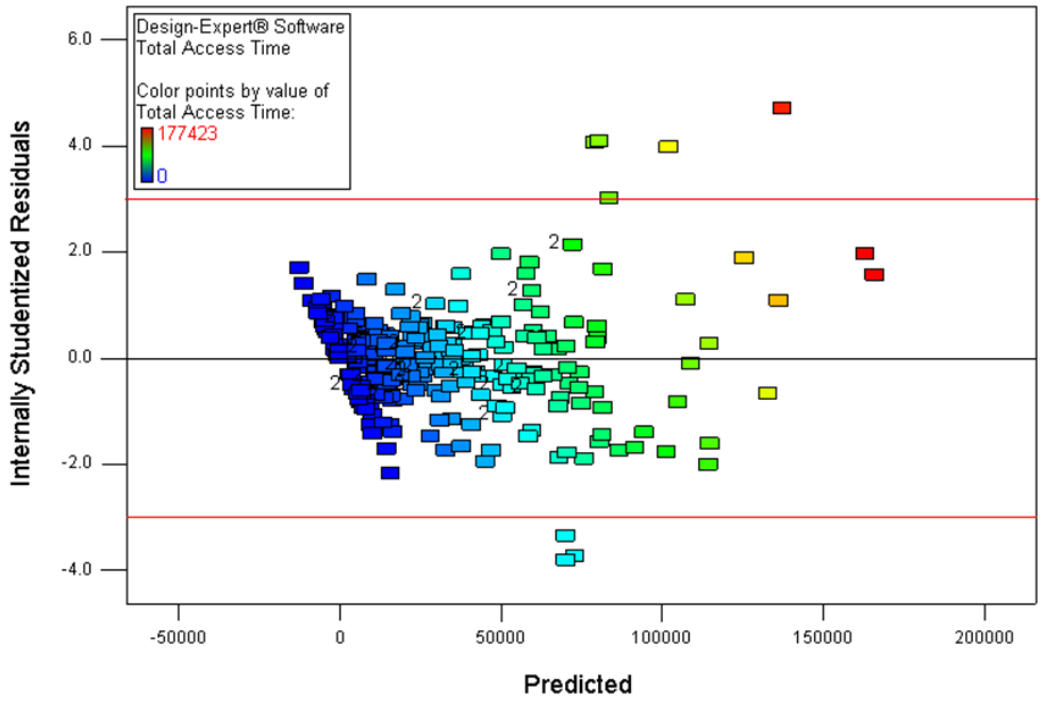

Figure 24. Plot of the Variance of the Data Fit Residuals

At first glance there appears to be some increase in the variance across the ascending predicted values since a number of points exist outside the ±3σ studentized residuals. However, from a more broad perspective, the variance seems to remain approximately constant and within about a ±2σ grouping. The assessment of Figure 24 is that there is no need for a transformation of the response data. Figure 24 is a second measure of validating the selection of the cubic model to fit the data.

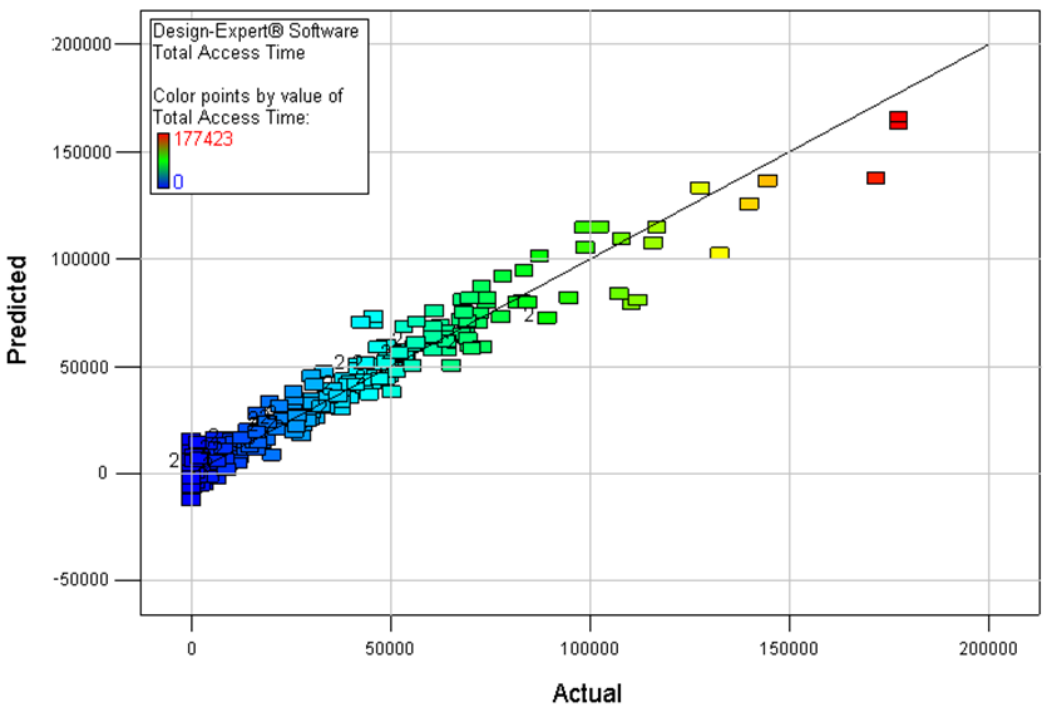

Figure 25. Cubic Polynomial Model Fit

Graphically, the cubic polynomial model fit does well to predict the data. There are a number of points that could either bring the fit into question or highlight particular difficult regions to model. The three turquoise-colored points that have some separation from the group of points along the fit-line are all 'semi-major axis, inclination, RAAN-plane' points of '6528, 1.5708, mid-offset.' The three red-colored points are all 'semi-major axis, inclination, RAAN-plane' points of '6528, 1.5708, equal.' The cluster of green-colored points below the fit-line to the right of the 100000-second-actual-gridline have no discernible connection. The yellow-colored point with separation from the fit-line is a 'semi-major axis, inclination, RAAN-plane' point of '6617, 1.5708, equal.' These points are too small of a sample size to draw firm conclusions about, but it should be noted that there are only eight test points for 'semi-major axis, inclination' of '6528,

1.5708’ and six of them deviate noticeably from the fit-line. Further there is a trend among the deviated-points that the mid-offset RAAN and equal RAAN factors are grouped together on opposite sides of the fit-line. The turquoise-colored points, which are mid-offset RAAN points, are over-predicted by the cubic model. The red-colored points and single yellow-colored point, which are equal RAAN points, are under-predicted by the cubic model. However, to make conclusions of the predictibility based on a single factor would be misleading. We can plot the model fit for each of the factors in Figure 26, Figure 27, Figure 28, Figure 29, and Figure 30. In observing all of the plots collectively, the only firm conclusion we can say is that there is typically a problem with the model fitting the data around the edge of the 2D test space for the semi-major axis and inclination factors, particuarly at the vertices of the test space in the experiment.

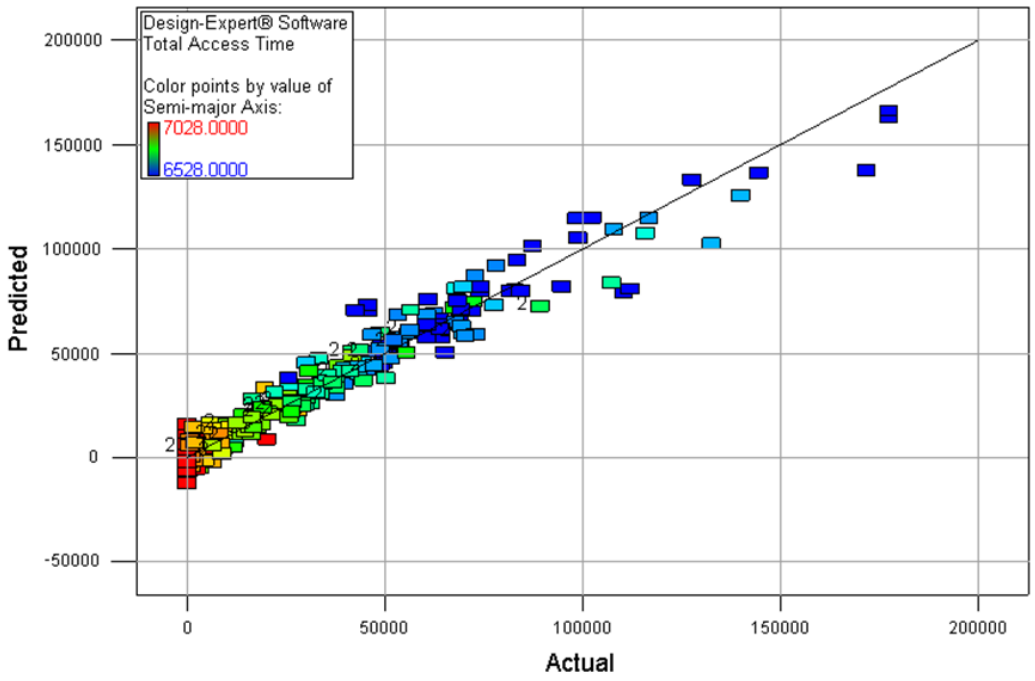

Figure 26. Cubic Polynomial Model Fit According to Semi-Major Axis (km)

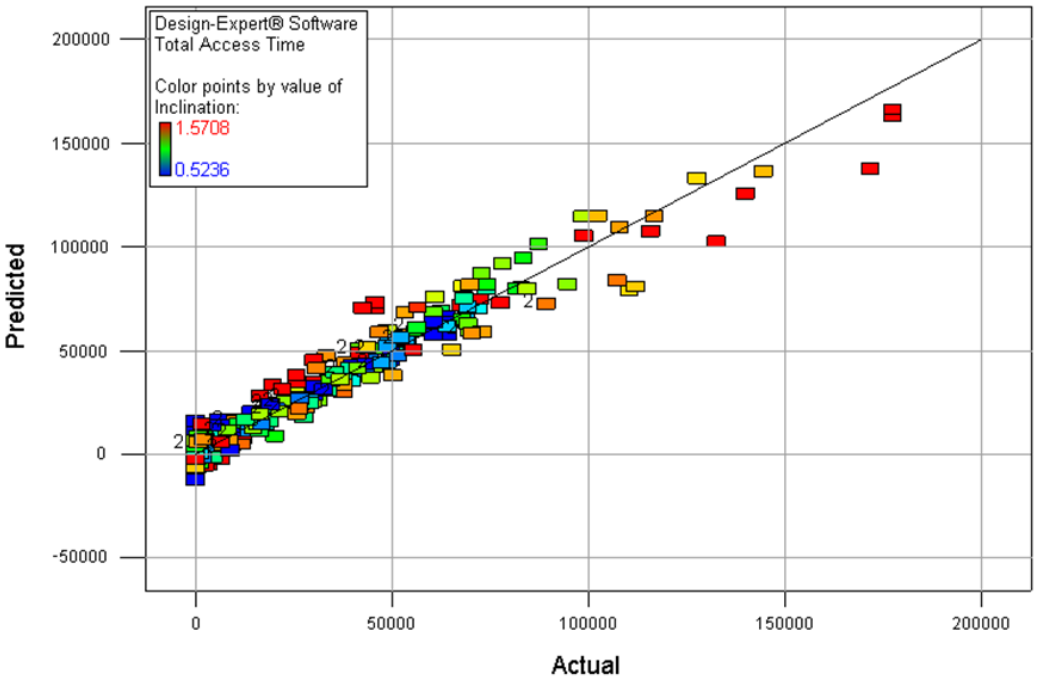

Figure 27. Cubic Polynomial Model Fit According to Inclination (rad)

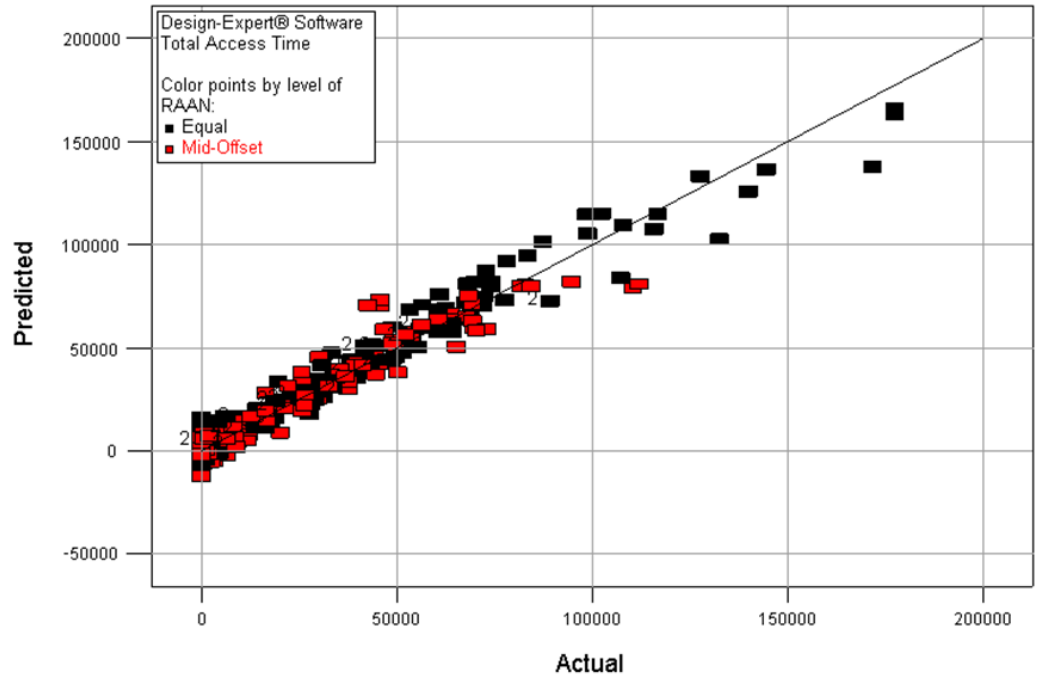

Figure 28. Cubic Polynomial Model Fit According to RAAN

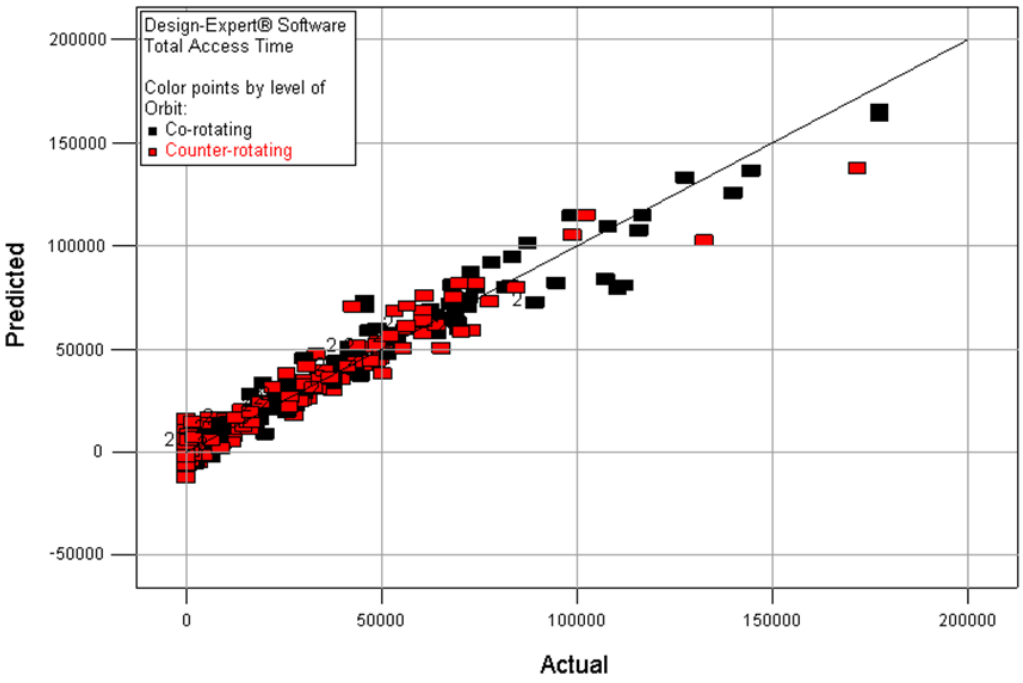

Figure 29. Cubic Polynomial Model Fit According to Orbit

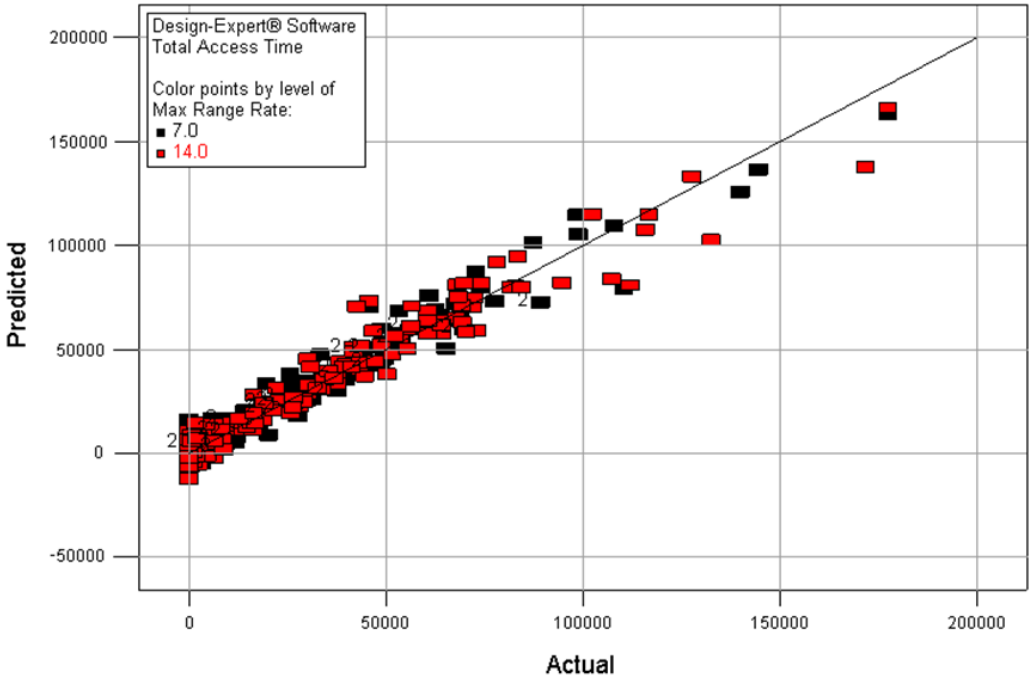

Figure 30. Cubic Polynomial Model Fit According to Max Range Rate

Now, as a consequence of having only two numeric factors, we can easily plot the full response surface given a particular set of the three categoric factors. Since the three categoric factors each have two levels, we have eight possible sets. Therefore, the following 16 figures are the eight response surfaces and their corresponding contour graphs for the total access time. The contour graph is the 2D projection of the response surface. For the reader, the sets are identified in the figure captions according to a three digit number where the first digit represents the RAAN, the second digit represents the Orbit, and the third digit represents the Max Range Rate. For all three digits, a zero represents the first level of the factor, namely Equal RAAN, Co-rotating Orbit, or 7.0 km/s Max Range Rate, and a one represents the second level of the factor, namely Mid-Offset RAAN, Counter-rotating Orbit, or 14.0 km/s Max Range Rate.

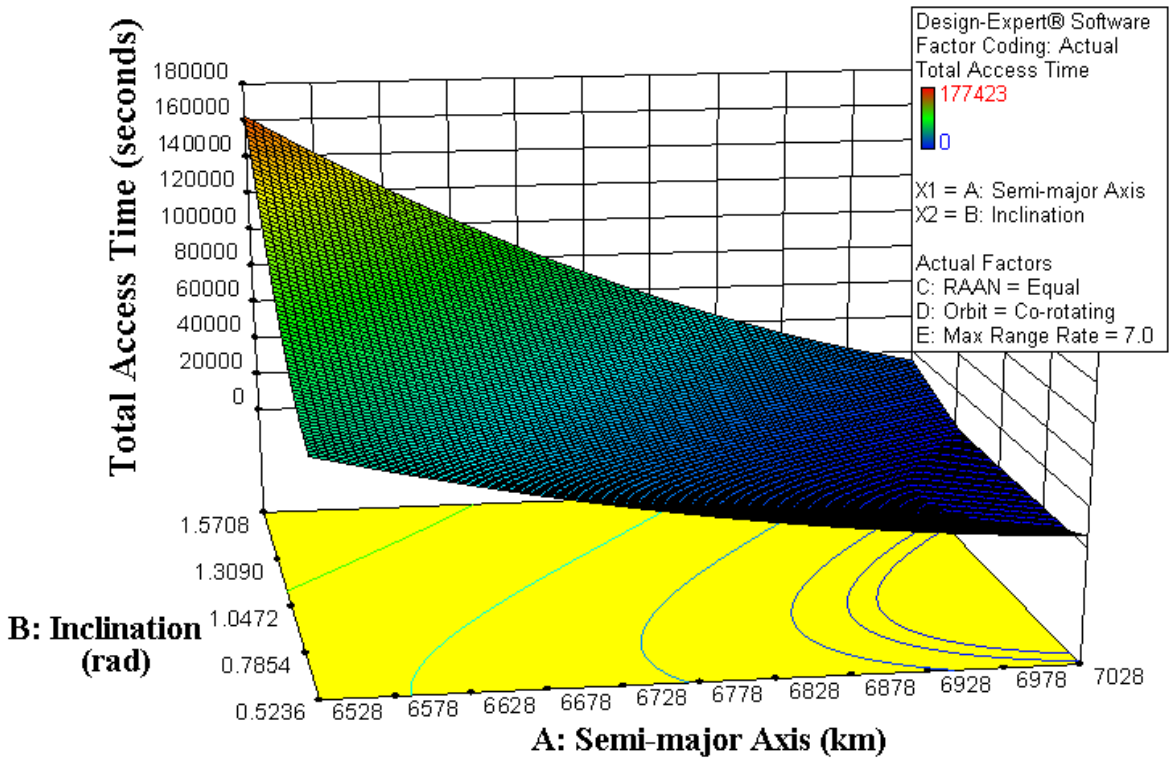

Figure 31. Total Access Time Response Surface – Categoric Set 000

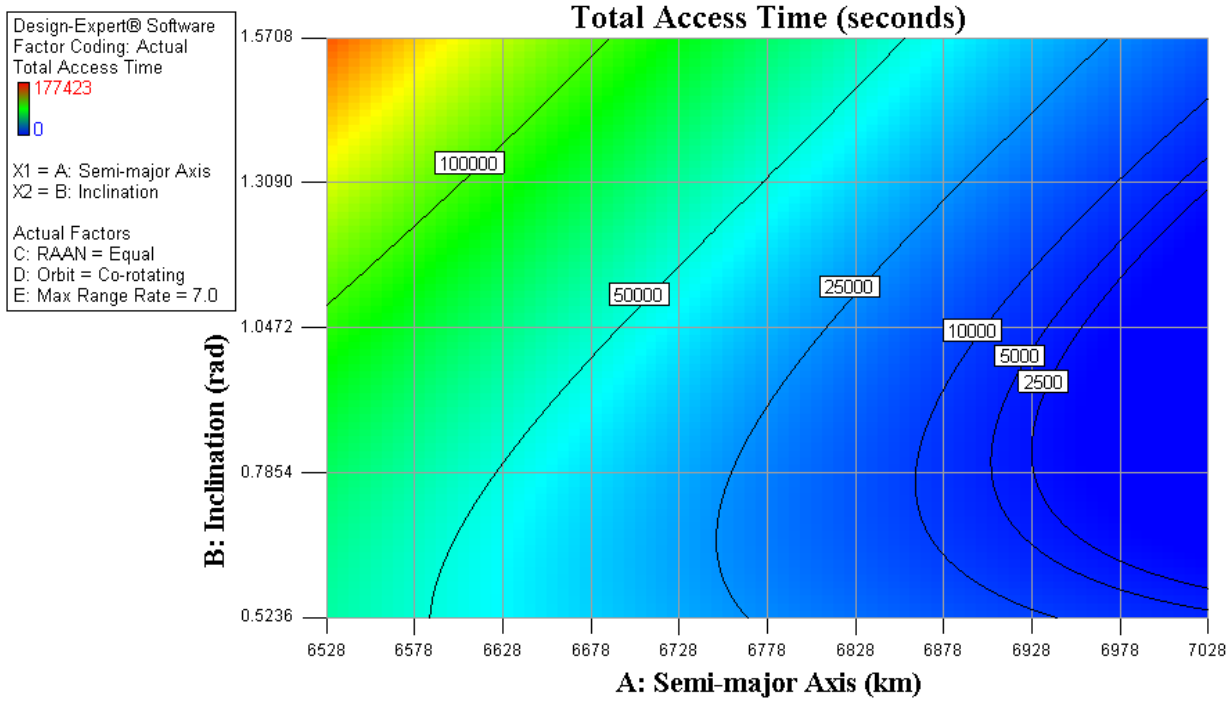

Figure 32. Total Access Time Contour Plot – Categoric Set 000

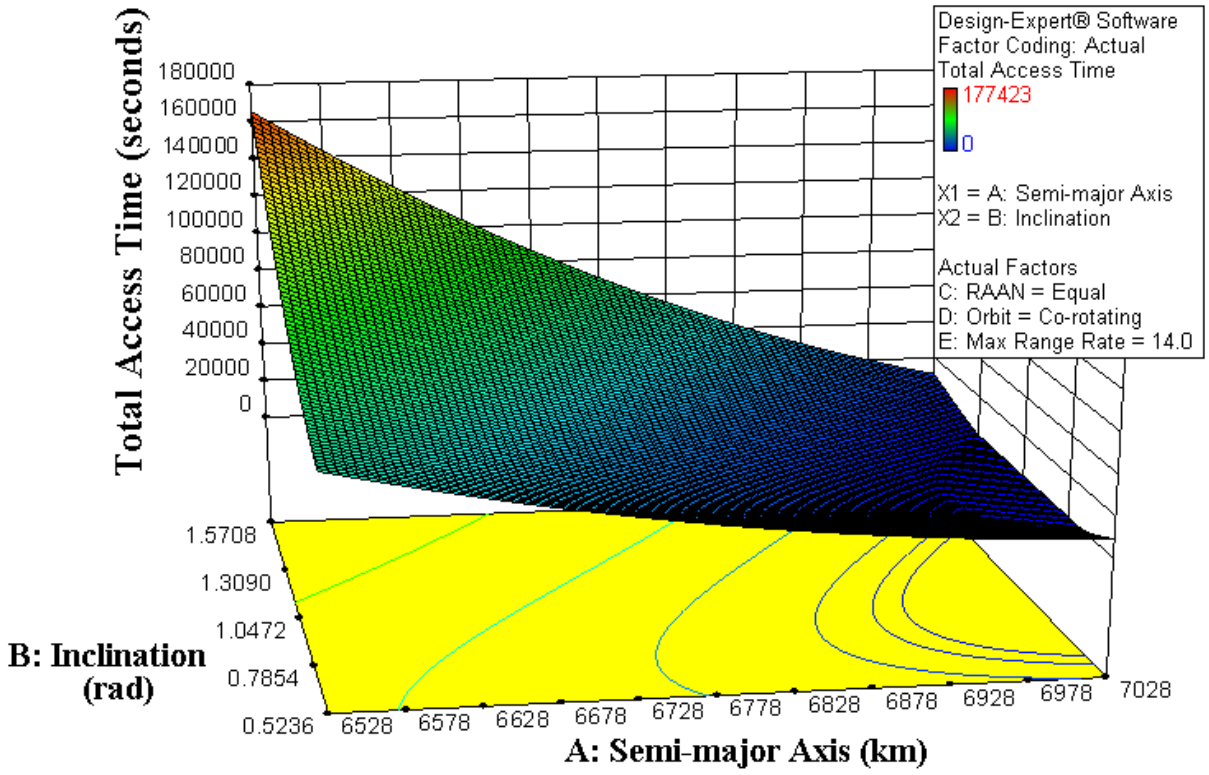

Figure 33. Total Access Time Response Surface – Categoric Set 001

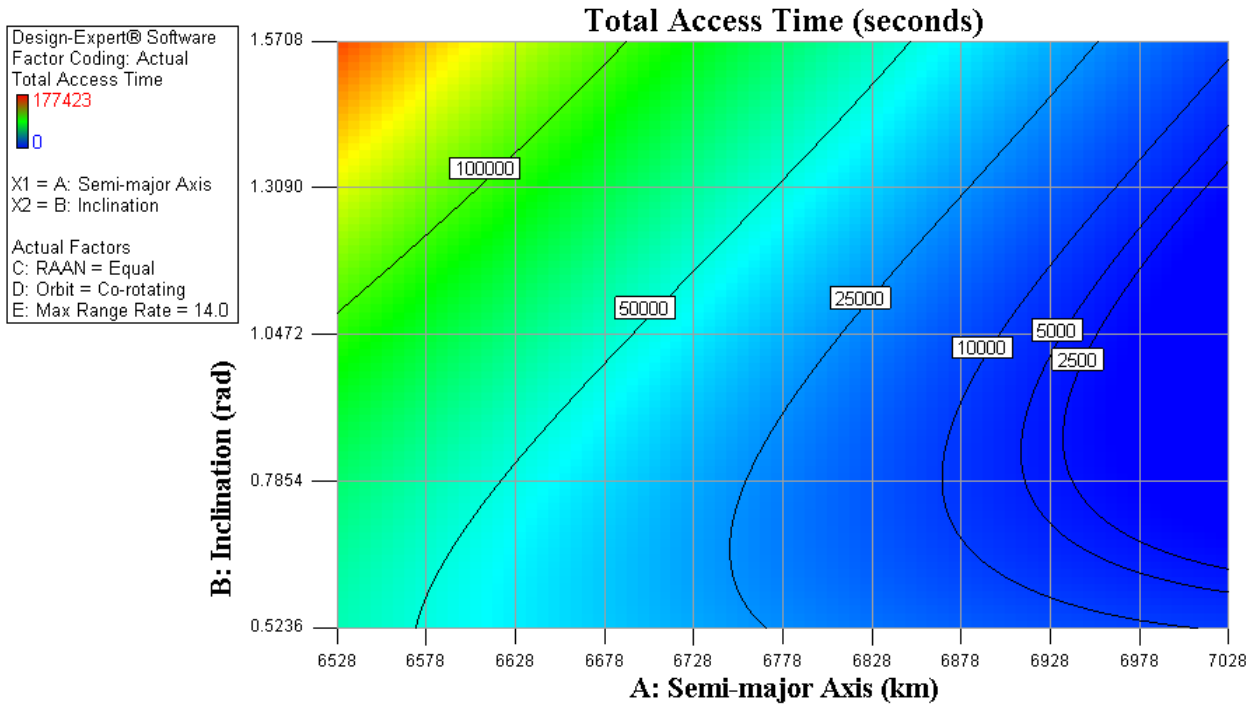

Figure 34. Total Access Time Contour Plot – Categoric Set 001

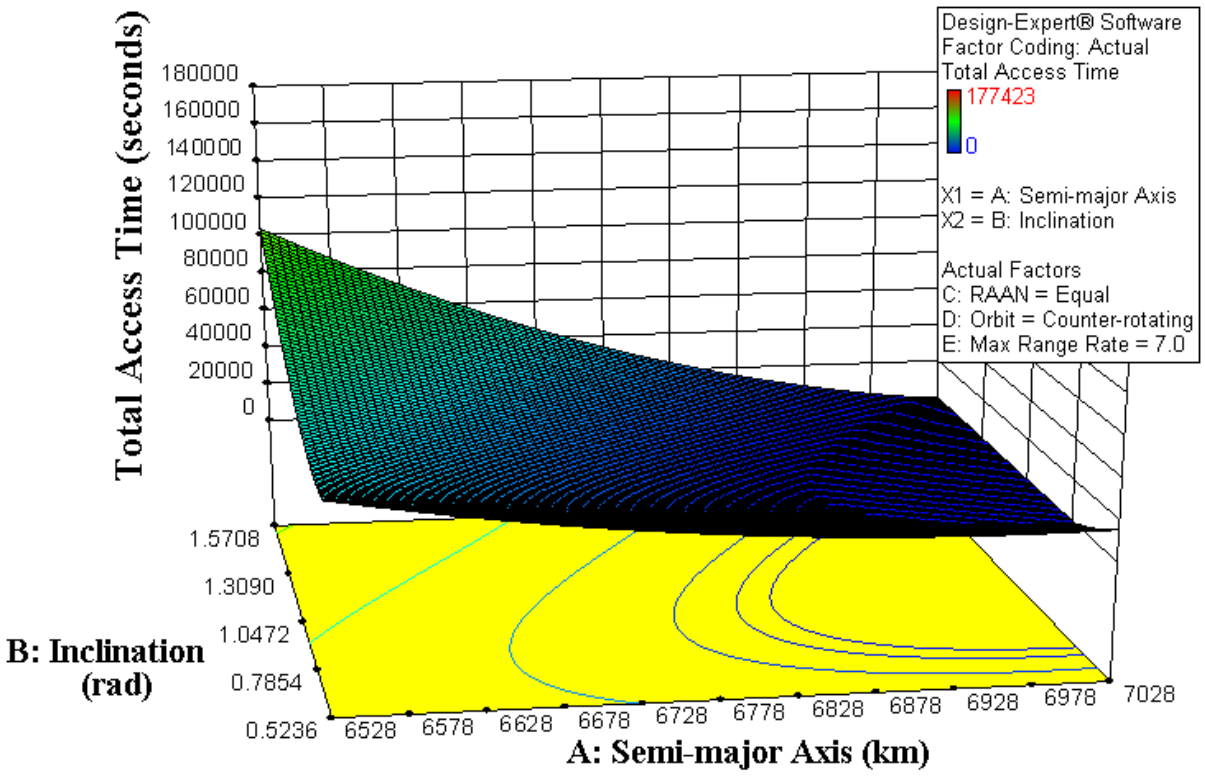

Figure 35. Total Access Time Response Surface - Categoric Set 010

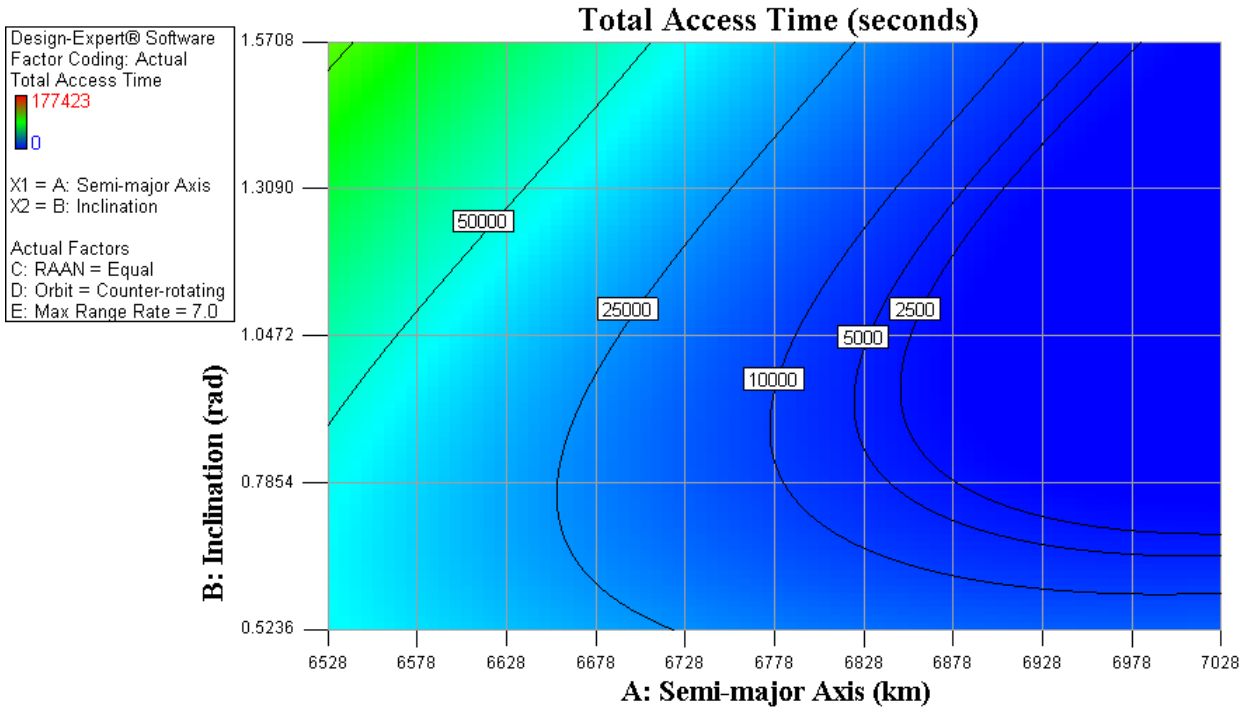

Figure 36. Total Access Time Contour Plot - Categoric Set 010

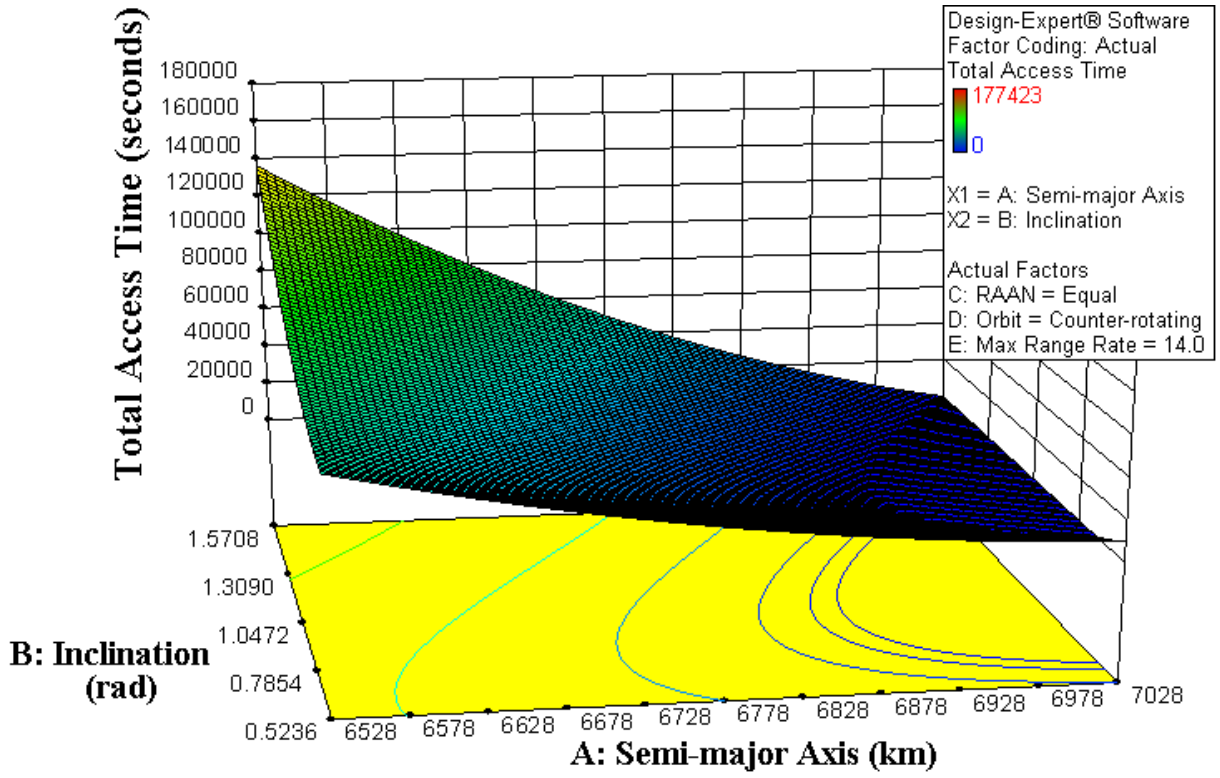

Figure 37. Total Access Time Response Surface – Categoric Set 011

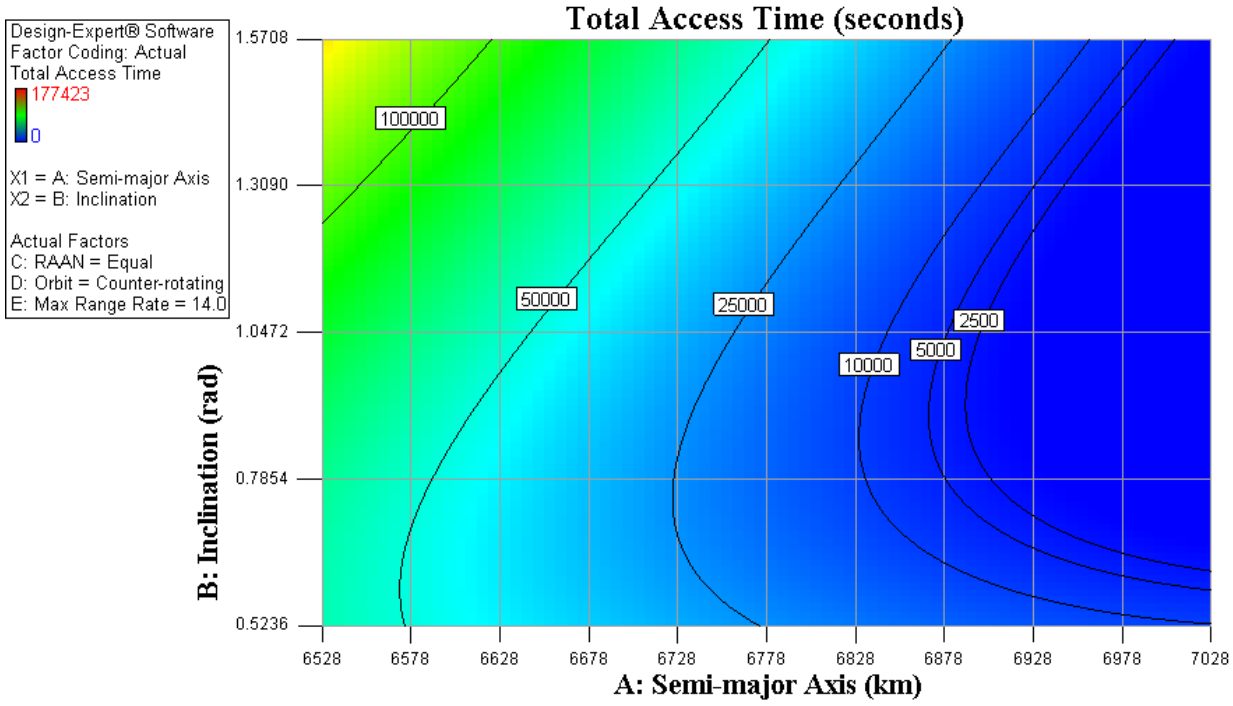

Figure 38. Total Access Time Contour Plot – Categoric Set 011

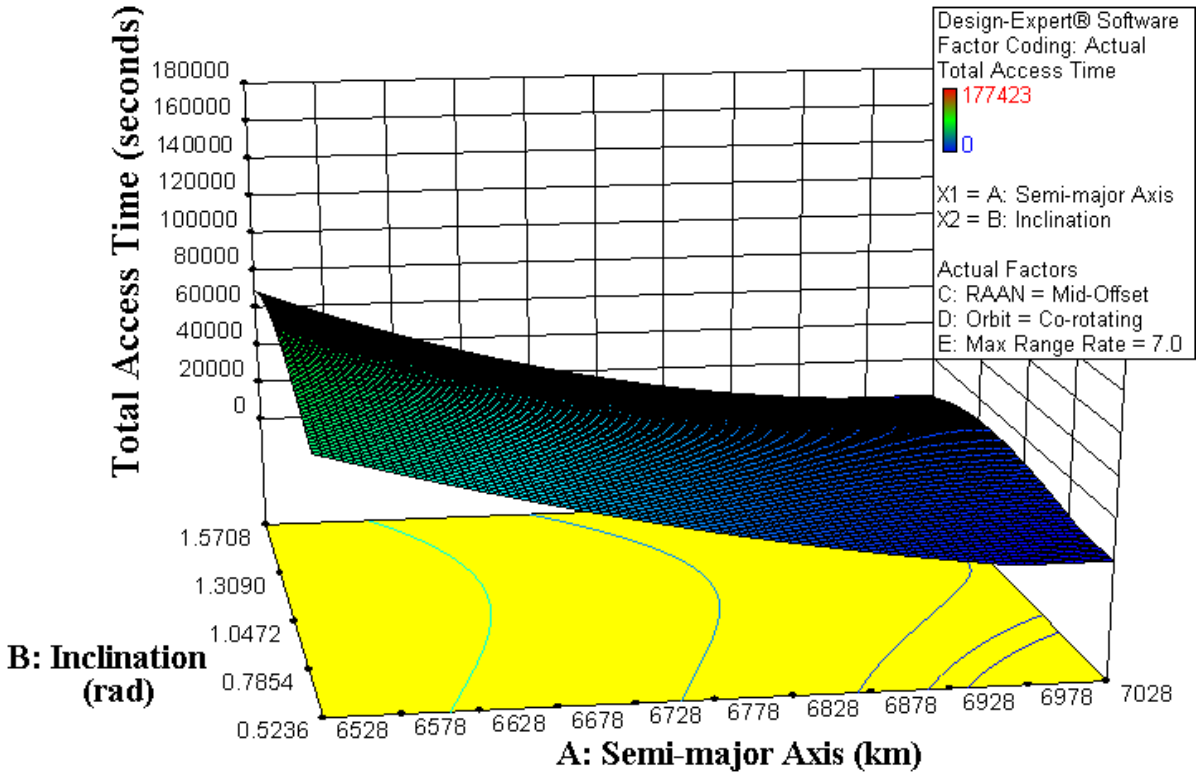

Figure 39. Total Access Time Response Surface – Categoric Set 100

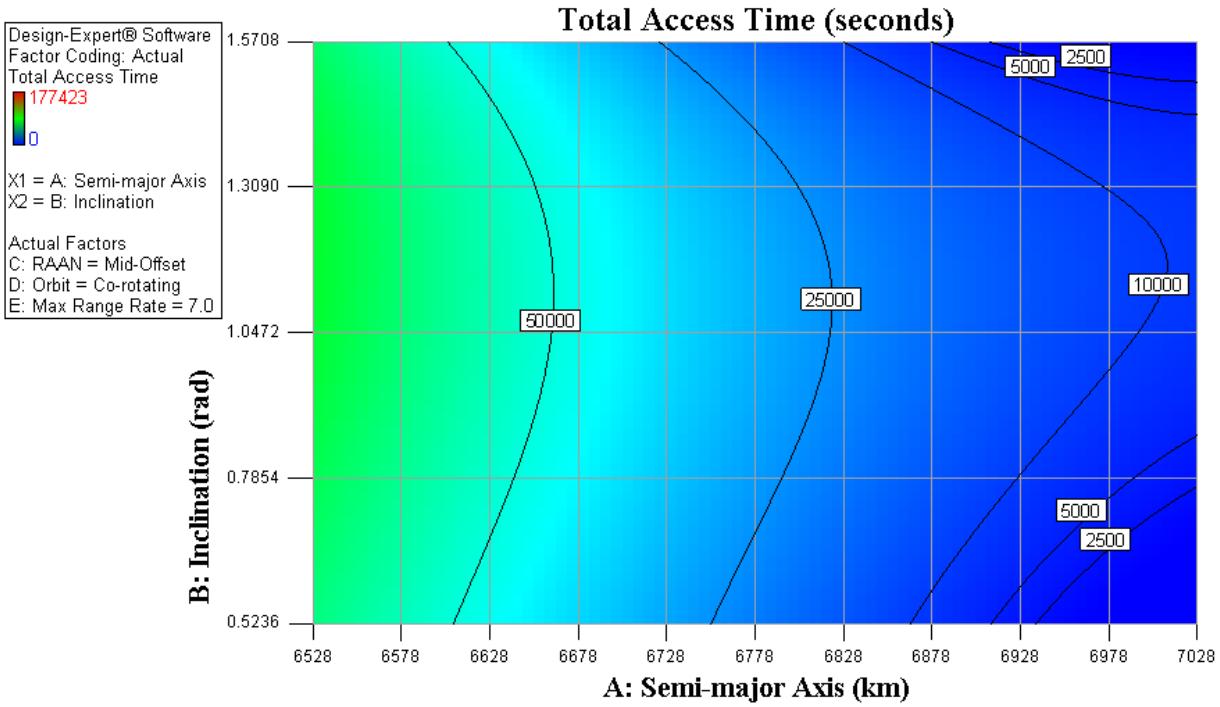

Figure 40. Total Access Time Contour Plot – Categoric Set 100

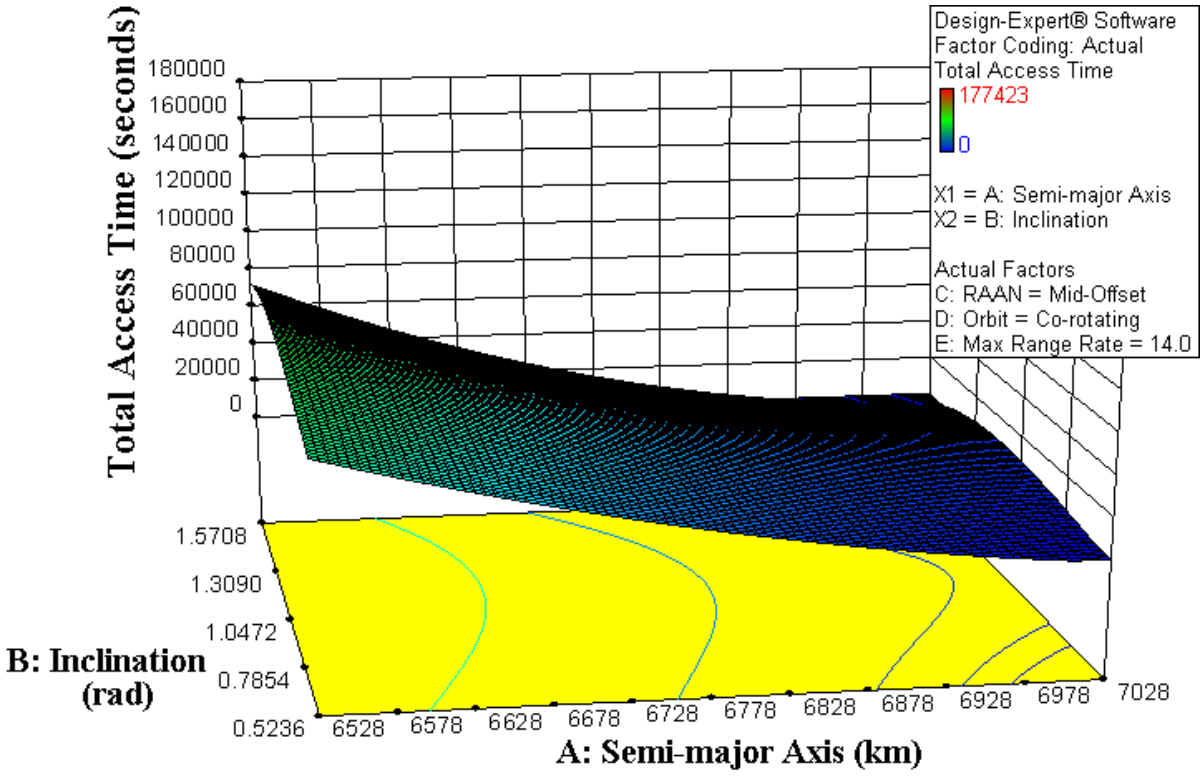

Figure 41. Total Access Time Response Surface – Categoric 101

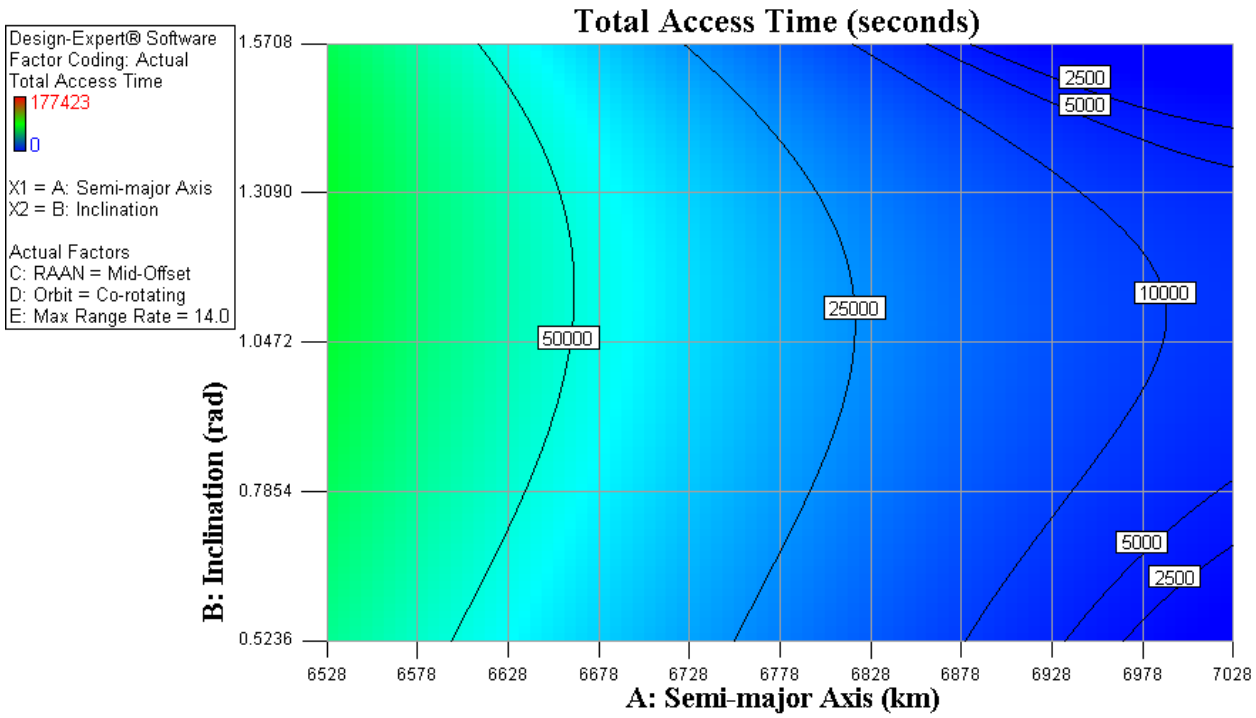

Figure 42. Total Access Time Contour Plot – Categoric 101

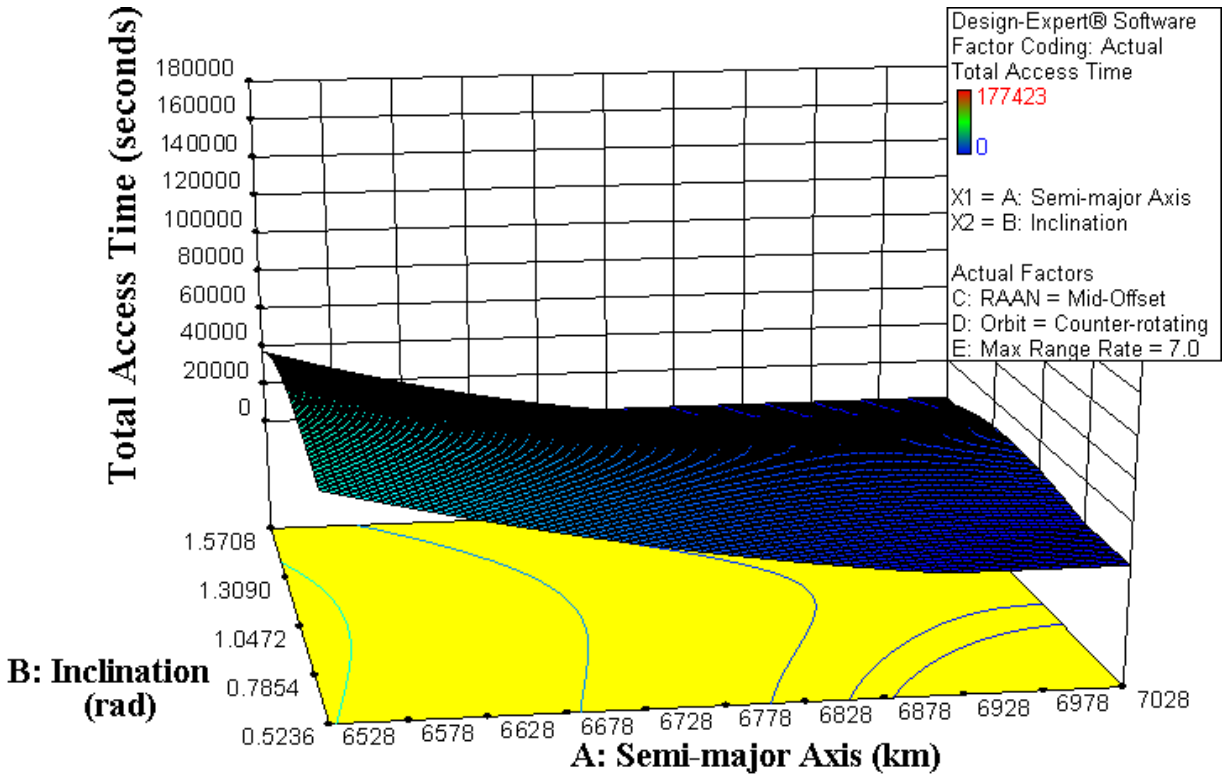

Figure 43. Total Access Time Response Surface – Categoric Set 110

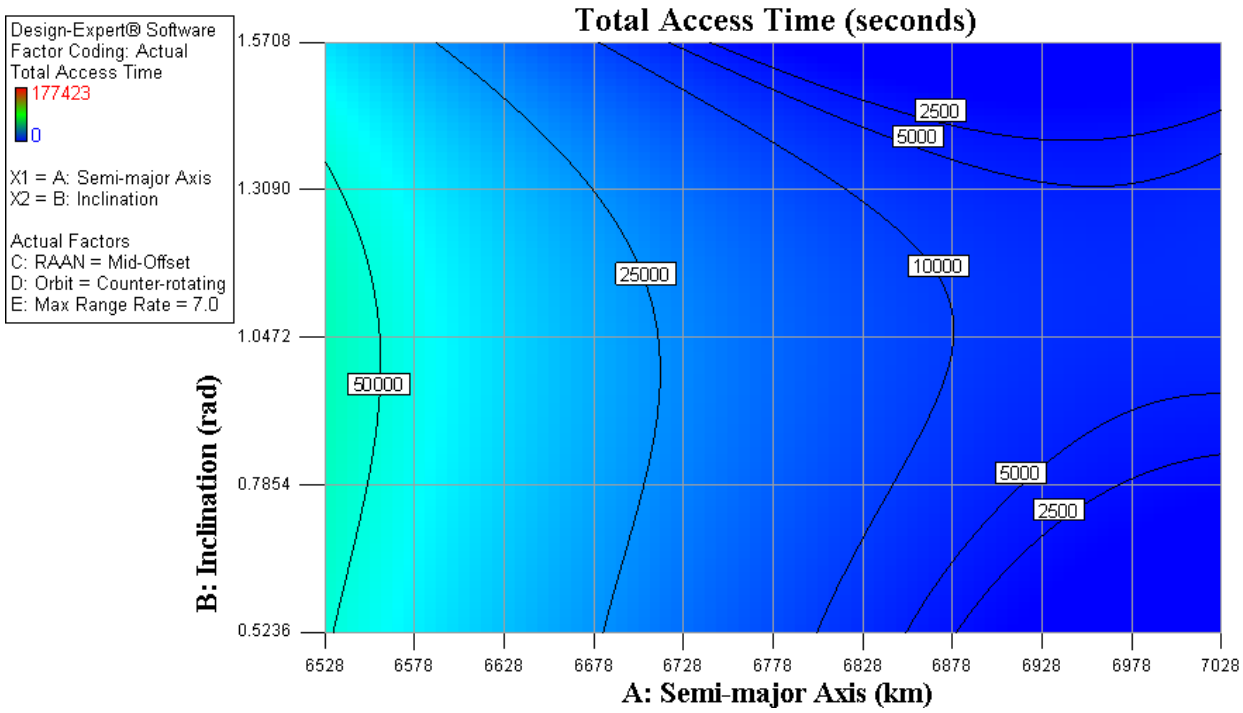

Figure 44. Total Access Time Contour Plot – Categoric Set 110

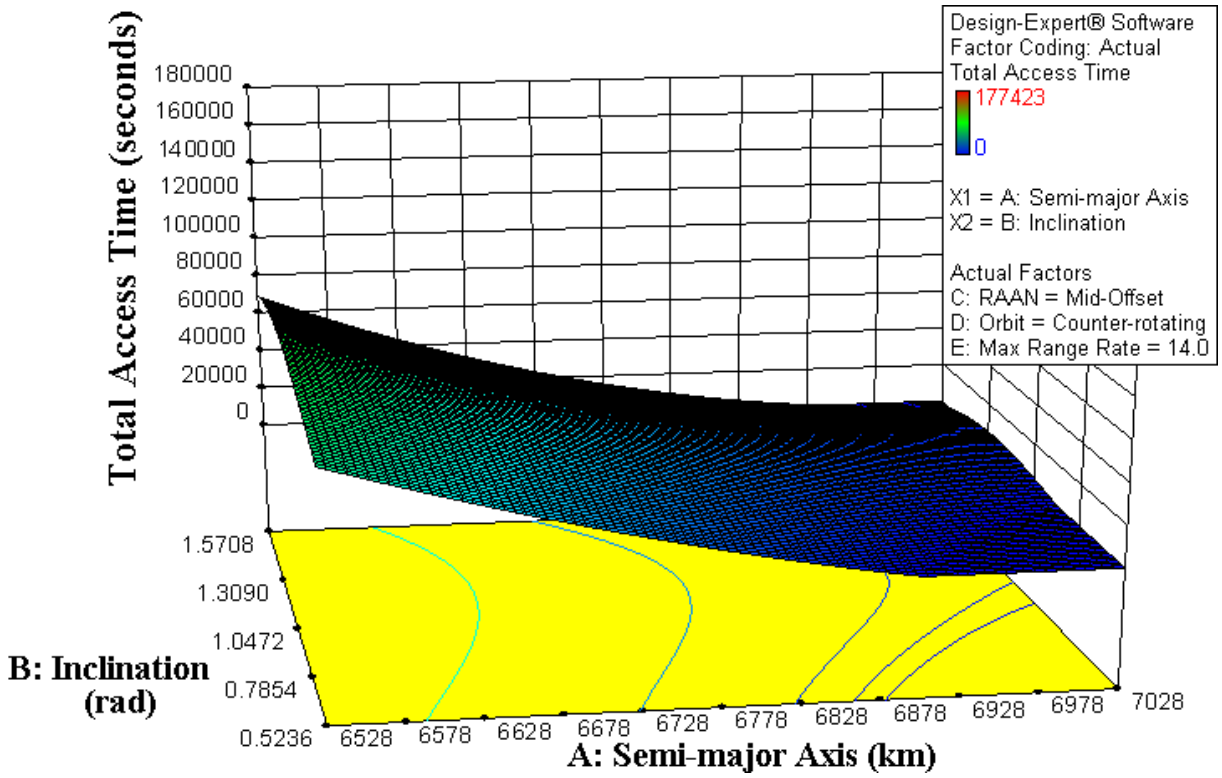

Figure 45. Total Access Time Response Surface – Categoric Set 111

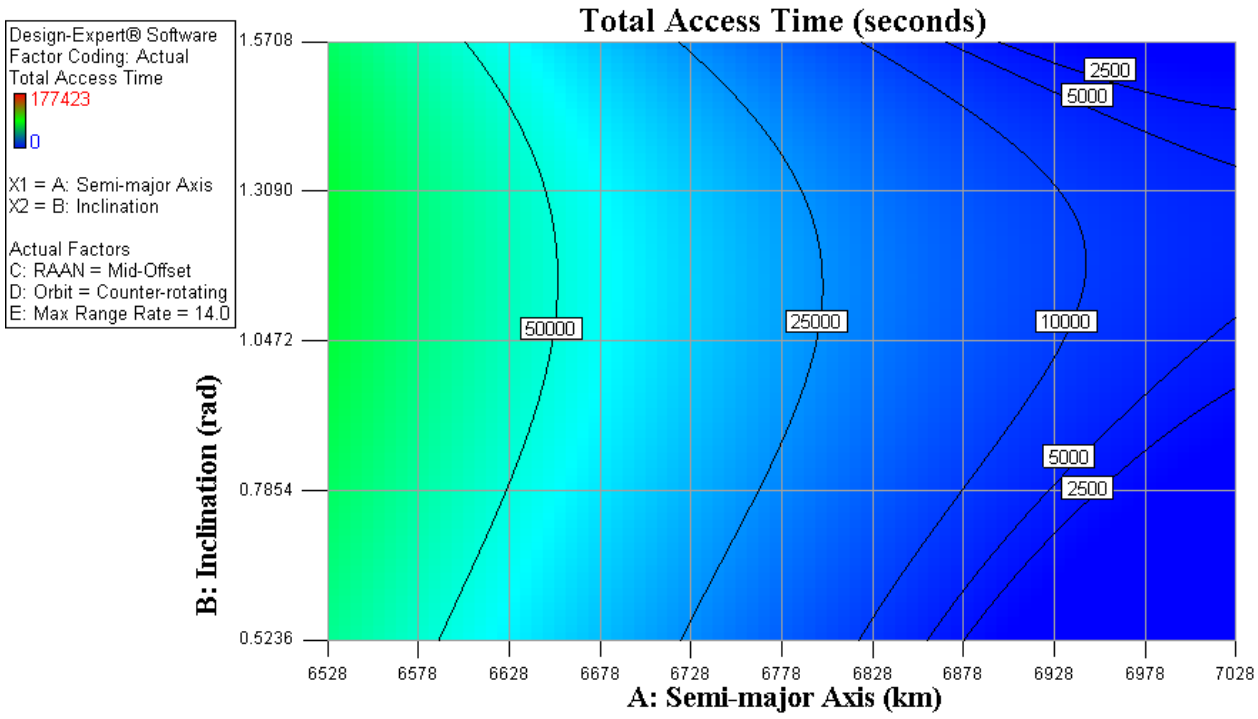

Figure 46. Total Access Time Contour Plot - Categoric Set 111

First, we can observe that the increase in the maximum range rate constraint does not impact the total access time overall for co-rotating orbits, but does impact the total access time overall for counter-rotating orbits. This agrees with our expectations for the purpose of the transceiver modification and discussion from Chapter Two. From a general broad perspective, the Doppler shift can actually improve on-orbit compared to the ground for the TestSat when co-rotating with the Iridium satellite constellation. However, the Doppler shift significantly increases compared to the ground for the TestSat when counter-rotating against the Iridium satellite constellation. We can particularly see the effect of this interaction when comparing plots of the same RAAN and Max Range Rate factor-levels. There is a noticeable reduction in total access time for counter-rotating orbits as compared to co-rotating orbits at the Max Range Rate level of 7 km/s. Again, Chapter Two showed that counter-rotating orbits would result in Doppler shifts that exceeded current transeiver capabilities, and therefore a reduction in total access time is expected. However, there is little to no impact to the total access time for counter-rotating orbits compared to co-rotating orbits at the Max Range Rate level of 14 km/s. Thus, the modification goal to double the permitted Doppler shift between the transceiver and satellite is justified and necessary to maximize the utility of the system.

Secondly, we can observe that the RAAN primarily impacts the total access time overall for higher inclinations. We can see this impact by comparing plots of the same Orbit and Max Range Rate factor-levels. If the TestSat has an equal RAAN value to that of one of the Iridium satellite constellation planes, then the total access time peaks as the inclination increases at a particular semi-major axis value. If the TestSat has a mid-offset

RAAN value compared to one of the Iridium satellite constellation planes, then the total access time peaks toward the middle of the inclination range space at a particular semi-major axis value. This also agrees with our expectations based on the initial assessments discussed in Chapter Three regarding the interaction between the inclination and the RAAN parameters over the analysis period of three days.

4.1.2 Validation of Cubic Model Fit for Total Access Time

The Iridium 9602 transceiver is projected to attach to one of three configurations, namely the International Space Station (ISS), a LEO satellite, or a rocket body. We will not attempt to validate the model fit for the case of the rocket body since tumbling will result in the transceiver antenna pointing directions other than zenith. For this thesis, we will only validate the cubic polynomial model fit against a sample ISS validation set of scenarios since the ISS also qualifies as a LEO satellite. The nominal ISS orbit also happens to lie within the center region of our model space.

The ISS has an orbit with a semi-major axis of approximately 6,790 km and an inclination of approximately 51.6 degrees. If we then select six random RAAN values for the ISS and assign a maximum range rate for each point, we can simulate the scenario in STK and check the access results against the predictions in Design Expert. For convenice Table 17 summarizes the STK simulation RAAN values with the categoric RAAN values as pertaining to the model fit prediction, and Table 18 provides the prediction and 95% confidence intervals from Design Expert with the actual results.

Table 17. ISS Sample Validation Simulations

Data Point	Max Range Rate (km/s)	STK RAAN (degrees)	Categoric RAAN	Categoric Orbit
1	7.0	20	Mid-Offset	Co-rotating
2	7.0	125	Equal	Co-rotating
3	7.0	190	Mid-Offset	Counter-rotating
4	7.0	308	Equal	Counter-rotating
5	14.0	105	Mid-Offset	Co-rotating
6	14.0	159	Equal	Co-rotating
7	14.0	240	Mid-Offset	Counter-rotating
8	14.0	340	Equal	Counter-rotating

Table 18. ISS Sample Validation Results

Data Point	Design Expert Predition (second)	Design Expert 95% CI Low (seconds)	Design Expert 95% CI High (seconds)	STK Actual (seconds)
1	27468	24317	30619	22362
2	22711	19573	25849	23908
3	16223	13057	19390	18397
4	8380	5244	11515	15624
5	27476	24333	30619	25003
6	22719	19518	25921	24361
7	23833	20642	27025	21302
8	15990	12815	19165	22607

Given a small sample of validation points within the center of our model space, we can say that the cubic polynomial model fit adequately predicts the total access time. Five of the eight validation points lie within the 95% confidence interval. The other three points comprise two prediction error cases. The first case is when the model under-predicts the total access time. It is not a problem for the LEO RSO to arrive on orbit and encounter longer-than-predicted access times, but before we launch we may eliminate a particular orbit because of low predictions for total access time. Two of the three error points over predict. The second case is when the model over-predicts the total access time. In this case, it is a significant problem for the LEO RSO to arrive on orbit and encounter shorter-than-predicted access times. This situation can result in a mission that fails to meet requirements. One point under predicts.

Therefore, given the small sample of validation points, we shall accept the cubic polynomial model as an adequate fit for the model space.

Finally we should emphasize that these results are based on an analysis period of three days. Over longer time periods, the RSO will transit through intervals of both rich and lean total access times due to the recession of the RAAN under the J_2 perturbation.

4.2 10-Second Window Results

The 10-second window results are calculated based on the access reports from STK simulations and the number of unique 10-second windows available within each of the access durations. Table 19 provides a brief list of examples for how the access durations were transformed into a count of 10-second windows.

Table 19. Example of Defining Unique 10-second Windows

Simulated Access Duration (seconds)	Number of Unique 10-Second Windows
10.15	1
17.94	1
22.63	2
35.48	3

All of the reports generated from STK simulations are constrained to report only those access durations of at least 10 seconds. These reports were imported into Microsoft Excel for analysis that focused on counting the number of unique 10-second windows available in each individual access of each simulated test point.

The test matrix evaluations are unchanged from response to response before data are collected. Therefore, the selection for the proper polynomial model fit for the 10-second window response relies on the same decisions made for the determination of the polynomial model fit for the total access time response. Consequently, we immediately disregard the fifth and sixth order polynomial model fits. We arrive at a similar decision point as that for the total access time response, where we need to make an engineering judgment between the quartic polynomial model and the cubic polynomial model. While not explicitly shown here, it turns out that the 10-second window response has nearly identical correlation constants and VIF values among the two models. Therefore, following the same judgment as the total access time response, we select the cubic polynomial model to fit the data from the STK simulations.

As it turns out, the trends in the 10-second window response match those as observed in the total access time results section discussed above. The only change lies with the absolute magnitude of the response values. Since the 10-second window response data is measuring the number of unique 10-second windows available, the response value is merely a counting parameter with no units and is an order of magnitude smaller than the total access time response.

4.3 Frequency of Access

In addition to the total access time over the period of three days, we are also concerned with the frequency of access. As before, the minimum access duration was constrained to 10 seconds, and then the number of those accesses is plotted versus the LEO RSO's orbital pass number. Unlike the total access time response, we do not want to formulate a statistical model fit, but instead we can plot a histogram for our data points. However, since we have 300 data points, only five representative histograms from data points across the model space are included explicitly in this thesis. All data points considered below have RAAN values of 94.8 degrees and maximum range rate constraints of 7 km/s. As a reference, in general we know that ground-based communications with a single ground station will have about two or three communication opportunities with approximate durations of 10 minutes each day.

The first data point considered is the sample ISS point at a semi-major axis of 6,790 km and an inclination of 51.6 degrees. Figure 47 shows the frequency of access for the LEO RSO to the Iridium satellite constellation.

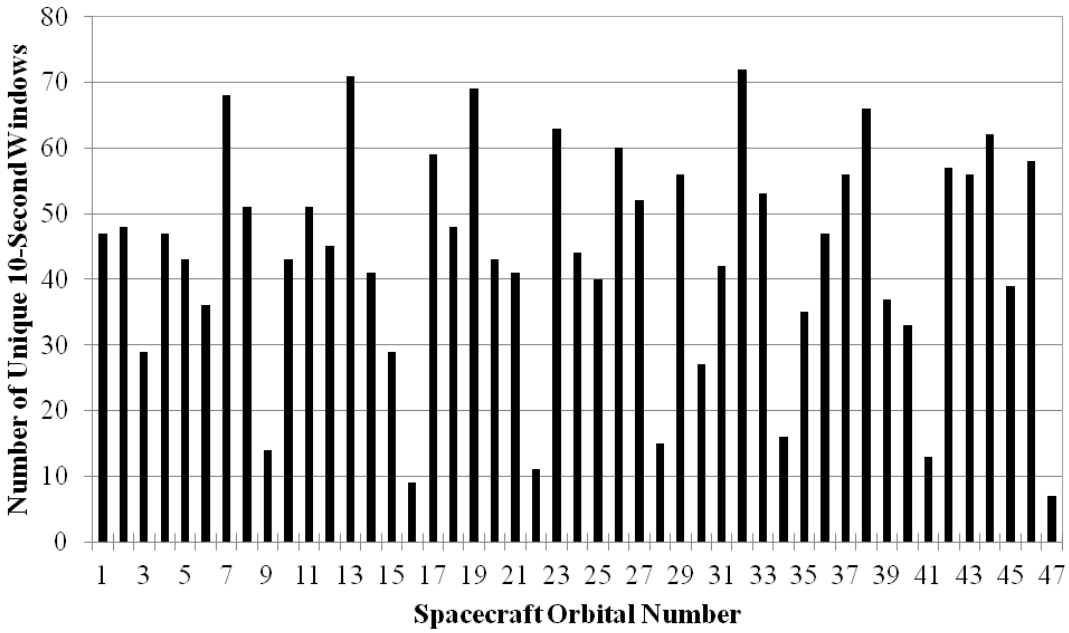

Figure 47. Histogram of 10-Second Accesses Per Orbit #1

Figure 47 exhibits periodic behavior and has a large difference between its maximum number of accesses in a particular orbit and its minimum number of accesses in a particular orbit. Generally speaking, there is a lot of potential 10-second access windows each RSO orbit.

The second data point considered is a semi-major axis of 6,600 km and an inclination of 35 degrees. Figure 48 shows the frequency of access for the LEO RSO to the Iridium satellite constellation.

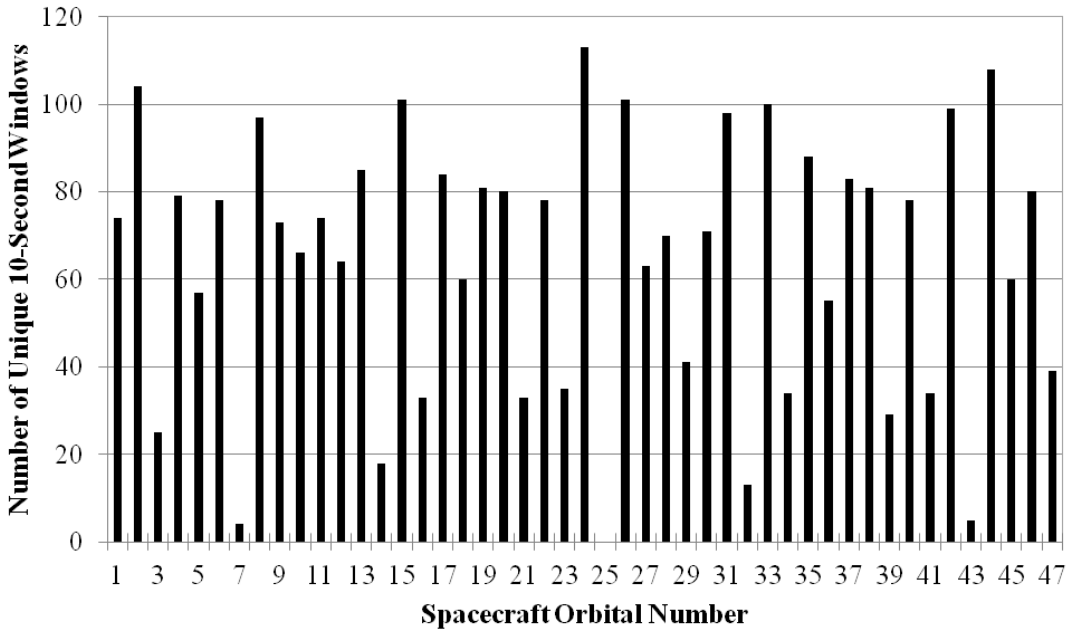

Figure 48. Histogram of 10-Second Accesses Per Orbit #2

Figure 48 does not exhibit a consistent periodic behavior. Further, the number of 10-second access windows is quite numerous during some orbits, but a few orbits have little access, including one orbit with no access windows. Generally speaking, there are a lot of 10-second access windows, but the trend orbit-to-orbit tends to follow large differences between successive orbits.

The third data point considered is a semi-major axis of 6,650 km and an inclination of 85 degrees. Figure 49 shows the frequency of access for the LEO RSO to the Iridium satellite constellation.

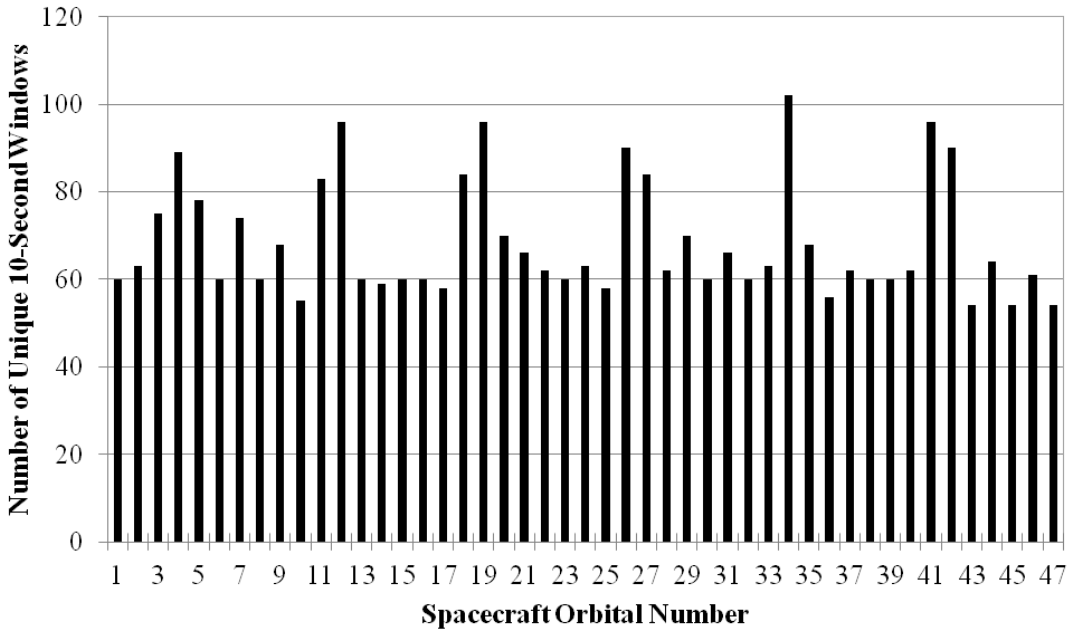

Figure 49. Histogram of 10-Second Accesses Per Orbit #3

Figure 49 exhibits an approximately consistent periodic behavior. The feature characteristics of this data point is that there are at least 50 10-second access windows each orbit, and that with the exception of some orbits with more numerous access windows, there is nearly a regularly consistent number of access windows orbit-to-orbit.

The fourth data point considered is a semi-major axis of 7,000 km and an inclination of 40 degrees. Figure 50 shows the frequency of access for the LEO RSO to the Iridium satellite constellation.

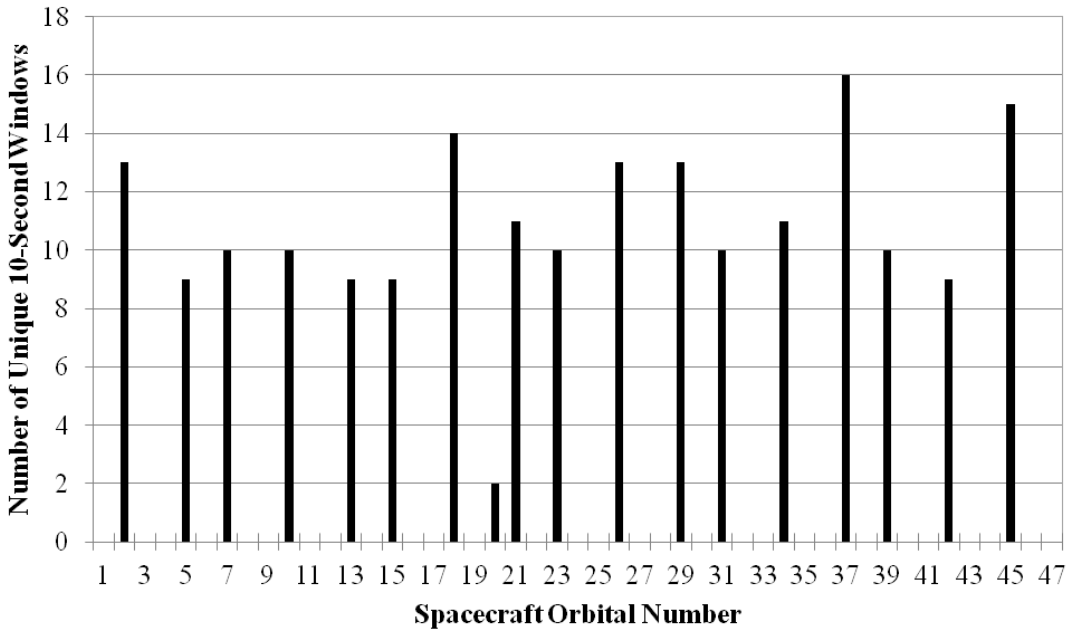

Figure 50. Histogram of 10-Second Accesses Per Orbit #4

Figure 50 exhibits a loosely periodic behavior for those orbits with access windows. Approximately have of the orbits do not have any access windows. Generally speaking, orbits with similar semi-major axis values and inclinations as the fourth data point are not desirable due to the regular blackouts and relatively low number of access windows on orbits with access.

The fifth data point considered is a semi-major axis of 6,900 km and an inclination of 80 degrees. Figure 51 shows the frequency of access for the LEO RSO to the Iridium satellite constellation.

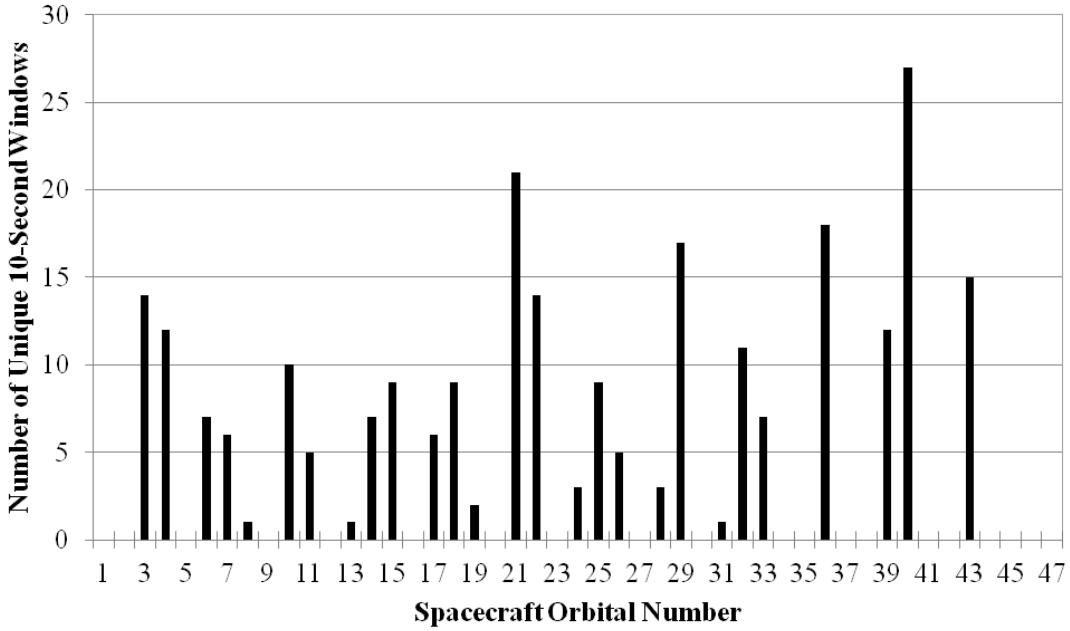

Figure 51. Histogram of 10-Second Accesses Per Orbit #5

Figure 51 does not exhibit a consistent periodic behavior. Approximately one-third of the LEO RSO orbits do not have any access windows. Generally speaking, orbits with similar semi-major axis values and inclinations as the fifth data point are not desirable due to the regular blackouts and relatively low number of access windows.

V. Conclusions and Recommendations

5.1 Chapter Overview

This chapter summarizes the thesis research and provides recommendations for future research efforts involving the study of communication between LEO RSOs and the Iridium Network satellite constellation.

5.2 Conclusions of Research

The utilization of the Iridium Network satellite constellation is feasible for LEO RSOs and provides significantly more communication opportunities in contrast to ground-based communications using a single ground station.

It is necessary to implement the Iridium 9602 transceiver firmware upgrade in order to achieve adequate access times when the LEO RSO is counter-rotating against the Iridium satellite constellation.

In general orbits with a lower semi-major axis and a higher inclination have higher total access times. The exception is when the LEO RSO has a RAAN that is offset from the Iridium satellite constellation planes, which trends toward more moderate inclinations for higher total access times.

In addition to the consideration of total access times, it is generally shown that orbits with a lower semi-major axis have more numerous 10-second access windows during a particular orbital pass. Then it was typically shown that orbits with higher inclinations exhibit a more regular behavior in the number of accesses between successive orbits. Orbits with lower inclinations or higher semi-major axis values do not exhibit regular behavior between successive orbits for the number of access windows. As

one of the potential first deployment locations of this capability, the ISS orbit is an adequate selection for flight testing the system. While a periodic behavior and noticeable differences between the maximum and minimum number of access windows exists, there are no blackouts and the worst case has about 10 to 15 minutes between access windows.

5.3 Significance of Research

This thesis demonstrates the feasibility of utilizing the Iridium Network satellite constellation. Further, it validates the need for AF funding to upgrade the Iridium 9602 transceiver in order to achieve regular access opportunities for counter-rotating orbits. This research also provides regimes of orbits based on the number of access windows per orbit, which provides critical communication capability information in order to properly select an orbit. For conjunction analysis applications, typically an orbit fit will be good for a couple of days and therefore almost all orbital regimes within this research are adequate. For SSA applications or other time-sensitive needs, it is necessary to avoid orbital regimes with blackouts in the number of access windows, as well as attempt to select an orbit that maximizes the number of access windows per orbit. Therefore, the AF can use the information provided in this research to appropriately select an orbit, or in actuality predict the total access time and the frequency of access for an orbit in order to sufficiently plan and account for the mission concept of operations.

5.4 Recommendations for Future Research

This thesis only studied circular orbits with the J_2 perturbation. It is recommended to expand the feasibility analysis to study the impact of eccentric orbits on the prediction variance. It could be possible that a solution as simple as computing a

correction factor based on the eccentricity can be applied to the cubic polynomial model of this thesis, or a completely new model may be required to fit simulation data. Along these thoughts, in order to increase the fidelity and fit of the model, higher order perturbations including atmospheric drag should be incorporated into the simulations.

Next, a closer analysis should be performed regarding the rate of change of the Doppler shift. Although not explicitly included in this thesis, data analysis of the STK access reports indicates that the rate of change of Doppler shift exceeds magnitudes calculated for ground-based communications with the Iridium Network. In some cases, the magnitudes increase by a factor of about eight. This may not exceed the capability of the communication link between the transceiver and satellite, but should be investigated.

Finally, we should call out that for longer analysis periods, the effects of the RAAN should average out similar to that of the true anomaly. This is due to the fact that the RAAN recesses under the effect of an oblate Earth (resulting J_2 perturbation). The recession rate of the RAAN is a function of the mean motion, semi-major axis, eccentricity and inclination. Referencing the J_2 equations found in Wiesel (34), we can compute a RAAN recession phase rate between a sample ISS orbit and the Iridium satellite constellation to be about 4.5 degrees per day. In other words, an analysis period of approximately 80 days will cycle the ISS RAAN completely through the relative range of RAAN values for a particular Iridium satellite constellation plane. The analysis period should in fact be tripled or even quadrupled to sufficiently average out the effects due to the RAAN. Results from this analysis would provide the long term averages of total access time and access windows dependent only on the semi-major axis, inclination and maximum range rate constraint.

5.5 Summary

In summary, the Iridium Network satellite constellation has been modeled in STK to simulate communication access from an RSO in LEO. An analysis period of three days was studied. Design Expert was used to implement the Design of Experiments technique in order to statistically quantify and predict the total access time and number of 10-second access windows.

Appendix I

Table 20. Orbital Elements of Iridium Satellite Constellation Model, Satellites 1-17

Satellite #	a (km)	e	i (deg)	ω (deg)	Ω (deg)	$\nu(t_o)$ (deg)
1	7151	0	86.4	0	0	0
2	7151	0	86.4	0	0	32.727
3	7151	0	86.4	0	0	65.455
4	7151	0	86.4	0	0	98.182
5	7151	0	86.4	0	0	130.909
6	7151	0	86.4	0	0	163.636
7	7151	0	86.4	0	0	196.364
8	7151	0	86.4	0	0	229.091
9	7151	0	86.4	0	0	261.818
10	7151	0	86.4	0	0	294.545
11	7151	0	86.4	0	0	327.273
12	7151	0	86.4	0	31.6	16.363
13	7151	0	86.4	0	31.6	49.091
14	7151	0	86.4	0	31.6	81.818
15	7151	0	86.4	0	31.6	114.545
16	7151	0	86.4	0	31.6	147.272
17	7151	0	86.4	0	31.6	179.999

Table 21. Orbital Elements of Iridium Satellite Constellation Model, Satellites 18-36

Satellite #	a (km)	e	i (deg)	ω (deg)	Ω (deg)	$\nu(t_o)$ (deg)
18	7151	0	86.4	0	31.6	212.726
19	7151	0	86.4	0	31.6	245.453
20	7151	0	86.4	0	31.6	278.180
21	7151	0	86.4	0	31.6	310.907
22	7151	0	86.4	0	31.6	343.634
23	7151	0	86.4	0	63.2	0
24	7151	0	86.4	0	63.2	32.727
25	7151	0	86.4	0	63.2	65.455
26	7151	0	86.4	0	63.2	98.182
27	7151	0	86.4	0	63.2	130.909
28	7151	0	86.4	0	63.2	163.636
29	7151	0	86.4	0	63.2	196.364
30	7151	0	86.4	0	63.2	229.091
31	7151	0	86.4	0	63.2	261.818
32	7151	0	86.4	0	63.2	294.545
33	7151	0	86.4	0	63.2	327.273
34	7151	0	86.4	0	94.8	16.363
35	7151	0	86.4	0	94.8	49.091
36	7151	0	86.4	0	94.8	81.818

Table 22. Orbital Elements of Iridium Satellite Constellation Model, Satellites 37-54

Satellite #	a (km)	e	i (deg)	ω (deg)	Ω (deg)	$\nu(t_o)$ (deg)
37	7151	0	86.4	0	94.8	114.545
38	7151	0	86.4	0	94.8	147.272
39	7151	0	86.4	0	94.8	179.999
40	7151	0	86.4	0	94.8	212.726
41	7151	0	86.4	0	94.8	245.453
42	7151	0	86.4	0	94.8	278.180
43	7151	0	86.4	0	94.8	310.907
44	7151	0	86.4	0	94.8	343.634
45	7151	0	86.4	0	126.4	0
46	7151	0	86.4	0	126.4	32.727
47	7151	0	86.4	0	126.4	65.455
48	7151	0	86.4	0	126.4	98.182
49	7151	0	86.4	0	126.4	130.909
50	7151	0	86.4	0	126.4	163.636
51	7151	0	86.4	0	126.4	196.364
52	7151	0	86.4	0	126.4	229.091
53	7151	0	86.4	0	126.4	261.818
54	7151	0	86.4	0	126.4	294.545

Table 23. Orbital Elements of Iridium Satellite Constellation Model, Satellites 55-66

Satellite #	a (km)	e	i (deg)	ω (deg)	Ω (deg)	$\nu(t_o)$ (deg)
55	7151	0	86.4	0	126.4	327.273
56	7151	0	86.4	0	158	16.363
57	7151	0	86.4	0	158	49.091
58	7151	0	86.4	0	158	81.818
59	7151	0	86.4	0	158	114.545
60	7151	0	86.4	0	158	147.272
61	7151	0	86.4	0	158	179.999
62	7151	0	86.4	0	158	212.726
63	7151	0	86.4	0	158	245.453
64	7151	0	86.4	0	158	278.180
65	7151	0	86.4	0	158	310.907
66	7151	0	86.4	0	158	343.634

Appendix II

Table 24. Angular Distribution for Iridium Satellite Spot Beams Model, Group 1

Spot Beam	Elevation	Azimuth
G1_Beam01	80°	0°
G1_Beam02	80°	120°
G1_Beam03	80°	240°

Table 25. Angular Distribution for Iridium Satellite Spot Beams Model, Group 2

G2_Beam01	65°	0°
G2_Beam02	65°	40°
G2_Beam03	65°	80°
G2_Beam04	65°	120°
G2_Beam05	65°	160°
G2_Beam06	65°	200°
G2_Beam07	65°	240°
G2_Beam08	65°	280°
G2_Beam09	65°	320°

Table 26. Angular Distribution for Iridium Satellite Spot Beams Model, Group 3

G3_Beam01	50°	0°
G3_Beam02	50°	24°
G3_Beam03	50°	48°
G3_Beam04	50°	72°
G3_Beam05	50°	96°
G3_Beam06	50°	120°
G3_Beam07	50°	144°
G3_Beam08	50°	168°
G3_Beam09	50°	192°
G3_Beam10	50°	216°
G3_Beam11	50°	240°
G3_Beam12	50°	264°
G3_Beam13	50°	288°
G3_Beam14	50°	312°
G3_Beam15	50°	336°

Table 27. Angular Distribution of Iridium Satellite Spot Beams Model, Group 4

G4_Beam01	30°	0°
G4_Beam02	30°	17.143°
G4_Beam03	30°	34.286°
G4_Beam04	30°	51.429°
G4_Beam05	30°	68.571°
G4_Beam06	30°	85.714°
G4_Beam07	30°	102.857°
G4_Beam08	30°	120°
G4_Beam09	30°	137.143°
G4_Beam10	30°	154.286°
G4_Beam11	30°	171.429°
G4_Beam12	30°	188.571°
G4_Beam13	30°	205.714°
G4_Beam14	30°	222.857°
G4_Beam15	30°	240°
G4_Beam16	30°	257.143°
G4_Beam17	30°	274.286°
G4_Beam18	30°	291.429°
G4_Beam19	30°	308.571°
G4_Beam20	30°	325.714°
G4_Beam21	30°	342.857°

Appendix III

Table 28. Reduced Cubic Polynomial Model Fit Results (A – B^2 terms)

Std. Dev.	**8191.25**						
Mean	**33038.57**						
Source	**Sum of Squares**	**df**	**Mean Squares**	**F-value**	**p-value**	**Std Error**	**VIF**
Model	3.13E+11	26	1.2E+10	179.5881	< 0.0001	921.859	
A	2.1E+11	1	2.1E+11	3131.575	< 0.0001	702.207	1.004
B	2.17E+09	1	2.17E+09	32.33443	< 0.0001	2064.91	8.627
C	2.24E+08	1	2.24E+08	3.344667	0.0685	742.775	2.467
D	9.62E+09	1	9.62E+09	143.3774	< 0.0001	473.821	1.004
E	1.81E+09	1	1.81E+09	26.9722	< 0.0001	474.016	1.004
AB	8.13E+09	1	8.13E+09	121.204	< 0.0001	1030.72	1.003
AC	4.81E+09	1	4.81E+09	71.68169	< 0.0001	702.950	1.005
AD	1.99E+09	1	1.99E+09	29.58944	< 0.0001	702.722	1.005
AE	1.32E+09	1	1.32E+09	19.73623	< 0.0001	702.649	1.005
BC	1.3E+10	1	1.3E+10	194.4436	< 0.0001	705.607	1.007
BD	1.81E+09	1	1.81E+09	26.97118	< 0.0001	704.533	1.004
BE	3.19E+08	1	3.19E+08	4.756975	0.0300	704.670	1.005
CD	9.22E+08	1	9.22E+08	13.74073	0.0003	474.132	1.005
DE	1.92E+09	1	1.92E+09	28.67739	< 0.0001	474.108	1.005
A^2	8.01E+09	1	8.01E+09	119.3111	< 0.0001	1249.98	1.005
B^2	1.91E+08	1	1.91E+08	2.844562	0.0928	1265.85	1.008

Table 29. Reduced Cubic Polynomial Model Fit Results (ABC – Error terms)

Source	Sum of Squares	Df	Mean Squares	F-value	p-value	Std Error	VIF
ABC	8.55E+09	1	8.55E+09	127.3814	< 0.0001	1030.98	1.003
ABD	2.71E+08	1	2.71E+08	4.037469	0.0455	1030.59	1.003
ABE	1.84E+08	1	1.84E+08	2.745781	0.0987	1031.04	1.004
ACD	2.72E+08	1	2.72E+08	4.048999	0.0452	702.866	1.006
ADE	1.27E+09	1	1.27E+09	18.95311	< 0.0001	702.702	1.005
BCD	1.45E+09	1	1.45E+09	21.60094	< 0.0001	705.443	1.007
BDE	4.17E+08	1	4.17E+08	6.210371	0.0133	704.723	1.005
A^2B	3.85E+08	1	3.85E+08	5.742259	0.0172	1814.34	2.463
B^2C	8.14E+09	1	8.14E+09	121.3071	< 0.0001	1265.20	2.473
B^3	2.9E+08	1	2.9E+08	4.318722	0.0386	2403.58	7.828
Residual	1.83E+10	273	67096574				
Lack of Fit	1.83E+10	254	72115609				
Pure Error	0	19	0				
Cor Total	3.32E+11	299					

Bibliography

(1) Bannach, Dane, et al. "Demonstration of Reliable Superior Worldwide Enabling Network Satellite." Team Final Report to Dr. Eric Swenson, Professor, AFIT/ENY. June 2011.

(2) Boiardt, Henric and Christian Rodriguez. "The Use of Iridium's Satellite Network for Nanosatellite Communications in Low Earth Orbit." *Proceedings of the Aerospace Conference, 2009 IEEE*. Big Sky, MT. March 2009.

(3) "Breakup Recorder Hits Ground Running." http://www.spaceref.com/news/viewpr.html?pid=33140. 30 March 2011.

(4) Department of Defense and National Intelligence Agency. *National Security Space Strategy Unclassified Summary*. http://www.defense.gov/home/features/2011/0111_nsss/docs/NationalSecurity/SpaceStrategyUnclassifiedSummary_Jan2011.pdf. January 2011.

(5) *Design Expert*. Version 8.0.7.1. Computer software. Stat-Ease Inc, Minneapolis, MN, 2010.

(6) Engineering Systems Learning Center. "Technical Success and Economic Failure." *Communications Satellite Constellations*. Massachusetts Institute of Technology. October 2003.

(7) Fankhauser, Stuart L. Vice-President for Network Operations and Customer Care, Iridium Communications Inc. Tempe, AZ. Facility Tour. 11 September 2012.

(8) Ilčev, Stojče Dimov. *Global Mobile Satellite Communications For Maritime, Land and Aeronautical Applications*. The Netherlands: Springer, 2005.

(9) *Iridium 9602*. Online Products page, Modems and Modules, www.iridium.com. McLean, VA: Iridium Communications Inc, July 2011.

(10) *Iridium SBD*. Online Products page, Data Services. www.iridium.com. McLean, VA: Iridium Communications Inc, Jul 2010.

(11) *Iridium Subscriber License Information*. Rev 1.26b. 09 February 2013. http://marine.rutgers.edu/~kerfoot/pub/slocum/RELEASE_6_32/src/doco/specifications/iridium-phone/IR_Lband.doc.rtf.

(12) "Japan's HTV cargo freighter proves useful to the end." http://www.spaceflightnow.com/h2b/htv2/110329entry/. 29 March 2011.

(13) Khan, Khudega Shahbaz. *Data Communication with a Nano-Satellite Using Satellite Personal Communication Networks*. MS thesis. School of Electrical Engineering and Computer Science, University of Central Florida. Orlando, FL. 2008.

(14) "Lead Increment Scientist's Highlights for Week of Sep 10, 2012." http://www.nasa.gov/mission_pages/station/research/news/wklysumm_week_of_sept10.html. September 2012.

(15) Lovell, T. Alan. Abstract of "Analysis of a New Nonlinear Solution of Relative Orbital Motion." *Proceedings of the 23rd International Symposium on Space Flight Dynamics*. Pasadena: October 2012

(16) Maher, Vaness Rian. *A Low Power Beacon for Transmitting Location Data via the Globalstar Satellite System*. MS thesis. Virginia Polytechnic Institute and State University. Blacksburg, VA. 2006.

(17) "Manual for ICAO Aeronautical Mobile Satellite Service." *Part 2 – Iridium*. Draft Version 4.0. http://legacy.icao.int/anb/panels/acp/wg/m/iridium_swg/ird-08/ird-swg08-ip05%20-%20ams(r)s%20manual%20part%20ii%20v4.0.pdf. 21 March 2007.

(18) McMahon, Margaret M. and Robert Rathburn. "Measuring Latency in Iridium Satellite Constellation Data Services." US Naval Academy, Computer Science Department. June 2005.

(19) Montgomery, Douglas C. *Design and Analysis of Experiments*. Hoboken, NJ: John Wiley & Sons, 2009.

(20) National Aeronautics and Space Administration. *KSC Research and Technology 2003 Annual Report*. NASA, 2003.

(21) National Aeronautics and Space Administration. *KSC Research and Technology 2004 Annual Report*. NASA, 2004.

(22) Pratt, Stephen R., et al. "An Operation and Performance Overview of the Iridium Low Earth Orbit Satellite System." *IEEE Communications Surveys*. Second Quarter, 1999.

(23) Schaub, Hanspeter and John L. Junkins. *Analytical Mechanics of Space Systems* (Second Ed). Reston, VA: AIAA, 2009.

(24) Simpson, James, et al. "Space Based Communications." Report for 40th Space Congress. NASA. 29 January 2003.

(25) Stringer, et al. "Analysis of a New Nonlinear Solution of Relative Orbital Motion." *Proceedings of the 23rd International Symposium on Space Flight Dynamics*. Pasadena: October 2012

(26) *The Global Network: Ground Infrastructure*. Online About page, Iridium Global Network, www.iridium.com. McLean, VA: Iridium Communications Inc, July 2012.

(27) *The Global Network: Satellite Constellation*. Online About page, Iridium Global Network, www.iridium.com. McLean, VA: Iridium Communications Inc, July 2012.

(28) "The Science of Breaking Up Via Space Station Re-Entry Investigation." http://www.sciencedaily.com/releases/2012/10/121012152319.htm. 12 October 2012.

(29) Topping, Russell T. Executive Vice-President, Celestech Inc. Electronic Message, attachment: Iridium proprietary satellite spot beam diagrams. September 2012.

(30) Topping, Russell T. Executive Vice-President, Celestech Inc. "Iridium Short Burst Data." Presentation to Air Force Institute of Technology, Aeronautical and Astronautical Engineering Department students and faculty. Air Force Institute of Technology, Wright-Patterson AFB, OH. July 2012.

(31) USSTRATCOM Space Control and Space Surveillance. http://www.stratcom.mil/factsheets/USSTRATCOM_Space_Control_and_Space_Surveillance/. Current as of May 2012.

(32) Vallado, David A. *Fundamentals of Astrodynamics and Applications*. Hawthorne, CA: Microcosm Press, 2007.

(33) Wertz, James R., et al. *Space Mission Engineering: The New SMAD*. Hawthorne, CA: Microcsom, 2011.

(34) Wiesel, William E. *Modern Astrodynamics* (Second Edition). Beavercreek, OH: Aphelion, 2010.

(35) Wiesel, William E. *Spaceflight Dynamics* (Third Edition). Beavercreek, OH: Aphelion, 2010.

REPORT DOCUMENTATION PAGE

Form Approved
OMB No. 074-0188

1. REPORT DATE *(DD-MM-YYYY)*	2. REPORT TYPE	3. DATES COVERED *(From – To)*
21-03-2013	Master's Thesis	May 2012 – March 2013

TITLE AND SUBTITLE

Feasibility Analysis on the Utilization of the Iridium Satellite Communications Network for Resident Space Objects in Low Earth Orbit

5a. CONTRACT NUMBER

5b. GRANT NUMBER

5c. PROGRAM ELEMENT NUMBER

6. AUTHOR(S)

Claybrook, John Robert, Civ, USAF

5d. PROJECT NUMBER

5e. TASK NUMBER

5f. WORK UNIT NUMBER

7. PERFORMING ORGANIZATION NAMES(S) AND ADDRESS(S)
Air Force Institute of Technology
Graduate School of Engineering and Management (AFIT/ENY)
2950 Hobson Way, Building 640
WPAFB OH 45433-8865

8. PERFORMING ORGANIZATION REPORT NUMBER

AFIT-ENY-13-M-04

9. SPONSORING/MONITORING AGENCY NAME(S) AND ADDRESS(ES)
Mr. Jason Guarnieri
Air Force Research Laboratory
Space Vehicles Directorate
3550 Aberdeen Ave., SE
Kirtland AFB, NM
505-853-7539
Jason.guarnieri@kirtland.af.mil

10. SPONSOR/MONITOR'S ACRONYM
AFRL/RVE

11. SPONSOR/MONITOR'S REPORT NUMBER(S)

12. DISTRIBUTION/AVAILABILITY STATEMENT
DISTRIBUTION STATEMENT A: APPROVED FOR PUBLIC RELEASE; DISTRIBUTION UNLIMITED

13. SUPPLEMENTARY NOTES

14. ABSTRACT

In recent years, space has become more congested and contested, particularly in low Earth orbit (LEO), generating the need for a low-latency capability to provide precise orbital knowledge and accurate space situational awareness information. This thesis investigates the feasibility of resident space objects (RSOs) in LEO communicating continuously with ground operators or users through the Iridium Satellite Communications Network. Due to the problem's complexity and required time for computation, a test-industry technique called Design of Experiments is implemented in order to efficiently study the feasibility of the communication link. Specifically, an optimal response surface method is chosen to design the computation test matrix of orbital parameters in Design Expert for simulations using Systems Tool Kit. The results provide a statistical polynomial model for predicting the total Iridium-network access times and windows under specified orbital parameters. Initial assessments and physical constraints provide the model-space envelope, including a discussion on representing specific orbital parameters within the model prediction space.

15. SUBJECT TERMS
LEO communication feasibility, Iridium Network, Design of Experiments, orbit determination, space situational awareness

16. SECURITY CLASSIFICATION OF:			17. LIMITATION OF ABSTRACT	18. NUMBER OF PAGES	19a. NAME OF RESPONSIBLE PERSON
a. REPORT	b. ABSTRACT	c. THIS PAGE			Wiesel, William E., PhD, Civ, USAF ADVISOR
U	U	U	UU	134	19b. TELEPHONE NUMBER *(Include area code)* 937-255-3636 ext 4312 (William.wiesel@afit.edu)

Standard Form 298 (Rev. 8-98)
Prescribed by ANSI Std. Z39-18